TWO-DIMENSIONAL EQUATIONS FOR THE ANALYSIS OF MICROSTRIP LINE DISPERSION AND STEP DISCONTINUITIES

BY

ALEXANDRU TUGULEA

A Thesis
Submitted to the Faculty of Graduate Studies
in Partial Fulfillment of the Requirements
for the Degree of

DOCTOR OF PHILOSOPHY

Department of Electrical and Computer Engineering
University of Manitoba
Winnipeg, Manitoba

National Library
of Canada

Acquisitions and
Bibliographic Services

395 Wellington Street
Ottawa ON K1A 0N4
Canada

Bibliothèque nationale
du Canada

Acquisitions et
services bibliographiques

395, rue Wellington
Ottawa ON K1A 0N4
Canada

Your file Votre référence

Our file Notre référence

0-612-53051-5

Canada

THE UNIVERSITY OF MANITOBA

FACULTY OF GRADUATE STUDIES

*****

COPYRIGHT PERMISSION PAGE

Two-Dimensional Equations for the Analysis of Microstrip Line Dispersion and Step Discontinuities

BY

Alexandru Tugulea

A Thesis/Practicum submitted to the Faculty of Graduate Studies of The University of Manitoba in partial fulfillment of the requirements of the degree

of

Doctor of Philosophy

TABLE OF CONTENTS

ACKNOWLEDGEMENTS

Many people have contributed in various ways to this thesis and their help and encouragement is kindly acknowledged.

My deepest appreciation is extended to Prof. I.R. Ciric who supervised the research and provided the guidance and unfailing support essential to the successful completion of the study.

I thank the members of my advisory committee, Prof. P.N. Shivakumar and Prof. E. Bridges for their help and constructive criticism.

I wish to thank Dr. P. Bhartia for graciously accepting to review my thesis.

I also wish to thank my friends Suzana and Dumitru Murgoi for helping me in good times and bad times, my colleague Koppada Srinivas for his warm friendship, and Keewatin Community College for support.

Finally I wish to thank my family for their support.

Abstract

It is shown how the two-dimensional equations for microwave planar circuits, which are in fact a generalization of the one-dimensional telegraphists' equations, can be derived through a rigorous theory based on Maxwell's equations.

These equations are used in the thesis to calculate the dispersion of the fundamental and of the higher-order modes of propagation on microstrip lines, the losses on microstrip lines, and the components of the equivalent circuit for symmetric, asymmetric, and cascaded microstrip lines.

The quasistatic parameters, necessary in the calculation of the modal dispersion, are determined using a new hybrid analytical-numerical approach. Four methods were developed, two of them being variational methods, together with theorems for the lower and upper bound of capacitance. Thus, the error in calculating the quasi-static parameters can be controlled.

The results obtained in calculating the dispersion are within the error of measurement range for experimental data. The proposed dispersion model permits also the inclusion of losses in the initial formulation. Thus, the attenuation and the phase constants can be obtained simultaneously.

Using the same model, the dispersion of the higher-order modes of propagation is obtained with an error of less then 1% when compared to the more accurate full-wave solution.

For symmetric and asymmetric step discontinuities, simple formulas for the components of the equivalent circuit are obtained. The results are in good agreement with those from the full-wave solution. the error being less then 1.5%.

In the case of cascaded microstrip lines, the proposed method reduces drastically the computation time while giving acceptable accuracy.

The two-dimensional equations can be successfully used up to the cutoff frequency of the first *TM* mode, well within the operation range of the microstrip lines.

LIST OF FIGURES

Fig. 7-6. Model for the structure in Fig. 7-5.

LIST OF TABLES

CHAPTER 1. INTRODUCTION

1.1. Methods of Microstrip Analysis

Transmission structures used as circuit elements in microwave circuits normally have a planar configuration. For such a configuration the element characteristics are determined by the dimensions in a single plane. For example, the width of a microstrip line on a given dielectric substrate can be adjusted to control its impedance. The required planar dimensions of these circuit elements can be conveniently obtained by photolithography and photoetching of thin films. Employment of such techniques at microwave frequencies has led to the development of microwave integrated circuits (Gupta and Singh, 1982).

There are several transmission structures that satisfy the requirement of being planar. The most common of these are the microstrip, the slotline, and the coplanar strips. Microstrip lines are widely used transmission structures, mainly due to the fact that the mode of propagation on microstrips is almost *TEM* (quasi-*TEM*). Pure *TEM* lines consist of two separate perfect conductors surrounded by a homogeneous linear dielectric. Only the triplate line belongs to this class. *TEM* modes are distinguished by having only transverse (to the direction of propagation) electric and magnetic field components. The *TEM* line is characterized by a phase velocity $v = c_0 / \sqrt{\varepsilon_r \mu_r}$ (c_0 is the velocity of light in free space, ε_r is the relative permittivity, μ_r is the relative permeability), and a characteristic impedance Z_c, both of which are frequency independent.

Quasi-*TEM* lines also have two separated conductors, but unlike pure *TEM* lines, the area containing fields is filled with an inhomogeneous dielectric. This is the case for microstrip lines, which are composed of a non-magnetic substrate layer ($\mu_r = 1$, $\varepsilon_r > 1$) and air. A *TEM* wave should have a velocity c_0 in air and $c_0 / \sqrt{\varepsilon_r}$ in the substrate, and this apparent contradiction is overcome by considering a quasi-*TEM* mode of propagation on the line. The quasi-*TEM* mode has at least one longitudinal field component along the direction of propagation and has the property of approaching a pure *TEM* mode as the frequency ω approaches zero.

The various methods of microstrip analysis available may be divided into three groups. In the first group, which comprises quasi-static methods, the propagation mode is considered to be pure *TEM* and the microstrip characteristics are calculated from the electrostatic capacitance of the structure. This type of an analysis is adequate for designing circuits at lower frequencies where the strip width and the substrate thickness are much smaller than the wavelength in the dielectric material.

In the second group, based on so-called dispersion models, the deviation from the TEM nature of the propagating field is accounted for quasi-empirically. Some parameters of the model are determined so that the final expression agrees with the known experimental (or exact theoretical) dispersion behavior of the microstrip. The methods in the third group take into account the hybrid nature of the mode of propagation. They are in fact full-wave analysis methods with both analytical and computational complexity, and they are not the subject of this thesis.

1.2. Statement of the Problem

The objectives of this research are:

- to investigate the applicability of the two-dimensional equations of microwave planar circuits in the study of microstrip lines;
- to develop an accurate and simple method for the calculation of the quasistatic parameters of microstrip lines;
- to construct a suitable model for microstrip lines that will allow the calculation of dispersion, losses, and higher-order modes by using the two-dimensional equations;
- to analyze the range of applicability of the models developed;
- to prove that the two-dimensional equations are derived, in some ideal cases, through a rigorous theory based on Maxwell's equations;
- to obtain simple formulas for the equivalent circuit for step and double step discontinuities in microstrip lines, employing the two-dimensional equations;
- to compare the quantitative results obtained with experimental data and with results from other models presented in the literature.

1.3. Quasistatic Parameters of Microstrip Lines

Circuits with inhomogeneous, non-magnetic dielectrics differ from homogeneous ones in that the phase velocity v depends not only on the relative permittivity ε_r of the substrate, but also on the distribution of the substrate in the field region and on the dimensions of the conductors. It is always bounded as $c_0/\sqrt{\varepsilon_r} < v < c_0$. The larger the volume of substrate (for a fixed thickness), the nearer is v to the value $c_0/\sqrt{\varepsilon_r}$. Therefore, for a complete description of a lossless, transversely inhomogeneous circuit, either the capacitance per unit length, C', and the inductance per unit length, L', are needed, or C' of the original circuit and C'_0 of the circuit of the same dimensions, but without substrate (that is, with a vacuum filling). Since L' is independent of ε_r, L' and C'_0 can be determined from one another since $c_0 = 1/\sqrt{L'C'_0}$.

For transversely inhomogeneous *TEM* circuits, the so-called effective (relative) permittivity (ε_{eff}) of the material is used instead of the phase velocity v of the wave. From the definition of the phase velocity, we have

$$\varepsilon_{eff} = \left(\frac{c_0}{v}\right)^2 = \left(\frac{\lambda_0}{\lambda}\right)^2 \tag{1.1}$$

where λ and λ_0 are the wavelengths in the presence and in the absence of the substrate, respectively; thus ε_{eff} is the relative permittivity of an equivalent homogeneous material that should fill the region outside conductors in order to obtain the same phase velocity as in the inhomogeneous original circuit. The effective permittivity ε_{eff} is given also by the following relationships:

$$\varepsilon_{eff} = \left(\frac{Z_{c0}}{Z_c}\right)^2 \tag{1.2}$$

$$\varepsilon_{eff} = \frac{C'}{C'_0}\ . \tag{1.3}$$

Equation (1.2) defines the characteristic impedance Z_c of the structure in terms of the characteristic impedance Z_{c0} in the absence of the substrate and of the effective permittivity. In a static analysis, all these three equations give the same value for ε_{eff}, always with $1 < \varepsilon_{eff} < \varepsilon_r$.

For quasi-*TEM* lines containing a layer of (isotropic) dielectric substrate material ($\varepsilon_r > 1$) and air ($\varepsilon = \varepsilon_0$), the capacitances C' and C'_0, and the circuit parameters Z_c, ε_{eff} cannot be determined exactly.

There are various methods available for calculating the electrostatic capacitances C' and C'_0. Wheeler (1965) used a conformal mapping approximation. Green's quasistatic analysis (Green, 1965) of microstrip lines was based on the numerical solution of Laplace's equation in finite difference form and is more suitable for enclosed microstrips. Silvester (1968) used an integral equation method, and Yamashita and Mittra (1968) employed a variational method in Fourier transform domain.

Kompa and Mehran (1975) used the planar waveguide model for microstrips. The static model (Figure 1-1 (b)) employs an ideal planar waveguide, which has the same characteristic impedance Z_c, effective permittivity ε_{eff}, phase velocity v, and wavelength λ as the original microstrip line (Figure 1-1 (a)). The planar waveguide is homogeneously filled with a fictitious dielectric which has the same relative permittivity ε_{eff} as the original microstrip line.

An ideal planar waveguide is defined as consisting of two parallel strip transmission-line conductors, with the field region bounded by magnetic walls (no normal component of the electric field, nor tangential component of the magnetic field), and with homogeneous electric and magnetic fields in the dielectric. The widths of the conductors in the model are set equal to the so-called effective conductor width w_{eff} to include the effect of the fields at the microstrip edges. The capacitance C' and the characteristic impedance Z_c of the planar waveguide model are given by

$$C' = \varepsilon_0 \varepsilon_{eff} w_{eff} / h \tag{1.4}$$

$$Z_c = \frac{\eta_0 \varepsilon_0 \sqrt{\varepsilon_{eff}}}{C'} = \frac{\eta_0 h}{w_{eff}\sqrt{\varepsilon_{eff}}} \quad ; \quad \eta_0 = 120\pi . \tag{1.5}$$

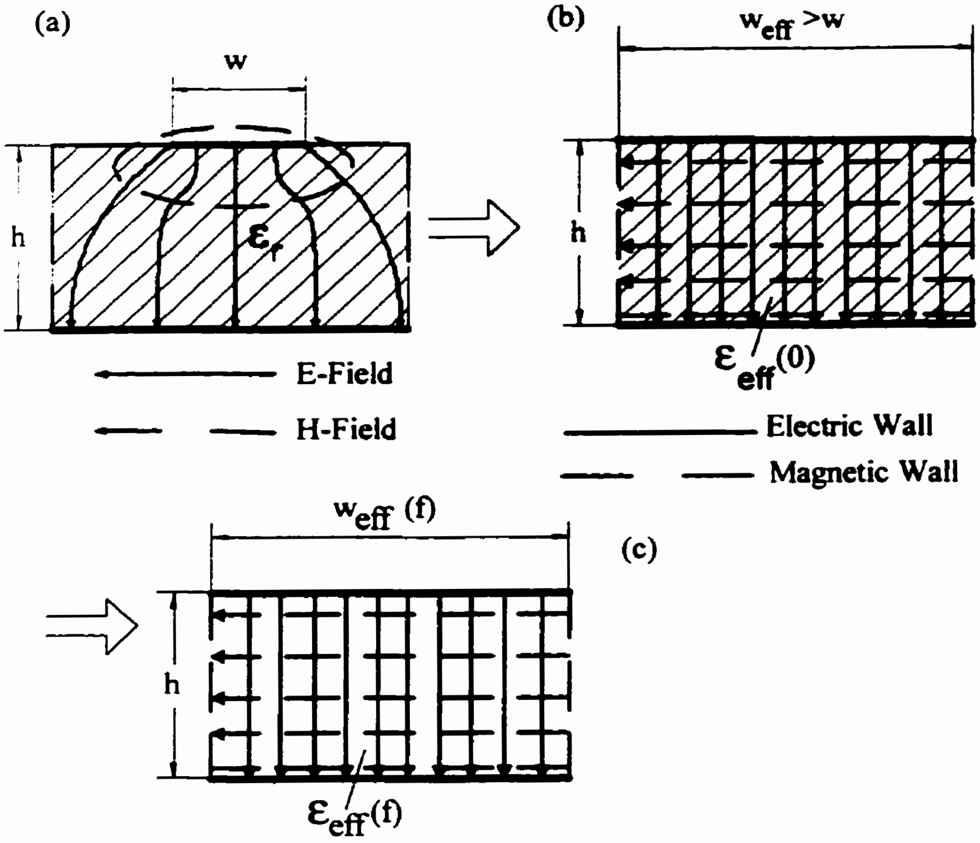

Fig. 1-1. Planar waveguide model for microstrip: (a) original circuit; (b) static model; (c) dynamic model.

The effective conductor width w_{eff} is determined from the circuit parameters Z_c and ε_{eff} as

$$w_{eff} = \frac{\eta_0 h}{Z_c \sqrt{\varepsilon_{eff}}} = \frac{\eta_0 h}{Z_{c0}} . \tag{1.6}$$

Frequency independent, static values of Z_c and ε_{eff} are used for the static planar waveguide model. For the dynamic model, frequency dependent values of ε_{eff} and w_{eff} are used.

1.4. Microstrip Dispersion

Numerous authors have tackled the problem of dispersion in microstrip lines (Carlin, 1973; Denlinger, 1971; Getsinger, 1973; Hoffmann, 1987; Jansen, 1978; Kirschning and Jansen, 1982; Kobayashi, 1982; Kobayashi, 1988; Kowalski and Pregla, 1971; Kuester and Chang, 1979; Mittra and Itoh, 1971; Pramanick and Bhartia, 1983; Pramanick and Bhartia, 1984; Schneider, 1972; Yamashita and Mittra, 1968; Yamashita *et al.*, 1979; Yamashita *et al.*, 1981) and they have proposed different models. Experimental data were also published (Edwards and Owens, 1976; Forzley and Bridges, 1992), as well as model comparisons and comparisons against experimental data (Atwater, 1988; Medina *et al.*, 1993; York and Compton, 1990).

Dispersion appears when the wave velocity depends on frequency and the fields tend to concentrate within the dielectric substrate producing an increase in the effective dielectric permittivity (Ramo *et al.*, 1994). The phenomenon of dispersion is due not only to losses in the stripline, ground plate, and dielectric, but also to the inhomogeneity of the dielectric. Indeed, consider the case of a microstrip, with the propagation velocity of the electromagnetic plane wave in air $c_0 = 1/\sqrt{\varepsilon_0 \mu_0}$, where ε_0 and μ_0 are the permittivity and permeability of free space, respectively. In the dielectric the propagation velocity becomes $v = c_0/\sqrt{\varepsilon_r}$, where $\varepsilon_r > 1$ is the relative permittivity of the dielectric substrate. It would seem that a wave can propagate with different velocities in the air and in the substrate, a fact which violates the boundary conditions at the air-dielectric interface, i.e., the conservation of the tangential components of the electric field intensity **E** and of the magnetic field intensity **H**, as well as the conservation of the normal components of the magnetic flux density **B** and of the electric flux density **D**. The conclusion is that there is a single velocity of propagation, dependent on frequency, $v(\omega)$, its value being between the previous two. Determination of $v(\omega)$ is possible by considering a higher order mode of propagation, either *TE* or *TM*, i.e. by considering either the longitudinal component of **H** or of **E**.

A variety of methods have been employed to determine the effective dielectric permittivity. There are two main ways of approaching this problem. The first uses a full-wave analysis and leads to numerical methods which are accurate and give good results as compared to experimental data. The second uses approximate formulas derived mainly by considering:

a) Coupled modes (*TEM* and *TE* or *TM*);

b) Single longitudinal-section electric (LSE) modes (Collin, 1992);

c) Curve-fitting to numerical solutions.

In the first category we mention Itoh and Mittra (1973) who have formulated the boundary value problem associated with the open microstrip line structure, in terms of a hybrid-mode representation. The equations obtained are transformed using the Ritz-Galerkin's method in the spectral domain to yield a characteristic equation for the dispersion of the open stripline. Denlinger (1971) utilizes a Fourier transform method in which the hybrid-mode solutions for a "fictitious" surface current at the substrate-air interface are combined in such a way as to represent the fields caused by a current distribution only over the region occupied by the conducting strip, assumed to be equal to that in the quasi-static case. Such full-wave solutions have been examined by Kuester and Chang (1979). These methods are computer time-consuming and do not yield closed-form equations.

In the second category we can mention Getsinger (1973) who uses the assumption that the quasi-*TEM* mode on microstrips is primarily a single longitudinal-section electric (LSE) mode which leads to a transmission line model whose dispersion behavior can be analyzed and related to that of the microstrip. He also uses an equivalent ridged waveguide model for the microstrip and determines a semi-empirical parameter from curve-fitting to experimental data, thus obtaining a simple formula. Schneider (1972) evaluates the frequency-dependent effective dielectric permittivity using the frequency at the inflection point as a function of the cutoff frequency of the lowest order *TE* surface wave mode. Carlin (1973) employs a pair of coupled lines which gives a simple model for microstrip dispersion. He considers a *TEM* transmission line and a *TE* line, and forms a distributed circuit from these two coupled lines. Kobayashi (1982) uses a *TEM* mode and a *TE* mode in order to improve Schneider's formula (Schneider, 1972). Pramanick and Bhartia (1983) derive expressions for the frequency dependence of the effective dielectric constant of the microstrip and the width of its equivalent planar waveguide model.

In the third category, that of curve-fitting to numerical solutions, we can mention Yamashita *et al.* (1979) who employ a numerical solution based on an integral equation method, obtaining a formula which is accurate up to 100 *GHz*. Kirschning and Jansen (1982) fit results from a full-wave, spectral-domain analysis. Kobayashi (1988) obtains an accurate formula by curve-fitting to the more precise numerical solution based on a more rigorous spectral-domain analysis.

Atwater (1988), using previously published experimental data, found that the formula given by Kirschning and Jansen (1982) was in fact the most accurate. York and Compton (1990) checked part of the models for various substrates ($2.2 \le \varepsilon_r \le 9.8$) and line impedances ($35\Omega \le Z_c \le 75\Omega$), and found that the best results are obtained by using the formulas given by Kirschning and Jansen (1982) and Kobayashi (1988).

We conclude that the available approximate formulas, with the exception of those in (Kobayashi, 1988) and (Yamashita *et al.*, 1981), are accurate only at "low" frequencies, usually up to 10 *GHz*, while there are numerical methods for field analysis which give more accurate results, but require time-consuming computations.

1.5. Dispersion Models

1.5.1. *Getsinger* Model

The longitudinal-section electric (LSE) mode (Collin, 1992) dispersion model of Getsinger (1973) (Figure 1-2) consists of a wave medium that allows LSE modes to propagate. The model is defined by electric ($E_{\text{tangential}}$ and $H_{\text{normal}} \to 0$) and magnetic (E_{normal} and $H_{\text{tangential}} \to 0$) walls. The dispersion model does not have exactly the same dispersion function ε_{eff} as the original circuit because the field distribution is different in the two cases. In microstrip lines the field is concentrated directly below the conductor edges (scattered fields). Near the strip transmission line edges, the electric field is mainly parallel and the magnetic field perpendicular to the dielectric boundary. These zones are indicated by the three regions I, II, and II′ of the planar waveguide model (Figure 1-2 (a)). The middle zone, a planar waveguide with dielectric of relative permittivity ε_r (the same as the substrate) and an arbitrarily chosen plate separation *h*, generates the parallel-plate capacitor field. The two zones, II and II′, represent the parts of the field in the air of the original structure. Since the air filled section is more extended than the substrate, the respective planar waveguide has a larger plate separation. Also, the **E**-field lines run parallel and the **H**-field lines run perpendicular to the dielectric boundary in the model. The dimensions b/a, c/h, and b/h are determined so that the dispersion given by the model matches as well as possible that of the original structure. The static values $Z_c(0)$ and $\varepsilon_{eff}(0)$ in the model and in the original line are matched by the choice of b/a and c/h. Hence, the dispersion function $\varepsilon_{eff}(f)$ from the model is determined by the transverse resonance method (Collin, 1992). Then b/h is obtained by matching $\varepsilon_{eff}(f)$ with the numerically determined dispersion function of the original circuit. This calculation (Getsinger, 1973) gives the dispersion function in the form

$$\varepsilon_{eff}(f)=\varepsilon_r-\frac{\varepsilon_r-\varepsilon_{eff}(0)}{1+G_1(f/f_{p1})^2} \tag{1.7}$$

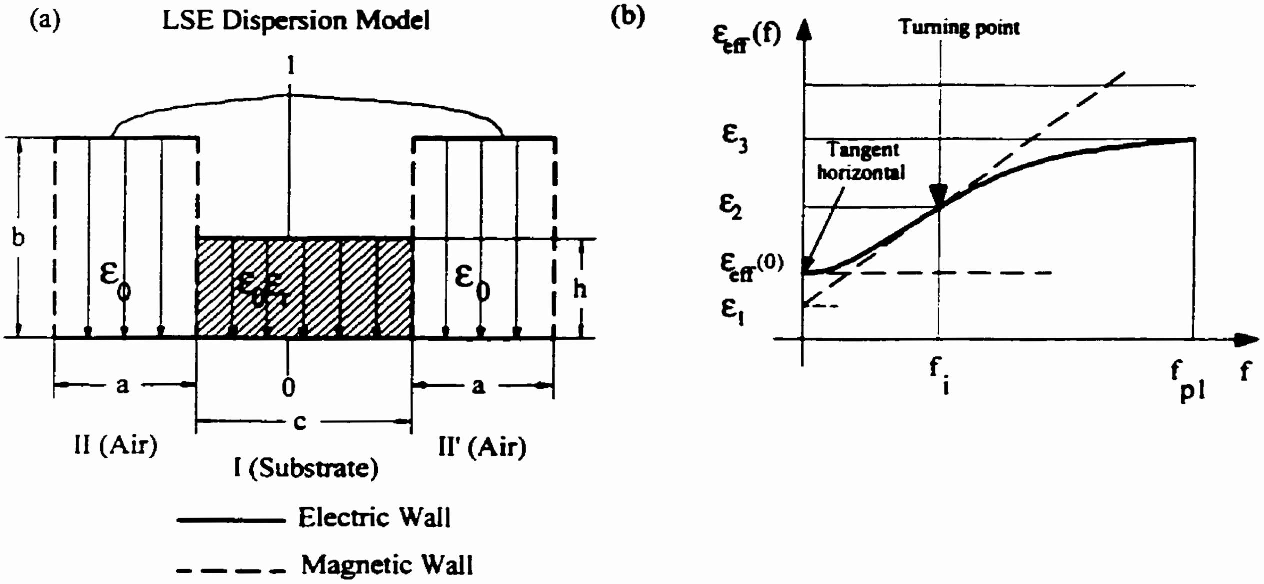

Fig. 1-2. LSE dispersion model of *Getsinger*: (a) model; (b) dispersion curve $\varepsilon_{eff}(f)$.

where

$$f_{p1}=\frac{c_0 Z_c(0)}{2h\eta_0} \tag{1.8}$$

$$G_1=0.6+0.009Z_c(0)\,. \tag{1.9}$$

G_1 is a dimensionless quantity chosen to match the dispersion function of the model with that of the original circuit. In (Getsinger, 1973) G_1 was determined by comparing ε_{eff} from the model with measurements at $f = 10\ GHz$ for microstrip lines with characteristic impedances $Z_c(0) = 15$ to 90Ω, and thicknesses of $0.635 \times 10^{-3} m$ and $1.27 \times 10^{-3} m$ for Al_2O_3 ceramic substrates ($\varepsilon_r \approx 10$). In Figure 1-2, the following notation is used for the quantities employed for matching:

$$\varepsilon_1 = \frac{9\varepsilon_{eff}(0) - \varepsilon_r}{8}\ ;\ \varepsilon_2 = \frac{3\varepsilon_{eff}(0) + \varepsilon_r}{4}\ ;\ \varepsilon_3 = \frac{\varepsilon_r G_1 + \varepsilon_{eff}(0)}{1 + G_1}\ .$$

The lower cutoff frequency f_{p1} of the first higher-order mode of the microstrip is determined by the transverse resonance method for the planar waveguide model in Section 1.3, with $w_{eff} = \lambda_{p1}/2$ and $\lambda_{p1} = c_0 / \left(f_{p1}\sqrt{\varepsilon_{eff}}\right)$ used in (1.6). As seen in Figure 1-2 (b), $\varepsilon_{eff}(f)$ increases with f from $\varepsilon_{eff}(0)$, where the function derivative is zero. The curve has a point of inflection (turning point) at $f_t = f_{p1}/\sqrt{3G_1}$ and tends toward $\varepsilon_{eff} = \varepsilon_r$ at $f = \infty$. The method described here has its limitations resulting from the fact that $\varepsilon_{eff}(f)$ was obtained from a specific, particular experimental set of data. As shown later on (Atwater, 1988; York and Compton, 1990), for substrates which are different from Al_2O_3 ($\varepsilon_r \neq 10$) and also for different thicknesses significant errors occur.

1.5.2. *Carlin* Model

A dispersion model proposed by Carlin (1973) consists of a coupled *TEM-TE* circuit (Figure 1-3). The idea of using coupled lines originates in the possibility of describing the dispersion in metallic waveguides partially filled with a dielectric by employing an infinite series of coupled *TE* and *TM* lines. In practice, only two coupled lines are used.

Carlin (1973) has modeled rectangular waveguides partially filled by a dielectric slab as two coupled *TE* lines, and circular waveguides with a concentric dielectric shell by coupled *TE* and *TM* lines. A microstrip line can be modeled by a *TEM* line electrically coupled with a *TE*

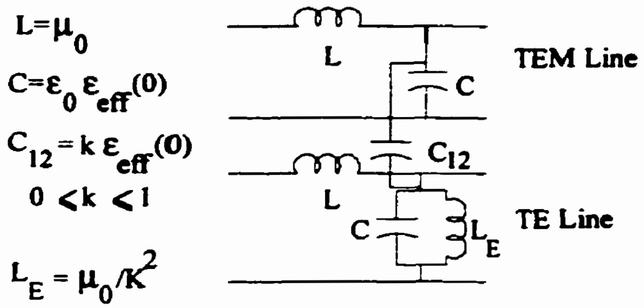

Fig. 1-3. Dispersion model from coupled TEM and TE lines.

line, as shown in Figure 1-3. One of the two lines must be a *TEM* line since the lowest cutoff frequency of the microstrip is zero, and only a *TEM* mode has this value of cutoff frequency. The second line is chosen to be a *TE* line since the first higher-order microstrip mode is a quasi-*TEM* mode. The frequency dependent effective permittivity $\varepsilon_{eff}(f) = (c_0/v)^2$ of the microstrip is derived from the phase velocity v of the propagating fundamental mode in the coupled system of conductors in the model. The circuit parameters in Figure 1-3 are determined by using the capacitive coupling coefficient k and the cutoff wavenumber K of the uncoupled *TE* mode. In this model:

$$\varepsilon_{eff}(f) = \varepsilon_{eff}(0)\left[1 + \frac{2k^2}{(f_{p2}/f)^2 + \sqrt{(2k)^2 + (f_{p2}/f)^4}}\right] \tag{1.10}$$

where

$$f_{p2} = \frac{c_0 Z_c(0)}{h\eta_0}\sqrt{\frac{k}{4.143 G_2}} \tag{1.11}$$

$$G_2 = 0.5 + 0.001 Z_c(0)^{3/2} \tag{1.12}$$

and f_{p2} is the frequency at which the turning point of the dispersion curve occurs for the *TE* line while G_2 is a dimensionless constant, similar to G_1 in (1.9). The improvement brought by this model with respect to the previous one (Getsinger, 1973) is that no recourse to interpolation for specific experimental dispersion data is required. However, the respective results have errors of 5% when compared to experimental data.

1.5.3. *Kobayashi* Formula

The formula proposed by Kobayashi (1988) is in fact a modified form of the equation (1.7) proposed by Getsinger (1973) and improved by Yamashita *et al.* (1979) and by Kirschning and Jansen (1982). Kobayashi's formula is

$$\varepsilon_{eff}(f) = \varepsilon_r - \frac{\varepsilon_r - \varepsilon_{eff}(0)}{1 + \left(f/f_{p1}\right)^m} \tag{1.13}$$

where f_{p1} and m have complicated forms depending on the microstrip dimensions, w and h. Results obtained using this formula will be presented in Chapter 4.

1.5.4. *Pramanick* and *Bhartia* Model

The dispersion model proposed by Pramanick and Bhartia (1984) is constructed by considering that microstrip dispersion is due to the coupling between a surface-wave mode and the LSE mode (Collin, 1992; Getsinger, 1973). This is the first model whose parameters are determined from a static equivalence analysis. The conventional microstrip line structure is shown in Figure 1-4 (a). The model shown in Figure 1-4 (b) preserves all the quasistatic characteristics of the original microstrip, but does not have any fringing field. The effective dielectric constants ε_I and ε_{II} of sections I and II, respectively, are obtained from y-directed resonances of the structures shown in Figure 1-4 (c) and (d), respectively, ε_I corresponding to the parallel-plate waveguide mode of the dielectric filled portion of the model and ε_{II} to the lowest order surface mode of the microstrip. The parameters u and v are obtained by imposing the condition that the model has the same electrical characteristics as the original microstrip.

From the y-directed resonances one obtains $\varepsilon_I = \varepsilon_r$ and

$$\varepsilon_{II} = \varepsilon_r + \left(\frac{\gamma_y}{k_0} \right) \tag{1.14}$$

where k_0 is the free-space propagation constant and γ_y is the phase constant. From the LSE model, by enforcing the fields H_z and E_y to be continuous at the interface between the two regions I and II, the following transcendental equation is obtained

$$\gamma_u \tanh(\gamma_u u) + \gamma_v \tanh(\gamma_v v) = 0 \tag{1.15}$$

which together with the relation

$$\gamma_v^2 = (\varepsilon_I - \varepsilon_{II}) k_0^2 + \gamma_u^2 \tag{1.16}$$

gives γ_u and γ_v. Once γ_u and γ_v are obtained, the frequency-dependent effective dielectric constant of the microstrip is determined as

$$\varepsilon_{eff}(f) = \varepsilon_I + \frac{\gamma_u^2}{k_0^2} = \varepsilon_{II} + \frac{\gamma_v^2}{k_0^2} \quad . \tag{1.17}$$

This method gives better results than the ones in (Carlin, 1973) and (Getsinger, 1973) when compared against experimental data.

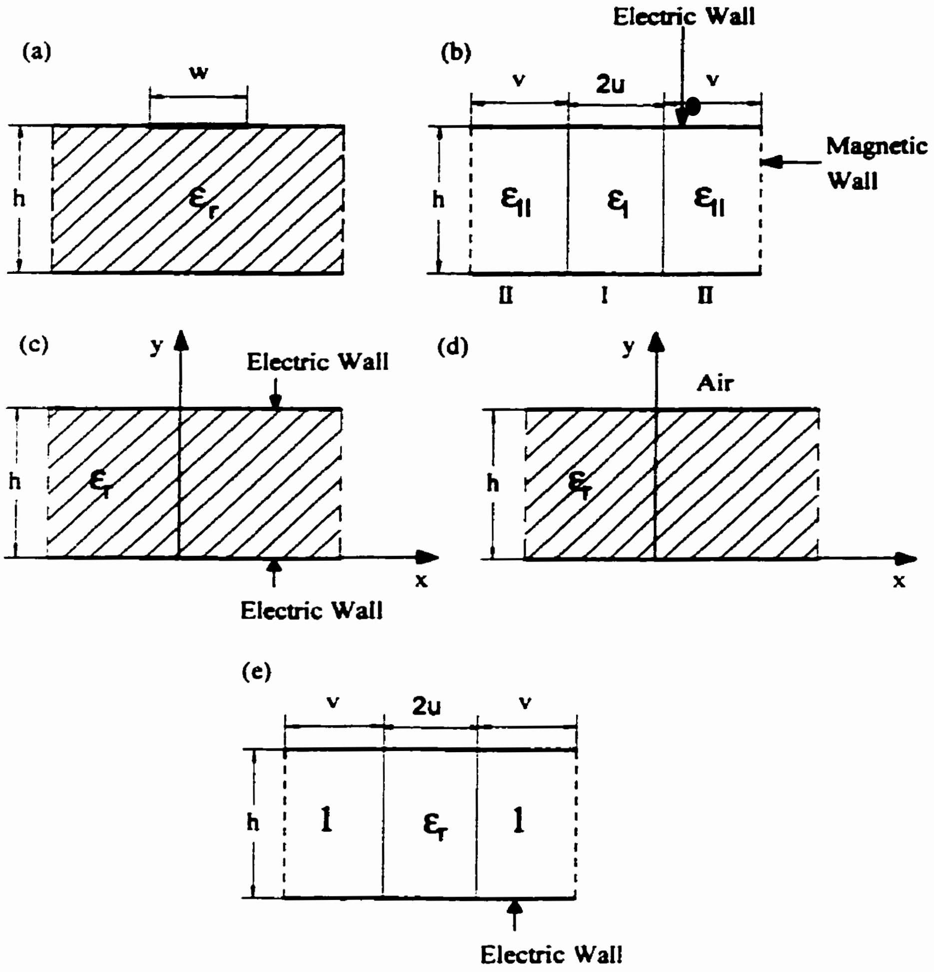

Fig. 1-4. (a) Microstrip line; (b) model of microstrip; (c) structure for analyzing y-directed resonance in region I; (d) structure for analyzing y-directed resonance in region II; (e) equivalent model at zero frequency.

1.6. Higher-Order Modes on Microstrips

The knowledge of the higher-order modes is important since they affect the usefulness of the microstrip line at high frequencies (Ermert, 1976). The modes that propagate along microstrips consist of a fundamental mode and an infinite number of higher-order modes. The fundamental mode has the lower cutoff frequency ($f = 0$) and this is normally the operating mode of the microstrips (Hoffmann, 1987). The interval between zero frequency and the cutoff frequency of the first higher-order mode is defined as the technical working range. Determination of the cutoff frequencies of the first two higher-order modes f_{HE1} and f_{HE2} is important because parasitic effects (such as extra signal losses) occur near these frequencies and can perturb the operation of the circuit.

The dynamic planar waveguide model, which is a generalization of the static planar waveguide model (Section 1.3), was used to produce diagrams and formulas for the cutoff frequencies f_{HEm} and the dispersion ($\varepsilon_{effHEm}(f)$) of the higher-order modes in open microstrips HE_m (Ermert, 1976; Kompa, 1975). For any arbitrary w_{eff} and h (1.6), the planar waveguide model, as the rectangular waveguide, has an infinite number of rectangular waveguide H_{mn} and E_{mn} modes, where m is the number of half-periods of the field amplitude along the width w_{eff} and n is the number of half-periods along the shorter side h (Figure 1-1). For the important practical case of thin substrates $h/\lambda_0 << 1$ and $n = 0$. Thus, planar waveguides support H_{m0} ($m = 0,1,2,\ldots$) modes, with the mode H_{00} (i.e. TEM) being the fundamental mode. Kompa (1975) determined a frequency dependent effective width $w_{eff}(f)$ and the cutoff frequencies of the first two higher-order modes H_{10} and H_{20} (corresponding to the HE_1 and HE_2 modes) of the microstrip. Comparisons of theoretically calculated cutoff frequencies f_{H10} and f_{H20} agree well with measurements of the cutoff frequencies f_{HE1} and f_{HE2} (Kompa, 1975; Kompa, 1976). Assuming that the measured dispersion behavior of the quasi-TEM mode, as well as that of the higher-order modes can be described by employing a planar waveguide model, an expression of the HE_m mode of the microstrip line is derived in the form

$$\lambda_{HEm} \approx \lambda_{Hm0} = \frac{\lambda_0}{\sqrt{\varepsilon_{eff}}\sqrt{1-(f_{c_m}/f)^2}} \tag{1.18}$$

with

$$f_{c_m} = \frac{mc_0}{2\sqrt{\varepsilon_{eff}}\, w_{eff}} \quad , \qquad m = 0,1,2,\ldots \tag{1.19}$$

$$\varepsilon_{eff} = \left(\frac{c_0}{f\lambda_{HE0}} \right)^2 \tag{1.20}$$

where $f_{c_m} \equiv f_{HEm}$. A rough estimation of the cutoff frequencies f_{HE1} and f_{HE2} derived from (1.19) gives (Hoffmann, 1987)

$$f_{HEm} \approx \frac{c_0 m Z_c}{2\eta_0 h} \tag{1.21}$$

where η_0 is the free-space impedance. Ermert (1976), using a transverse connection of a pair of bifurcated waveguides and employing a transverse mode-matching technique, obtains the fundamental and the first two higher-order modes. Results published by Ermert (1976) are slightly better than those given by Kompa (1975). Other authors, for example Kobayashi (1982), have used a simple formula for the cutoff frequency of the first higher-order mode

$$f_{TE10} = \frac{c_0}{4h\sqrt{\varepsilon_r - 1}} \tag{1.22}$$

(since H has a longitudinal component, the HE_m higher-order modes are also called *quasi* H_{m0} (Ermert, 1976; Kompa, 1975) or *quasi* TE_{m0} modes (Hoffmann, 1987; Kobayashi, 1982)). This formula introduces significant errors with respect to experimental data published by Ermert (1976) and Kompa (1975).

1.7. Microstrip Discontinuities

A transmission line discontinuity is a variation from a straight and longitudinally homogeneous circuit. At the discontinuity the electric and magnetic fields and the current lines are distorted as compared with those of a longitudinally homogeneous circuit. To account for this, the discontinuities are analyzed as individual elements (one-, two-, n-port), described in general by the frequency dependent n-port scattering parameters $S_{ij}(f)$. The discontinuities are often approximated at low frequencies by an equivalent circuit of lumped L and C elements.

Microstrip discontinuities consist of abrupt changes in strip conductor width from w_1 to w_2, without any change in substrate thickness h or permittivity ε_r. These discontinuities are used in low-pass filters and in impedance transformer circuits. The field discontinuities are due to the increase in current density from the wider to the narrower conductor, and also due to scattered electric (fringing) fields on the front edge of the wider conductor. The current compression generates a series inductance L_s and the scattered fields generate a parallel capacitance C_p, as shown in the equivalent circuit of Figure 1-5 (b). These are referred to the cross-sectional plane T at the step location. The following methods can be applied to step discontinuity analysis (Akhtarzad and Jahus, 1975; Easter *et al.*, 1978; Garg and Bahl, 1978; Giannini *et al.*, 1992; Gopinath *et al.* 1976; Kompa, 1973; Kompa, 1976; Kompa, 1978; Koster and Jansen, 1986; Levy, 1999; Neidert and Reilly, 1974; Oliner, 1955; Prouty *et al.*, 1997; Railton and Rozzi, 1988; Silvester and Benedek, 1972; Thomson and Gopinath, 1975; Wolf *et al.*, 1972; Xu *et al.*, 1989):

1. Fullwave analysis of the original structure (Akhtarzad and Jahus, 1975; Koster and Jansen, 1986; Xu *et al.*, 1989), including the air-substrate dielectric inhomogeneity; this method is valid for all frequencies encountered in practice;
2. For low frequencies, a static numerical analysis of the original structure can be used, with frequency independent values for L_S (Thomson and Gopinath, 1975);
3. A dynamic analysis can be employed for step discontinuities by using the fundamental planar waveguide mode (Kompa, 1978) to generate approximate equations for the frequency dependent values of L_S (equivalent circuits in Figure 1-5 (b,c,e));
4. A full-wave analysis based on the planar waveguide model, with fundamental and higher-order modes (Kompa, 1973; Kompa, 1976; Kompa, 1978), is used to obtain values for frequency dependent scattering parameters $S_{ij}(f)$ of the equivalent two-port (equivalent circuits in Figure 1-5 (d,f)) of the conductor discontinuity;

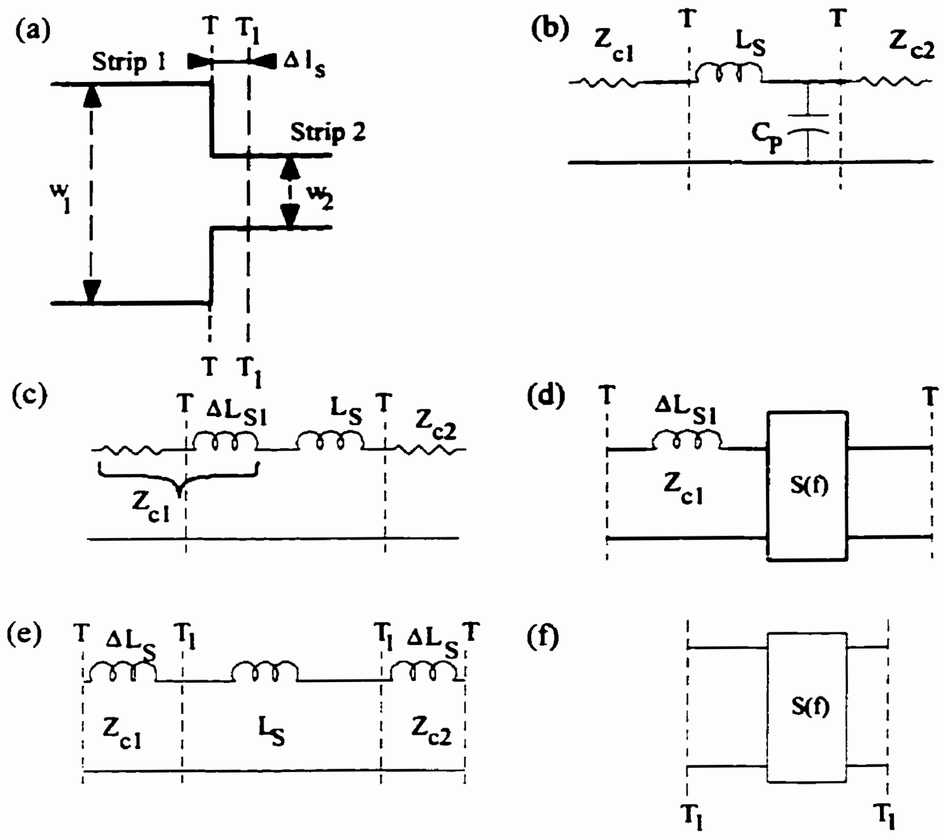

Fig. 1-5. Step discontinuity: (a) original circuit; (b) lumped element equivalent circuit; (c) equivalent circuit with conductor extension, using the inductance ΔL_{s1} instead of the capacitance C_p ; (d) inclusion of the forward scattered fields by the extension ΔL_{s1} in the general S-parameter equivalent circuit from the planar waveguide model; (e) lumped element equivalent circuit with variable reference plane T_1 ; (f) general S-parameter equivalent circuit for planar waveguide analysis with higher-order modes.

5. Experimental determination of the equivalent circuit reactive elements L_s and C_p (Easter *et al.*, 1978; Neidert and Reilly, 1974);
6. Approximate equations are used for the equivalent circuit reactive elements (Garg and Bahl, 1978) from the approximations of the static numerical results.

In static approximations, the frequency independent reactive elements L_s and C_p in the equivalent circuit (Figure 1-5 (b)) are separately determined by various methods. C_p can be obtained from a numerical static analysis of the original structure by using Green functions C_p (Easter *et al.*, 1978), assuming the conductor thickness $t = 0$. The functional dependence of the static capacitance is

$$C_p = hf(w_1/h, w_2/h, \varepsilon_r) \ . \tag{1.23}$$

L_s can be determined by static analysis of the original structure using the Galerkin method (Gopinath *et al.*, 1976). Due to the static approximation, L_s is constant for all values of ε_r and its functional dependence is

$$L_s = hf(w_1/h, w_2/h) \ . \tag{1.24}$$

Expressions for the static L_s and C_p, derived from numerical results, are given in elements (Garg and Bahl, 1978). If both sections 1 and 2 of the step (Figure 1-5 (a)) are replaced by their planar waveguide models, it is assumed that the transfer properties of the planar waveguide conductor discontinuity are the same as those of the original conductor step. The two planar waveguides are joined at the reference plane T. The front face of conductor 1 is then closed by a magnetic wall. The planar waveguide model only allows us to determine the effects of the current concentration or field discontinuity within the planar waveguide (i.e. L_s). The effect of the scattered electric fields at the front edge of the wider conductor cannot be determined. If only the fundamental mode is used in the planar waveguide model (i.e. higher order modes are ignored), then there are simple equations for L_s (Kompa, 1978; Oliner, 1955), due to the closed, homogeneously filled field region of the planar waveguide. Oliner (1955) proved that the discontinuities in the planar waveguide model can be converted into rectangular waveguide discontinuities, for which the equivalent circuits are given in standard reference works, such as (Montgomery *et al.*, 1948). By using this method, the inductance of the equivalent circuits in Figure 1-5 (b,c,e) is derived as (Oliner, 1955)

$$\frac{2\pi f L_s}{Z_{c1}} = \frac{4w_{eff1}}{\delta\lambda_1}\ln\left[1\Big/\sin\left(\frac{\pi}{2}\frac{w_{eff2}}{w_{eff1}}\right)\right] \tag{1.25}$$

where $\delta = 2$ for symmetrical steps. If w_{eff1} and w_{eff2} are taken from (1.6) for the static approximation, then

$$L_s = h\frac{2\mu_0}{\delta\pi}\ln\left[1\Big/\sin\left(\frac{\pi}{2}\frac{Z_{c1}}{Z_{c2}}\right)\right] . \tag{1.26}$$

There are various expressions for the inductance L_s which are valid at frequencies higher than those considered in (1.25) and (1.26) (Kompa, 1978). The frequency dependent L_s becomes infinitely large at the first cut-off frequency.

The previously described hybrid-mode analysis includes only the fundamental mode for the step discontinuity. The analysis can be extended to include the HE_n higher modes. These higher-order modes are excited at all discontinuities. The modes generated, depending on frequency, represent propagating waves or evanescent fields, which affect the properties of the discontinuity. A rigorous analytical description of these properties is extremely difficult (Gopinath *et al.*, 1976). By splitting the discontinuity into sections and employing characteristic waves matching at each section of the discontinuity, the frequency dependent scattering parameters $S_{ij}(f)$ of the equivalent circuits in Figure 1-5 (d,f) can be obtained by using various numerical methods.

In Chapter 2, the two-dimensional equations for microwave planar circuits are introduced, along with associated uniqueness theorems. Chapter 3 describes the methods proposed for calculating the quasistatic parameters of microstrip lines necessary in obtaining the dispersion on the basis of the models presented in Chapter 4. In Chapter 5 it is shown how the model employed in calculating the dispersion of the fundamental mode can also be used to obtain the dispersion of the higher-order modes. Microstrip step discontinuities are the subject of Chapter 6. Two simple examples of microstrip resonators are analyzed in Chapter 7 using the same two-dimensional equations. Finally, the conclusions of this thesis are presented in Chapter 8.

CHAPTER 2. TWO-DIMENSIONAL EQUATIONS FOR MICROWAVE PLANAR CIRCUITS

2.1. Definition of Planar Circuit Field Quantities

In planar structures the propagation of microwaves is two-dimensional if the thickness of the structure is much less than the minimal wavelength of the microwave spectrum. The following simplifications related to the structure of the electromagnetic field are assumed (Radulet and Tugulea, 1983):

a) The modes of propagation have the electric field ***E*** normal to the plates of the structure, while the magnetic field ***H*** is parallel to these plates (Figure 2-1).

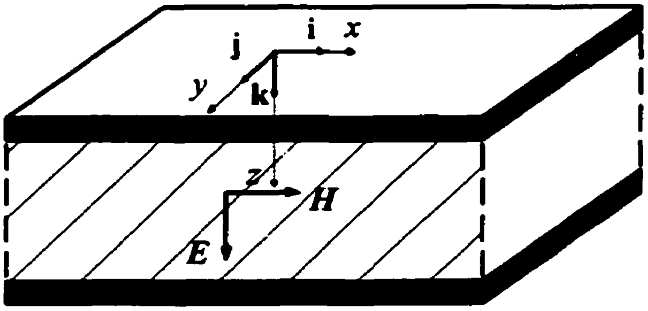

Fig. 2-1. Segment of an arbitrarily shaped planar structure showing the fields orientation.

If the system of coordinates is chosen as in Figure 2-1, the fields can be expressed as

$$\boldsymbol{E} = \mathbf{k}E_z(x,y,t) \tag{2.1}$$

$$\boldsymbol{H} = \mathbf{i}H_x(x,y,t) + \mathbf{j}H_y(x,y,t) \tag{2.2}$$

b) The fields are independent of the coordinate normal to the plates.

Equations (2.1) and (2.2) describe rigorously only the case of the lossless structures. For lossy structures there is also a tangential component of the electric field which is neglected. For two opposite points of the plates, M and M', an electric voltage can be defined as (Figure 2-2)

$$u(x,y,t)=\int_{M}^{M'}\mathbf{E}d\mathbf{r}=E_z h\ . \tag{2.3}$$

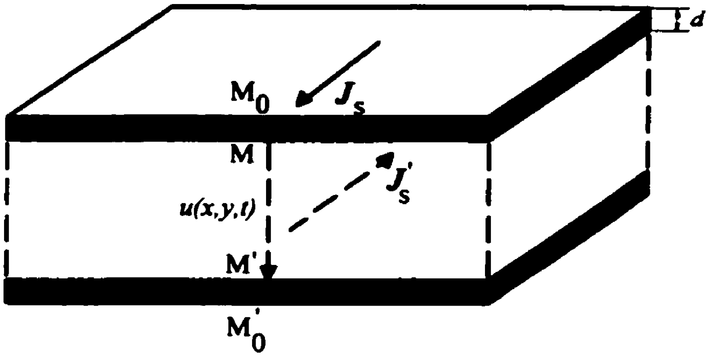

Fig. 2-2. Voltage between plates and the direction of surface current density.

For each of the plates a surface current density of the equivalent current layer can be defined as

$$J_s(x,y,t)=\int_{M_0}^{M}J(x,y,z,t)dz \tag{2.4}$$

$$J_s'(x,y,t)=\int_{M_0'}^{M'}J'(x,y,z,t)dz\ . \tag{2.5}$$

The instantaneous current densities J and J' in the conducting plates are in general nonuniform due to the skin effect. In the case where the thickness d of the plates is much less than the penetration depth, the current densities are assumed independent of z and therefore

$$J_s=Jd \tag{2.6}$$

$$\boldsymbol{J}_s' = \boldsymbol{J}d\,. \tag{2.7}$$

The boundary conditions for the magnetic field are

$$\boldsymbol{H}_M = \boldsymbol{J}_s \times \mathbf{k} = \boldsymbol{H}_{M'} = \mathbf{k} \times \boldsymbol{J}_s' \tag{2.8}$$

yielding

$$\boldsymbol{J}_s(M,t) = -\boldsymbol{J}_s'(M',t) \tag{2.9}$$

and

$$H_x = J_{sy} \tag{2.10}$$

$$H_y = -J_{sx}\,. \tag{2.11}$$

The conduction current density through the dielectric medium is

$$J_z = \sigma E_z \tag{2.12}$$

where σ is the conductivity of the dielectric. Finally one can observe that the fundamental quantities in the field theory of the planar circuits are $\boldsymbol{E}$ and $\boldsymbol{H}$ while in the circuit theory the corresponding quantities are u and $\boldsymbol{J}_s$. The relationships between the two theories are ensured by Equations (2.3) and (2.8).

2.2. Definition of Planar Circuit Parameters

In Figure 2-3 an elementary parallelepiped $ABCDA'B'C'D'$ is considered, which will enable us to define the two-dimensional parameters. On the opposite faces $ABCD$ and $A'B'C'D'$

the electric charges are equal

$$\pm\Delta q = \pm\rho_s \Delta x \Delta y = \pm\varepsilon E_z \Delta x \Delta y$$

where ρ_s is the surface charge density and ε is the permittivity of the material between the plates. The elementary capacitance is

$$\Delta C = \frac{\Delta q}{u} = \frac{\varepsilon}{h}\Delta x \Delta y \ .$$

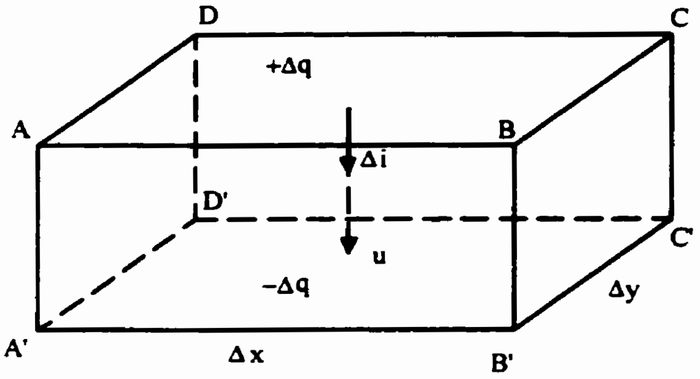

Fig. 2-3. Definition of the capacitance and the conductance.

Thus, the capacitance per unit area is

$$C = \lim_{\Delta x, \Delta y \to 0} \frac{\Delta C}{\Delta x \Delta y} = \frac{\varepsilon}{h} \ . \tag{2.13}$$

The conduction current through the dielectric medium is

$$\Delta i = J_z \Delta x \Delta y = \sigma E_z \Delta x \Delta y$$

and the elementary conductance is

$$\Delta G = \frac{\Delta i}{u} = \frac{\sigma}{h}\Delta x \Delta y \, .$$

The conductance per unit area is

$$G = \lim_{\Delta x, \Delta y \to 0} \frac{\Delta G}{\Delta x \Delta y} = \frac{\sigma}{h} \, . \tag{2.14}$$

In Figure 2-4 two rectangularly contours $\Gamma_x = abb'a'$ and $\Gamma_y = cdd'c'$ are considered.

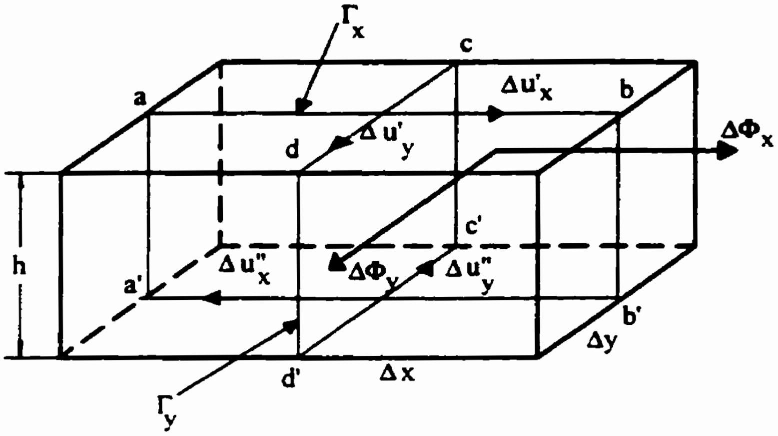

Fig. 2-4. Definition of the inductance and the resistance.

The magnetic fluxes through the surfaces bounded by the considered contours are

$$\Delta\Phi_x = \mu_x H_x h \Delta y = \mu_x J_{sy} h \Delta y$$

$$\Delta\Phi_y = \mu_y H_y h \Delta x = -\mu_y J_{sx} h \Delta x \, .$$

The inductances per square are

$$L_x = -\lim_{\Delta x \to 0} \frac{\Delta \Phi_y}{J_{sx} \Delta x} = \mu_y h \tag{2.15}$$

$$L_y = \lim_{\Delta y \to 0} \frac{\Delta \Phi_x}{J_{sy} \Delta y} = \mu_x h \ . \tag{2.16}$$

For isotropic media ($\mu_x = \mu_y \equiv \mu$) $L_x = L_y = \mu h$. The voltages along the plates are (Figure 2-4)

$$\Delta u_x = \Delta u'_x + \Delta u''_x = J_{sx} \Delta x \left(\frac{1}{\sigma'_{sx}} + \frac{1}{\sigma''_{sx}} \right)$$

$$\Delta u_y = \Delta u'_y + \Delta u''_y = J_{sy} \Delta y \left(\frac{1}{\sigma'_{sy}} + \frac{1}{\sigma''_{sy}} \right) .$$

The resistances per square are

$$R_x = \lim_{\Delta x \to 0} \frac{\Delta u_x}{J_{sx} \Delta x} = \frac{1}{\sigma'_{sx}} + \frac{1}{\sigma''_{sx}} \equiv \frac{1}{\sigma_{sx}} \tag{2.17}$$

$$R_y = \lim_{\Delta y \to 0} \frac{\Delta u_y}{J_{sy} \Delta y} = \frac{1}{\sigma'_{sy}} + \frac{1}{\sigma''_{sy}} \equiv \frac{1}{\sigma_{sy}} \tag{2.18}$$

where σ'_{sx}, σ''_{sx}, σ'_{sy}, and σ''_{sy} are the surface conductivities for the upper plate (′) and for the lower plate (″) in the x and y directions, respectively. For isotropic media ($\sigma_{sx} = \sigma_{sy} \equiv \sigma_s$) $R_x = R_y \equiv 1/\sigma_s$, $\sigma_s = \sigma_c d$, where σ_c is the conductivity of the plates.

2.3. First and Second Order Equations

Applying *Faraday*'s law to the contours Γ_x and Γ_y (Figure 2-5) one obtains

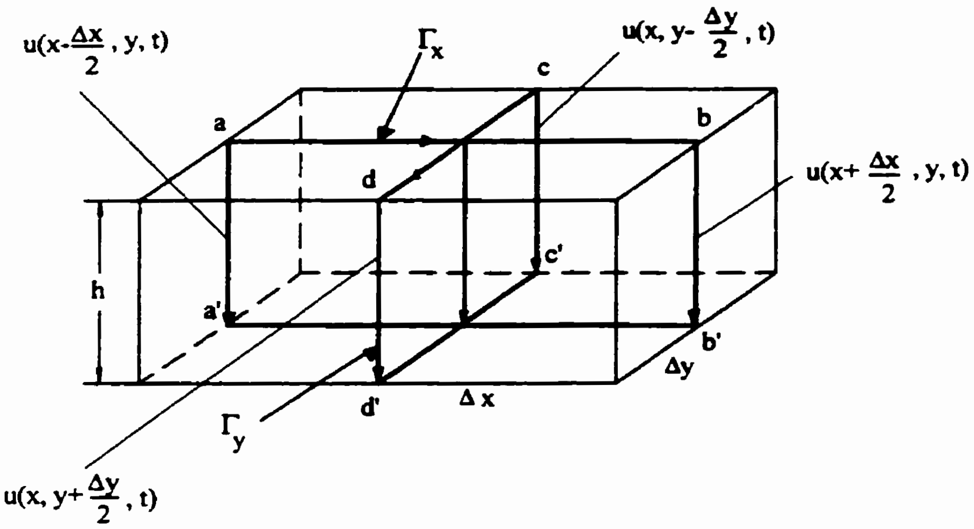

Fig. 2-5. Relative to the derivation of the first order two-dimensional equations.

$$-u\left(x-\frac{\Delta x}{2},y,t\right)+\Delta u'_x+u\left(x+\frac{\Delta x}{2},y,t\right)+\Delta u''_x=-\frac{\partial}{\partial t}\left(-\Delta\Phi_y\right)$$

$$-u\left(x,y-\frac{\Delta y}{2},t\right)+\Delta u'_y+u\left(x,y+\frac{\Delta y}{2},t\right)+\Delta u''_y=-\frac{\partial}{\partial t}\left(\Delta\Phi_x\right) .$$

Dividing by Δx and Δy, respectively, one obtains for $\Delta x \to 0$ and $\Delta y \to 0$ the following equations

$$-\frac{\partial u}{\partial x}=R_x J_{sx}+L_x\frac{\partial J_{sx}}{\partial t} \tag{2.19}$$

$$-\frac{\partial u}{\partial y}=R_y J_{sy}+L_y\frac{\partial J_{sy}}{\partial t} . \tag{2.20}$$

$$\overline{\mathbf{R}} = \begin{bmatrix} R_x & 0 \\ 0 & R_y \end{bmatrix}, \qquad \overline{\mathbf{L}} = \begin{bmatrix} L_x & 0 \\ 0 & L_y \end{bmatrix} \tag{2.21}$$

the Equations (2.19) and (2.20) can be expressed in tensor form as

$$-\mathbf{i}\frac{\partial u}{\partial x} - \mathbf{j}\frac{\partial u}{\partial y} = \overline{\mathbf{R}} \cdot \boldsymbol{J}_s + \overline{\mathbf{L}} \cdot \frac{\partial \boldsymbol{J}_s}{\partial t}$$

or

$$-\nabla u = \overline{\mathbf{R}} \cdot \boldsymbol{J}_s + \overline{\mathbf{L}} \cdot \frac{\partial \boldsymbol{J}_s}{\partial t} \tag{2.22}$$

where

$$\nabla \equiv \mathbf{i}\frac{\partial}{\partial x} + \mathbf{j}\frac{\partial}{\partial y}$$

is the two-dimensional *del* operator.

For isotropic media ($R_x = R_y \equiv R$, $L_x = L_y \equiv L$) (2.22) becomes

$$-\nabla u = R\boldsymbol{J}_s + L\frac{\partial \boldsymbol{J}_s}{\partial t} \ . \tag{2.23}$$

Applying the law of conservation of electric charge on a closed surface Σ around the upper plate in Figure 2-6 one obtains

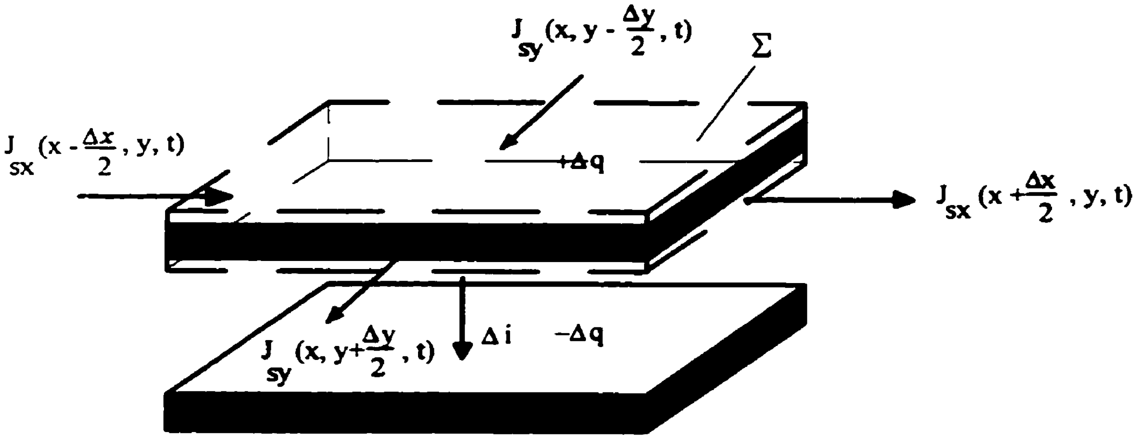

Fig. 2-6. Relative to the application of the law of conservation of electric charge.

$$-J_{sx}\left(x-\frac{\Delta x}{2},y,t\right)\Delta y+J_{sx}\left(x+\frac{\Delta x}{2},y,t\right)\Delta y-J_{sy}\left(x,y-\frac{\Delta y}{2},t\right)\Delta x+$$
$$J_{sy}\left(x,y+\frac{\Delta y}{2},t\right)\Delta x+J_{z}\Delta x\Delta y=-\frac{\partial}{\partial t}(\Delta q).$$

Dividing by $\Delta x\Delta y$ and taking $\Delta x \to 0$, $\Delta y \to 0$ gives

$$-\frac{\partial J_{sx}}{\partial x}-\frac{\partial J_{sy}}{\partial y}=Gu+C\frac{\partial u}{\partial t}$$

or

$$-\nabla\cdot\mathbf{J}_{s}=Gu+C\frac{\partial u}{\partial t}\ . \qquad (2.24)$$

The Equations (2.23) and (2.24) are called the instantaneous first order two-dimensional equations of propagation for planar circuits.

For an isotropic and homogeneous structure one can obtain the classical one-dimensional equations, assuming that only the *TEM* mode propagates, by replacing the per square and per unit area parameters from Equations (2.23) and (2.24) with the per length parameters as follows

$$i = J_s w \quad R' = \frac{R}{w} \quad L' = \frac{L}{w} \quad G' = Gw \quad C' = Cw$$

where w is the width of the strip.

For time-harmonic fields the first-order equations can be written in a phasor form as

$$-\nabla U = R\mathbf{J}_s + j\omega L\mathbf{J}_s \tag{2.25}$$

$$-\nabla \cdot \mathbf{J}_s = GU + j\omega CU \tag{2.26}$$

where U and $\mathbf{J}_s$ are complex quantities, functions of the space coordinates only. The modulus of U and $\mathbf{J}_s$ are the rms values of u and J_s. Losses in the material between the conductors can be taken into account by using complex values for the permittivity and permeability in C and L,

$$\varepsilon = \varepsilon_0 \varepsilon_r (1 - j\tan\delta)$$

$$\mu = \mu_0 \mu_r (1 - j\tan\alpha)$$

where δ is the dielectric loss angle and α is the magnetic loss angle of the material. The skin effect in the plates can also be taken into consideration.

For isotropic circuits, the second order equations are obtained by taking the divergence of (2.25) and by substituting (2.26) into the resulting equations. Thus, the following complex equations are derived:

$$\nabla^2 U - \gamma^2 U = 0 \tag{2.27}$$

$$\nabla^2 \mathbf{J}_s - \gamma^2 \mathbf{J}_s = 0 \tag{2.28}$$

where $\gamma^2 = (R + j\omega L)(G_s + j\omega C_s)$.

2.4. Power Conservation in Planar Microwave Circuits

Starting from the first order instantaneous equations, by cross-multiplication with J_s and u we obtain the following identity

$$-\nabla \cdot (uJ_s) = (\overline{\mathbf{R}} \cdot J_s) \cdot J_s + Gu^2 + \frac{\partial}{\partial t}\left[\frac{1}{2}Cu^2 + \frac{1}{2}(\overline{\mathbf{L}} \cdot J_s) \cdot J_s\right].$$

Integrating over the surface S_Γ of the circuit conductor, after some elementary integral transformation, we obtain

$$\oint_\Gamma uJ_s \cdot \mathbf{n}_{in} dl = \int_{S_\Gamma} \left[(\overline{\mathbf{R}} \cdot J_s) \cdot J_s + Gu^2\right] dS + \frac{d}{dt}\int_{S_\Gamma}\left[\frac{1}{2}Cu^2 + \frac{1}{2}(\overline{\mathbf{L}} \cdot J_s) \cdot J_s\right] dS = P_J + \frac{dW_{em}}{dt} \tag{2.29}$$

where Γ is the contour of S_Γ and $\mathbf{n}_{in}$ is the inward normal.

For a m-port circuit in which the voltages at the terminals are u_k and the currents through the terminals are i_k, (2.29) yields

$$\sum_{k=1}^{m} u_k i_k = P_J + \frac{dW_{em}}{dt} \tag{2.30}$$

where $\sum_{k=1}^{m} u_k i_k$ is the electromagnetic power received from the outside sources,

$$P_J = \int_{S_\Gamma} \left[\left(\overline{\mathbf{R}} \cdot J_s \right) \cdot J_s + G u^2 \right] dS \tag{2.31}$$

is the Joule power (losses), and

$$W_{em} = \int_{S_\Gamma} \left[\frac{1}{2} C u^2 + \frac{1}{2} \left(\overline{\mathbf{L}} \cdot J_s \right) \cdot J_s \right] dS = W_e + W_m \tag{2.32}$$

is the electromagnetic energy stored in the circuit, with W_e the energy stored in the electric field and W_m the energy stored in the magnetic field.

For the time-harmonic conditions the power conservation for an isotropic material is expressed in the form

$$\sum_{k=1}^{n} U_k I_k^{*} = \int_{S_\Gamma} \left[(R\mathbf{J}_s) \cdot \mathbf{J}_s^{*} + G U^2 \right] dS + 2 j\omega \int_{S_\Gamma} \left[\frac{1}{2} (L\mathbf{J}_s) \cdot \mathbf{J}_s^{*} - \frac{1}{2} C U^2 \right] dS \tag{2.33}$$

or

$$S = P + jQ \tag{2.34}$$

where S is the apparent complex power, P is the active power, and $Q = 2\omega\left(\widetilde{W}_m - \widetilde{W}_e\right)$ is the reactive power, with $\widetilde{W}_m$ and $\widetilde{W}_e$ being the time average values of the magnetic and electric energies stored in the circuit.

2.5. Uniqueness Theorems

2.5.1. Uniqueness Theorems for the Instantaneous Equations

The uniqueness theorems are important for the correct formulation and solution of problems relative to the propagation equations. From the equation of power conservation (2.29), the following *theorem* can be proved:

The surface current density $\mathbf{J}_s$ *and the voltage* u *at any point on the surface* S_Γ *bounded by* Γ *of a planar circuit conductor are uniquely determined if the following uniqueness conditions are given:*

Ic) Initial conditions: $\mathbf{J}_s(x,y,0)$ *and* $u(x,y,0)$; $\forall\ x,y \in S_\Gamma$

Bc1) Boundary conditions: $J_{sn} = \mathbf{J}_s \cdot \mathbf{n}_{in}$ *or* $u(x,y,t)$; $\forall\ x,y \in \Gamma$.

If the planar circuit is a m-port the conditions Bc1 are replaced by

Bc2) Boundary conditions: $u_k(t)$ *or* $i_k(t)$; $k = 1,2,\ldots,m$.

Indeed for zero values of the quantities in the boundary conditions, the power conservation equation gives

$$P_J + \frac{dW_{em}}{dt} = 0 \ .$$

By integration in time we have

$$W_{em}(t) - W_{em}(0) = -\int_0^t P_J dt \leq 0$$

since P_J is positive definite. With zero initial conditions we have $W_{em}(0) = 0$ and, on the other hand, $W_{em}(t)$ is a positive function, $W_{em}(t) \geq 0$. Thus, we must have $P_J = 0$, $W_{em}(t) = 0$, and therefore $J_s(t) = 0$, $u(t) = 0$. If we consider now two different solutions which correspond to the same nonzero initial conditions (Ic) and boundary conditions (Bc), their difference corresponds to the zero Ic and Bc, and is thus identically zero. Therefore, the two solutions are identical.

2.5.2. Uniqueness Theorems for the Complex Equations

For time-harmonic fields, the initial conditions are no longer necessary and the uniqueness of the solutions is ensured by boundary conditions Bc1 or Bc2 . In phasor form these conditions are

$$\text{Bc1) } J_{sn} = \mathbf{J}_{sn} \cdot \mathbf{n}_{in} \text{ or } U(x,y)\,;\ \forall\ x,y \in S_\Gamma$$

or

$$\text{Bc2) } U_k \text{ or } I_k\,;\ k = 1,2,\ldots,m\ .$$

If $S = 0$, this implies either $U_k = 0$ or $I_k = 0$. Under these conditions

$$P = \int_{S_\Gamma} \left[(R\mathbf{J}_s) \cdot \mathbf{J}_s^* + GU^2 \right] dS = 0$$

and

$$Q = 2\omega \int_{S_\Gamma} \left[\frac{1}{2}(L\mathbf{J}_s) \cdot \mathbf{J}_s^* - \frac{1}{2} CU^2 \right] dS = 0\ .$$

<u>Case I (Lossy Structures)</u>

Either $R \neq 0$ or $G \neq 0$, or both are different from zero.

1) $R \neq 0$ and $G = 0$ implies $\mathbf{J}_s = 0$. If $\mathbf{J}_s = 0$ then

$$\widetilde{W}_m = \int_{S_\Gamma} \frac{1}{2}(L\mathbf{J}_s) \cdot \mathbf{J}_s^* dS = 0$$

and since $Q = 0$ we also have

$$\widetilde{W}_e = \int_{S_\Gamma} \frac{1}{2} C U^2 dS = 0 \Rightarrow U = 0 .$$

Proof:

Assume that $U_1, U_2, \ldots, U_m$ are known and that two distinct solutions U', $\mathbf{J}_s'$ and U'', $\mathbf{J}_s''$ exist. Obviously $U_1' = U_1'', \ldots, U_m' = U_m''$. Let $U_d = U' - U''$ and $\mathbf{J}_{sd} = \mathbf{J}_s' - \mathbf{J}_s''$ be the solution corresponding to the difference voltage U_d. Then $U_{dk} = 0$ and

$$\sum_{k=1}^{m} U_{dk} I_{dk}^{*} = S_d = P_d + jQ_d = 0 \Rightarrow U_d = 0 \text{ and } \mathbf{J}_{sd} = 0 .$$

This means $\mathbf{J}_s' \equiv \mathbf{J}_s''$ and $U' \equiv U''$, i.e. the solution is unique.

2) If $G \neq 0$ and $R = 0 \Rightarrow U = 0$ then $\widetilde{W}_e = 0 \Rightarrow \widetilde{W}_m = 0$ and $\mathbf{J}_s = 0$.

3) If $R \neq 0$ and $G \neq 0 \Rightarrow \mathbf{J}_s = 0$ and $U = 0$.

Case II (Lossless structures)

If $R = 0$, $G = 0$, then $P = 0$.

With $S = 0$ we have $Q = 0$, which implies $\widetilde{W}_m = \widetilde{W}_e$ and two cases are possible.

1) $\widetilde{W}_m = 0$ and $\widetilde{W}_e = 0$ only when the initial conditions are zero.

2) $\widetilde{W}_m = \widetilde{W}_e \neq 0$ only when the initial conditions are different from zero. Therefore the equation $\widetilde{W}_m - \widetilde{W}_e = 0$ has a number, finite or infinite, of discrete solutions which are the resonant frequencies of the planar circuit structure.

This is why the resonant frequencies of the planar lossless circuit structure may be calculated by looking for the solutions of the two-dimensional telegraphists' equations, assuming zero boundary conditions.

2.6. Network Equations for Microwave Planar Circuits

The network equations express the link between the two categories of boundary conditions for the microwave planar circuits. For multiport circuits under time-harmonic conditions, the uniqueness theorem states that the two-dimensional telegraphists' equations have unique solutions for lossy circuits if either the voltages at the terminals or the currents are known. Thus, the voltages determine an unique solution for the currents and viceversa. If the circuits are linear the link between the two sets of quantities is expressed through linear and homogeneous relations,

$$U_k = \sum_{j=1}^{m} Z_{kj} I_j \ , \quad k = 1,2,\ldots,m$$

or

$$I_j = \sum_{k=1}^{m} Y_{jk} I_k \ , \ j = 1,2,\ldots,m \ .$$

In matrix notation, the above relations are

$$[U] = [Z]\ [I]$$

or

$$[I] = [Y]\ [U]$$

where $[Y] = [Z]^{-1}$ and $[Z]$ are nonsingular if the boundary conditions are imposed correctly.

For lossless circuits when there is no unique solution the corresponding matrices are singular. Now the equations

$$\det[Z] = 0 \text{ or } \det[Y] = 0$$

generate the associated eigenvalues.

The network equations allow the treatment of the planar circuits as ordinary circuits in the schemes used in various microwave techniques.

CHAPTER 3. METHODS FOR CALCULATING THE QUASISTATIC PARAMETERS OF MICROSTRIP LINES

3.1. Potential Analysis

In this chapter the quasistatic parameters used in the two-dimensional equations analyzed in Chapter 2 are evaluated by employing four new methods. These parameters are the characteristic impedance $Z_c(0)$ and the effective dielectric constant $\varepsilon_{eff}(0)$, at zero frequency. They are calculated from the capacitances per unit length C' of the original circuit and C'_0 of the same circuit, but without a dielectric substrate. Considering the inhomogeneity of the structure presented in Figure 3-1 (a), C' has been determined by employing numerical methods such as finite-differences method (Green, 1965; Salazar-Parma *et al.*, 1998), variational methods (Bryant and Weiss, 1968), integral equation methods (Silvester, 1968) and the method of lines (Schulz and Pregla, 1980).

The effective dielectric constant at zero frequency is defined as $\varepsilon_{eff}(0) = C'/C'_0$. The inductance per unit length in the absence of the substrate is determined by using the permittivity ε_0 and the permeability μ_0 of free space, as $L'_0 = \varepsilon_0 \mu_0 / C'_0$. Assuming the substrate to be non-magnetic and the strip line and ground base to be perfect conductors, the characteristic impedance at zero frequency is obtained as

$$Z_c(0) = \sqrt{\frac{L'_0}{C'}} = \frac{\sqrt{\varepsilon_0 \mu_0}}{C'_0} \frac{1}{\sqrt{\varepsilon_{eff}(0)}} = \frac{\eta_0}{2W_0} \frac{\varepsilon_0}{\sqrt{\varepsilon_{eff}(0)}} \tag{3.1}$$

where W_0 is the electrostatic energy per unit length of the structure without substrate, for a unit voltage between the strip and the ground, and $\eta_0 \cong 120\pi$ is the free space impedance. These relations are used to characterize the quasi-*TEM* mode at frequencies lower than 1 GHz.

For the structure in Figure 3-1 (a), we need to find solutions for the electrostatic field in two cases: the microstrip without substrate ($\varepsilon_r = 1$ everywhere) and the microstrip with substrate ($\varepsilon_r = 1$ in air and $\varepsilon_r \neq 1$ in substrate). The first problem has an analytical solution and can be solved using conformal mapping (Collin, 1992) while the second one does not have such

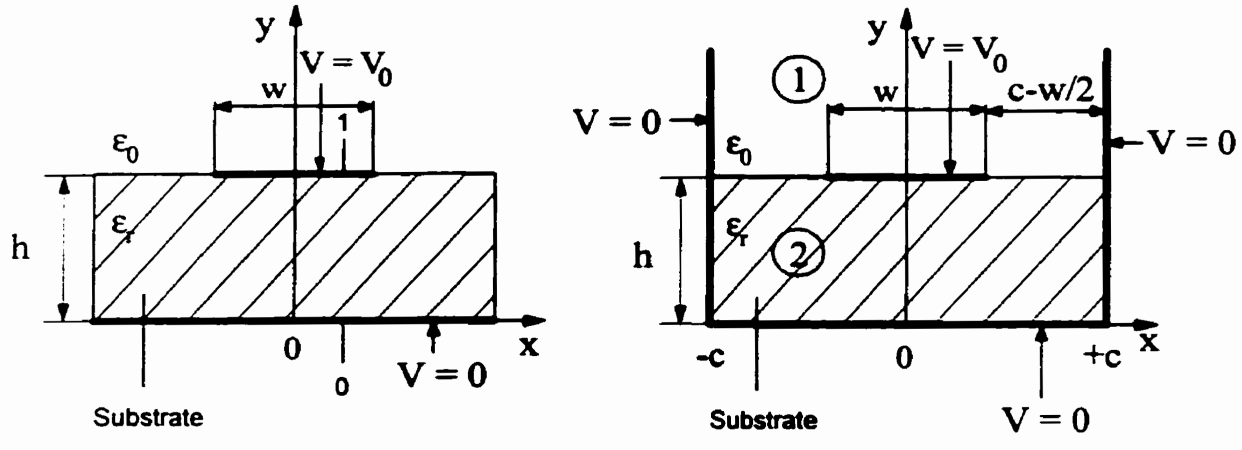

Fig. 3-1. (a) Microstrip geometry; (b) shielded microstrip.

a solution and can be solved using numerical methods. The following assumptions are made:

a) The mode of propagation is *TEM* (the electric and magnetic field intensity vectors are situated in a plane perpendicular to the direction of propagation);

b) The ground base and the strip line are perfect conductors ($\sigma \to \infty$) and the strip has zero thickness;

c) The dielectric is perfect, homogeneous, isotropic and non-magnetic ($\varepsilon_r =$ constant, $\sigma = 0$, $\mu = \mu_0$).

We observe that the extension of the ground base and of the dielectric in the x direction is never infinite. Therefore we may choose the model in Figure 3-1 (b), where $c >> w$, such that the introduction of the lateral walls practically does not affect the result.

For the calculation of C', we solve the electrostatic field problem in the region defined by $y > 0$ and bounded by the two electric walls. The potentials V_1 and V_2 in the two subregions (1) and (2) satisfy the two-dimensional Laplace equation

$$\frac{\partial^2 V_1}{\partial x^2}+\frac{\partial^2 V_1}{\partial y^2}=0 \qquad \text{for } x\in[-c,c],\ y\in(h,\infty)$$

$$\frac{\partial^2 V_2}{\partial x^2}+\frac{\partial^2 V_2}{\partial y^2}=0 \qquad \text{for } x\in[-c,c],\ y\in[0,h), \tag{3.2}$$

under the following boundary conditions

$$V_1(x,\infty)\to 0,\ V_1(\pm c,y)=0$$

$$V_2(x,0)\to 0,\ V_2(\pm c,y)=0$$

$$V_1(x,h)=V_2(x,h)=V_0 \qquad \text{for } x\in[-w/2,w/2] \tag{3.3}$$

and the continuity equations

$$V_1(x,h)=V_2(x,h) \qquad \text{for } y=h,\ x\in(-c,-w/2)\cup(w/2,c)$$

$$\varepsilon_0\frac{\partial V_1}{\partial y}=\varepsilon\frac{\partial V_2}{\partial y} \qquad \text{for } y=h,\ x\in(-c,-w/2)\cup(w/2,c). \tag{3.4}$$

The solutions in the two subregions are obtained by applying the method of separation of variables, in the form

$$V_1(x,y)=\sum_{k=1}^{\infty}A_k e^{-\lambda_k(y-h)}\cos\lambda_k x \qquad ,\ y>h$$

$$V_2(x,y)=\sum_{k=1}^{\infty}B_k\frac{\sinh\lambda_k y}{\sinh\lambda_k h}\cos\lambda_k x \qquad ,\ y\in(0,h] \tag{3.5}$$

where $\lambda_k=(2k-1)\pi/2c$, which satisfy the first two conditions in (3.3). From the first condition in (3.4) we obtain $A_k\equiv B_k$ with A_k yet to be determined from the second condition in (3.4). The complete solutions can be obtained if the potential distribution at $y=h$ is known. On the strip the potential $V=V_0$ is given while that on the dielectric is unknown. Thus, the problem must be solved numerically.

3.2. Proposed Solution Methods

3.2.1. Point Matching Hybrid Method

The boundary between the two subregions, at $y = h$, is divided in $2(M + N)$ equal intervals, where $2N$ points are on the strip and $2M$ are on the dielectric. One interval will have the length $\Delta x_i = c/(M + N)$. Due to the symmetry, $V(x, y) = V(-x, y)$, only $M + N + 1$ points are used. Therefore the problem is solved only for $x \geq 0$. On the strip we impose the Dirichlet condition $V = V_0$, which gives

$$V_1(x_i, y) = V_2(x_i, y) = \sum_{k=1}^{N+M+1} A_k \cos \lambda_k x_i = V_0 \tag{3.6}$$

where $i = 0,1,\ldots, N$ and $x_i = i\Delta x$. The last point on the strip is $x_N = N\Delta x = w/2$. For the next M points we impose the second condition from (3.4). Thus,

$$\varepsilon \sum_{k=1}^{N+M+1} A_k \lambda_k \coth \lambda_k h \cos \lambda_k x_i = -\varepsilon_0 \sum_{k=1}^{N+M+1} A_k \lambda_k \cos \lambda_k x_i \,, \quad i = N+1, \ldots, N+M \tag{3.7}$$

and $x_{M+N} = (M + N)\Delta x = c$. The following system of $(N + M + 1)$ equations with $(N + M + 1)$ unknowns is obtained

$$\begin{aligned} &\sum_{k=1}^{N+M+1} A_k \cos \lambda_k x_i = V_0 \,, \quad i = 0,1,\ldots, N \quad (x_0 = 0) \\ &\sum_{k=1}^{N+M+1} A_k \lambda_k (\varepsilon_r \coth \lambda_k h + 1) \cos \lambda_k x_i = 0 \,, \quad i = N+1, \ldots, N+M \,. \end{aligned} \tag{3.8}$$

By solving the system of equations (3.8) we obtain the coefficients $A_1, \ldots, A_{N+M+1}$ which give the approximate solution in the form of truncated series. The electrostatic energy per unit length is calculated from

$$W = \frac{\varepsilon}{2}\int_{D_x}(\nabla V)^2 dv = \frac{\varepsilon_0}{2}\oint_{\Sigma_1} V_1 \frac{\partial V_1}{\partial n_{ext}} dS + \frac{\varepsilon}{2}\oint_{\Sigma_2} V_2 \frac{\partial V_2}{\partial n_{ext}} dS$$

$$= \varepsilon_0 \int_0^c - V_1 \frac{\partial V_1}{\partial y} dx + \varepsilon \int_0^c V_2 \frac{\partial V_2}{\partial y} dx \qquad \text{[J/m]}$$

where Σ_1 and Σ_2 are the boundaries of the two subregions (1) and (2), respectively and n_{ext} is the outward normal. Therefore,

$$W \cong \frac{1}{2} \sum_{k=1}^{N+M+1} A_k^2 \lambda_k (\varepsilon_r \coth \lambda_k h + 1)\varepsilon_0 c$$

$$W_0 \cong \frac{1}{2} \sum_{k=1}^{N+M+1} A_{k_0}^2 \lambda_k (\coth \lambda_k h + 1)\varepsilon_0 c$$

where W_0 is the energy of the structure without substrate and A_{k_0} are the solutions of Equations (3.8) with $\varepsilon_r = 1$. The capacitances per unit length are

$$C_0' = \frac{2W_0}{V_0^2} \quad ; \quad C' = \frac{2W}{V_0^2}$$

If $V_0 = 1$, then $C_0' = 2W_0$ and $C' = 2W$.

3.2.2. Improved Flux Matching Hybrid Method

In a second method we use the same procedure as in the first one, but instead of employing the condition of continuous normal component of the electric flux density vector across the boundary between the two subregions at every point x_i, we impose the continuity of the electric flux along each small interval Δx_i on the dielectric boundary outside the strip. Thus, only the second equation (3.7) is modified to

$$\varepsilon \sum_{k=1}^{N+M+1} A_k \lambda_k \coth \lambda_k h \int_{x_i}^{x_{i+1}} \cos \lambda_k x dx = -\varepsilon_0 \sum_{k=1}^{N+M+1} A_k \lambda_k \int_{x_i}^{x_{i+1}} \cos \lambda_k x dx \tag{3.9}$$

and hence

$$\sum_{k=1}^{N+M+1} A_k (\varepsilon_r \coth \lambda_k h + 1)(\sin \lambda_k x_{i+1} - \sin \lambda_k x_i) = 0 , \quad i = N+1, \ldots, N+M . \tag{3.10}$$

Finally, we obtain a system of $(N + M + 1)$ equations with $(N + M + 1)$ unknowns in the form

$$\begin{gathered} \sum_{k=1}^{N+M+1} A_k \cos \lambda_k x_i = V_0 , \quad i = 0,1,\ldots,N \\ \sum_{k=1}^{N+M+1} A_k (\varepsilon_r \coth \lambda_k h + 1) \sin \lambda_k \frac{x_{i+1} - x_i}{2} \cos \lambda_k \frac{x_{i+1} - x_i}{2} = 0 \ , \ i = N+1, \ldots, N+M . \end{gathered} \tag{3.11}$$

The electrostatic energies and the capacitances per unit length are obtained as in the first method.

3.2.3. Variational Method for Potentials

A third proposed technique is based on the fact that the solution of the Laplace equation in a domain corresponds to the minimum electrostatic energy in that domain. This is true even if the domain is piecewise homogeneous, as in the case of microstrip. We use the same discretization employed in the first two methods, but this time instead of solving for the coefficients A_k we choose the potentials at the points x_i on the interface as unknowns,

$$\begin{aligned} & V(x_i) = V_0 , \quad i = 0,1,\ldots,N \\ & V(x_j) = V_j , \quad j = N+1, \ldots, N+M-1 \\ & V_{N+M} = V(c) = 0 . \end{aligned} \tag{3.12}$$

On the dielectric interface, at $y = h$, the potential is linearly interpolated on each interval Δx_j,

$$V(x) = \alpha_j x + \beta_j \quad \text{for} \quad x \in (x_j, x_{j+1}),\ y = h. \tag{3.13}$$

Since at $y = h$

$$V(x) = \sum_{k=1}^{\infty} A_k \cos \lambda_k x \tag{3.14}$$

the Fourier coefficients are given by

$$A_k = \frac{2}{c} \int_0^c V(x) \cos \lambda_k x dx = \frac{2}{c} \left[V_0 \int_0^w \cos \lambda_k x dx + \sum_{j=N}^{N+M-1} \int_{x_j}^{x_{j+1}} (\alpha_j x + \beta_j) \cos \lambda_k x dx \right] \tag{3.15}$$

where

$$\begin{aligned} &\alpha_j x_j + \beta_j = V_j \\ &\alpha_j x_{j+1} + \beta_j = V_{j+1}. \end{aligned} \tag{3.16}$$

Performing the integrals in (3.15) and rearranging the terms after $_j$

$$A_k = \sum_{j=N}^{N+M} B_{kj} V_j \tag{3.17}$$

where the coefficients B_{kj} are known. The electric energy per unit length is determined as in Section 3.2.1, from

$$W = \frac{\varepsilon}{2} \int_{D_\Sigma} (\nabla V)^2 dv = \frac{\varepsilon_0}{2} \oint_{\Sigma_1} V_1 \frac{\partial V_1}{\partial n_{ext}} dS + \frac{\varepsilon}{2} \oint_{\Sigma_2} V_2 \frac{\partial V_2}{\partial n_{ext}} dS, \tag{3.18}$$

with the energy stored outside and inside the dielectric given, respectively, by

$$W_1 = \frac{c}{2}\varepsilon_0 \sum_{k=1}^{N+M+1} \lambda_k A_k^2 \tag{3.19}$$

and

$$W_2 = \frac{c}{2}\varepsilon \sum_{k=1}^{N+M+1} \lambda_k A_k^2 \coth \lambda_k h \,. \tag{3.20}$$

With (3.17), the total energy per unit longitudinal length is

$$W = W_1 + W_2 = \frac{c}{2} \sum_{k=1}^{N+M+1} \lambda_k (\varepsilon_0 + \varepsilon \coth \lambda_k h)\left(\sum_{j=N}^{N+M} B_{kj} V_j \right)^2 . \tag{3.21}$$

Minimizing *W* with respect to the unknown potentials *V* we obtain

$$\frac{\partial W}{\partial V_l} = c \sum_{k=1}^{N+M+1} \lambda_k (\varepsilon_0 + \varepsilon \coth \lambda_k h)\left(\sum_{j=N}^{N+M} B_{kj} V_j \right) B_{kl} = 0 \,, \; l = N+1, \ldots, N+M-1 \,. \tag{3.22}$$

The following system of nonhomogeneous equations with M-1 equations in M-1 unknowns, $V_{N+1}, \ldots, V_{N+M-1}$, is obtained

$$a_{l0} V_0 + \sum_{j=N+1}^{N+M-1} a_{lj} V_j = 0 \tag{3.23}$$

where

$$a_{lj} \equiv \sum_{k=1}^{N+M+1} \lambda_k (1 + \varepsilon_r \coth \lambda_k h) B_{kj} B_{kl} \,. \tag{3.24}$$

Once this system is solved, the coefficients A_k are calculated from (3.17) and the energy W from (3.19)-(3.21). The capacitance per unit length is finally obtained,

$$C' = \frac{2W}{V_0^2} \; . \tag{3.25}$$

Similarly, for the microstrip without substrate ($\varepsilon = \varepsilon_0$),

$$C_0' = \frac{2W_0}{V_0^2} \; . \tag{3.26}$$

Then, the effective dielectric constant $\varepsilon_{eff}(0)$ at zero frequency is obtained as

$$\varepsilon_{eff}(0) = \frac{C'}{C_0'} = \frac{W}{W_0} . \tag{3.27}$$

The computer program has to be run twice in order to obtain $\varepsilon_{eff}(0)$ and the characteristic impedance of the microstrip line. With the coefficients A_k determined, the analytical expressions in (3.5) allow the calculation of the electric potential and field intensity at any point in the region considered.

3.2.4. Theorem for Upper Bound of Capacitance

Consider the capacitor in Figure 3-2.

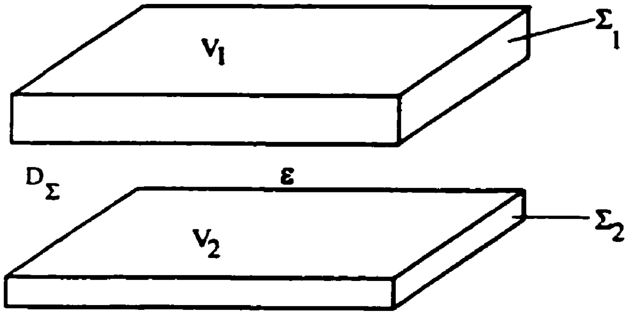

Fig. 3-2. The armatures of a capacitor.

If the dielectric is nonhomogeneous, the equation satisfied by the electric potential is

$$\nabla \cdot (\varepsilon \nabla V) = 0 \tag{3.28}$$

with the boundary conditions $V = V_1$ and $V = V_2$ on the conductor surfaces Σ_1 and Σ_2, respectively. The capacitance can be expressed as

$$C = \frac{q}{V_1 - V_2} = \frac{2W}{(V_1 - V_2)^2}\,. \tag{3.29}$$

Let U be a function which does not satisfy the Equation (3.28) ($\nabla \cdot (\varepsilon \nabla U) \neq 0$), but satisfies the boundary conditions $U = V_1$ on Σ_1 and $U = V_2$ on Σ_2, and let $u = V - U$. On Σ_1 and Σ_2, $u = 0$. The energy W^s which would correspond to U is calculated as

$$W^s = \frac{1}{2}\int_{D_\Sigma} \varepsilon (\nabla U)^2 dv = \frac{1}{2}\int_{D_\Sigma} \varepsilon [\nabla (V - u)]^2 dv =$$

$$=\frac{1}{2}\int_{D_\Sigma}\varepsilon(\nabla V)^2dv+\frac{1}{2}\int_{D_\Sigma}\varepsilon(\nabla u)^2dv-\int_{D_\Sigma}\varepsilon\nabla V\cdot\nabla u dv. \tag{3.30}$$

But

$$-\int_{D_\Sigma}\varepsilon\nabla V\cdot\nabla u dv=-\int_{D_\Sigma}\nabla\cdot(u\varepsilon\nabla V)dv=-\oint_{\Sigma_1+\Sigma_2}u\varepsilon(\nabla V)\cdot\mathbf{n}dS=0 \tag{3.31}$$

since $\nabla\cdot(\varepsilon\nabla V)=0$ (the exact solution) and $u=0$ on Σ_1 and Σ_2. Thus,

$$W^s=W+\frac{1}{2}\int_{D_\Sigma}\varepsilon(\nabla u)^2dv>W. \tag{3.32}$$

Hence

$$C^s=\frac{2W^s}{(V_1-V_2)^2}>\frac{2W}{(V_1-V_2)^2}=C \tag{3.33}$$

with C^s being an upper bound of the exact value C of the capacitance.

The method presented in Section 3.2.3 builds a function U from two functions V_1 and V_2, defined in two subregions, which satisfy the Laplace equation everywhere except on the dielectric boundary. By minimizing W^s we approach the exact value W.

3.2.5. Variational Method for Electric Charges

A fourth method is being proposed to enable us to control the error introduced in the variational approach in Section 3.2.3. Consider again the general solution in (3.5) and a discretization of the dielectric boundary in $2(M+N)$ intervals. The free electric charge density $\rho_s(x)$ is different from zero on the strip line and zero on the dielectric boundary. The values of $\rho_s(x)$ at the discretization points on the strip are unknown. From the condition

$$D_{2n} - D_{1n} = \rho_s(x) \tag{3.34}$$

where D_{1n} and D_{2n} are the electric flux densities in the two regions (see Figure 3-1 (b)), the charge density is obtained in the form

$$\rho_s(x) = \sum_{k=1}^{\infty} \lambda_k A_k \left(\varepsilon \coth \lambda_k h + \varepsilon_0\right) \cos \lambda_k x \, . \tag{3.35}$$

Using the Fourier series expansion

$$\rho_s(x) = \sum_{k=1}^{\infty} R_k \cos \lambda_k x \tag{3.36}$$

the coefficients R_k are expressed as

$$R_k = \frac{2}{c} \sum_{i=0}^{N} \left(\int_{x_i}^{x_{i+1}} \rho_s(x) \cos \lambda_k x dx \right) \tag{3.37}$$

with

$$A_k = \frac{R_k}{\lambda_k \varepsilon_0 \left(\varepsilon_r \coth \lambda_x x + 1\right)} \, . \tag{3.38}$$

Using again a linear interpolation for $\rho_s(x)$, Equation (3.37) can be written in the form

$$R_k = \sum_{i=0}^{N} \beta_{ki} \rho_{si} \tag{3.39}$$

where ρ_{si} are the unknown values of $\rho_s(x)$ at the discretization points and the coefficients β_{ki} are known. The expression of the electric energy is minimized with respect to ρ_{si},

$$\frac{\partial W}{\partial \rho_{si}} = 0, \quad i = 0, 1, \ldots, N, \tag{3.40}$$

which yields a system with $N+1$ equations in $N+1$ unknowns. Since the total charge per unit length of strip is given,

$$\int_{-w/2}^{w/2} \rho_s(x) dx = q_0 , \tag{3.41}$$

the system (3.40) is in fact reduced to a system of N equations in N unknowns, giving ρ_{si} and then R_k and A_k, and finally the energy. The capacitances are calculated as shown in the previous Sections.

3.2.6. Theorem for Lower Bound of Capacitance

Consider in Figure 3-2 the electric charge $+q$ on the armature Σ_1 and $-q$ on Σ_2. The capacitance is expressed now as

$$C = \frac{q}{V_1 - V_2} = \frac{q^2}{2W} . \tag{3.42}$$

Let U be a function that satisfies the equation $\nabla \cdot (\varepsilon \nabla U) = 0$ but does not satisfy the boundary conditions, $U \neq V$ on Σ_1 and on Σ_2. Assume that U gives the same charge on the two armatures

$$q = \oint_{\Sigma_1} \varepsilon \frac{\partial U}{\partial n_{ext}} dS = -\oint_{\Sigma_2} \varepsilon \frac{\partial U}{\partial n_{ext}} dS \tag{3.43}$$

and let $U = V - u$. The associated energy is

$$W' = \frac{1}{2}\int_{D_\Sigma} \varepsilon(\nabla U)^2 dv = \frac{1}{2}\int_{D_\Sigma} \varepsilon(\nabla V)^2 dv + \frac{1}{2}\int_{D_\Sigma} \varepsilon(\nabla u)^2 dv - \oint_{\Sigma_1+\Sigma_2} V(\varepsilon\nabla u)\cdot \mathbf{n}dS \tag{3.44}$$

since $\nabla\cdot(\varepsilon\nabla u) = 0$. The last integral in (3.44) can be developed as

$$-\oint_{\Sigma_1+\Sigma_2} V(\varepsilon\nabla u)dS = -(V_1 q_{u1} - V_2 q_{u2}) = 0, \tag{3.45}$$

the charges corresponding to u being zero (U and V give the same charge on Σ_1 and Σ_2). Thus

$$W' = W + \frac{1}{2}\int_{D_\Sigma} \varepsilon(\nabla u)^2 dv > W\ . \tag{3.46}$$

Hence

$$C' = \frac{q^2}{2W'} < \frac{q^2}{2W} = C \tag{3.47}$$

with C' being a lower bound of the exact value C of the capacitance. The last two proposed methods provide the bounds C^s and C'.

3.3. Numerical Results and Conclusions

The performance of the method in 3.2.2 was compared with that of the method of lines (Hoffmann, 1987; Schulz and Pregla, 1980) for w/h=0.02, 0.03, 0.04, 0.05, 0.1, 0.15, 0.2, 0.3, 0.4, 0.6, 0.8, 1.0, 1.2, 1.4, 1.6, 1.8, 2.0, 2.5, 3.0, 3.5, 4.0, 5.0, and 10.0, and for relative permittivities ε_r=2.1, 2.3, 2.5, 3.78, 9.6, 10.0, 11.9, 12.9, and 16. For microstrip lines without substrate ($\varepsilon_r = 1$), the method of lines has an accuracy of 0.12% on average with a maximum error of 0.2% for $Z_c(0)$, with respect to the exact values determined by the method of conformal mapping. The integral equations method using Green's function (Silvester, 1968) generates results which differ from those obtained by the method of lines by 0.3% on average for $\varepsilon_{eff}(0)$, with a maximum of 0.4%, and by 0.8% on average for $Z_c(0)$, with a maximum of 2%.

For the calculation of $\varepsilon_{eff}(0)$ we set $c - w/2 = 10w$ in the case of $w/h > 1$ and $c - w/2 = 10h$ in the case of $w/h \leq 1$. Taking the number of discretization points $M + N = 300$, the proposed method gives results for $\varepsilon_{eff}(0)$ with an average of 0.26% difference from the results obtained by the method of lines (Hoffmann, 1987), with a maximum difference of 0.4%. In this case the computer time, employing a HP 300 *MHz* Personal Computer, is 15 seconds. If the number of points is increased to 500, the differences are on average 0.14% (maximum 0.3%). The computer time increases to 50 seconds. In Table 3-1, the convergence of the results versus the total number of points *M*+*N* is presented. In Tables 3-2 and 3-3 results are presented for all four developed methods (in Sections 3.2.1, 3.2.2, 3.2.3, and 3.2.5), the number of discretization points being 300. Knowing that the method proposed in 3.2.3 provides an upper bound of capacitance and the method proposed in 3.2.5 provides a lower bound, the maximum error can be defined as

$$\text{Error}(\%) = \frac{\lfloor \varepsilon_{eff}(0) \rfloor_{\max} - \lfloor \varepsilon_{eff}(0) \rfloor_{\min}}{\lfloor \varepsilon_{eff}(0) \rfloor_{\max}} \times 100$$

where $\varepsilon_{eff}(0)_{\max}$ and $\varepsilon_{eff}(0)_{\min}$ are the values obtained by applying the methods in Sections 3.2.3 and 3.2.5, respectively.

M+*N*	$\varepsilon_{eff}(0)$
20	1.774
30	1.759
40	1.750
150	1.749
200	1.747
300	1.745

Table 3-1. Convergence of the method in 3.2.2 for ε_r =2.3 and w/h = 0.15.

w/h	Polyolefin substrate $\varepsilon_r = 2.3$					
	(1)	(2)	(3)	(4)	(5)	(6)
0.03	1.715	1.716	1.719	1.719	1.718	0%
0.15	1.745	1.747	1.745	1.746	1.748	0.05%
1.0	1.834	1.834	1.833	1.834	1.838	0.05%
2.0	1.903	1.904	1.904	1.904	1.904	0%
3.0	1.952	1.952	1.953	1.953	1.953	0%
10.0	2.100	2.101	2.101	2.101	2.098	0%

w/h	Alumina ceramic substrate $\varepsilon_r = 9.6$					
	(1)	(2)	(3)	(4)	(5)	(6)
0.03	5.674	5.688	5.705	5.706	5.692	0.01%
0.15	5.869	5.878	5.869	5.871	5.873	0.03%
1.0	6.429	6.428	6.428	6.430	6.448	0.03%
2.0	6.885	6.890	6.887	6.888	6.890	0.01%
3.0	7.213	7.217	7.218	7.218	7.213	0%
10.0	8.221	8.224	8.233	8.234	8.214	0.01%

Table 3-2. Results obtained for the effective dielectric constant: (1) method in 3.2.1; (2) method in 3.2.2; (3) method in 3.2.3; (4) method in 3.2.5; (5) results in [24]; (6) maximum error.

w/h	Polyolefin substrate $\varepsilon_r = 2.3$					
	(1)	(2)	(3)	(4)	(5)	(6)
0.03	253.47	253.86	254.16	254.18	255.51	0.0%
0.15	177.73	178.86	179.98	180.03	180.46	0.0%
1.0	92.75	92.77	92.94	92.95	93.30	0.0%
2.0	64.34	64.41	64.53	64.55	64.52	0.0%
3.0	49.90	49.97	50.00	50.02	49.96	0.0%
10.0	19.87	19.92	19.96	19.98	20.02	0.01%

w/h	Alumina ceramic substrate $\varepsilon_r = 9.6$					
	(1)	(2)	(3)	(4)	(5)	(6)
0.03	139.80	139.94	140.29	140.33	140.27	0.0%
0.15	98.19	98.30	98.33	98.35	98.38	0.0%
1.0	49.96	50.01	50.07	50.11	49.76	0.0%
2.0	34.17	34.15	34.30	34.33	33.90	0.0%
3.0	25.74	25.72	25.80	25.88	25.98	0.003%
10.0	9.93	9.96	10.06	10.11	10.12	0.004%

Table 3-3. Results obtained for the characteristic impedance (Ω): (1) method in 3.2.1; (2) method in 3.2.2; (3) method in 3.2.3; (4) method in 3.2.5; (5) results in [24]; (6) maximum error.

The following general conclusions can be drawn.

- The theorems on upper and lower bounds of the capacitance proved in Sections 3.2.4 and 3.2.6 are general theorems that are not restricted to microstrip lines only. Collin (1992), for example, uses similar theorems for the calculation of the upper and lower bounds of impedance, employing Green's functions, for a stripline with a rectangular inner conductor.

- These proposed methods allow the calculation of the upper and lower bounds of impedance, and of the effective dielectric constant, at zero frequency.

- The hybrid analytical-numerical methods presented in this Chapter can also be used for various other structures such as:
    - Microstrip lines with a top shield;
    - Shielded mirostrip lines;
    - Coupled microstrip lines;
    - Slot lines;
    - Coplanar lines.

CHAPTER 4. MICROSTRIP DISPERSION ANALYSIS

4.1. Introduction

Wide spread use of microstrips has made the accurate computation of microstrip parameters increasingly important. Numerous researchers have implemented both approximate and rigorous numerical techniques to calculate microstrip line characteristic impedances and phase velocities. When confronted with using either a rigorous numerical technique or an approximate solution, the microwave circuit designer must choose between more rigorous, but time consuming computer algorithms, and relatively simple closed form expressions with limited ranges of validity and degrees of uncertainty. In all cases, reliable experimental data is required to verify the numerical approach or to determine the limitations of an approximate expression. Extractions of experimental data, however, is expensive and time consuming; this explains the fact that only limited experimental results are available in the literature for comparison of performance of various microstrip dispersion models (York and Compton, 1990; Forzley and Bridges, 1992).

Comparisons among different dispersion models were published by Verma and Kumar (1998), Atwater (1988), Edwards and Owens (1976), Kuester and Chang (1979), and York and Compton (1990).

Verma and Kumar (1998) compared results based on the available dispersion models with those from a numerical solution and not with experimental data. This is why comparisons with the empirical formula proposed by Verma and Kumar (1998) will not be performed in this thesis.

Atwater (1988) compared the performance of various models using published experimental data "taken from each curve by measurements on an enlarged photocopy". The author concludes that the model published by Kirschning and Jansen (1982) is the most accurate (rms error 2.3% for the data employed).

Edwards and Owens (1976) published an extensive set of experimental data covering the frequency range of 2-18 *GHz*. The measurements were performed on a single type of substrate (sapphire) using ring resonator techniques and the frequency error was estimated at less than 2 *MHz*. They concluded that the model proposed by Getsinger (1973) is sufficiently accurate for practical purposes.

York and Compton (1990) published results for microstrip dispersion over the range of 1-18 *GHz*, measured using the method of gap-coupled resonator pairs. The estimated errors were ± 1 *MHz* in frequency, ± 0.05 ***mm*** for length, corresponding to about 0.8% in the measured permittivity. These authors concluded that the model proposed by Kobayashi (1988) is the most accurate, yielding rms errors of 0.73% when compared to experimental data, which is significantly lower than 2.5% as reported by Atwater (1988). This difference is mainly due to the way the experimental data were extracted from a graph as opposed to having first-hand measured experimental results. From the available literature, we remark that:

- none of the published empirical equations allow the analysis of the higher-order modes and their dispersion;
- there is no empirical formula that can evaluate the microstrip losses.

In order to evaluate the accuracy of the results obtained on the basis of the model proposed in this thesis, in comparison with that of the results from existing models, a full-wave analysis has been performed for all the cases considered. Among the most recent software packages, the Sonnet (1999), for example, uses a method of moments solution to calculate the dispersion on a microstrip line. The line has to be enclosed in a box made of perfect conductor walls. Obviously, the dispersion characteristics computed by applying such a full-wave analysis depend on:

- the dimensions of the box containing the strip line, and;
- the number of cells used in the discretization of the region considered.

When using this type of analysis, one should truncate the field region and choose the number of cells in such a way that the results obtained have a controllable accuracy. Since a benchmark solution does not exist, in this work we proceed as follows:

- first, using a reliable method to calculate the static parameters of the microstrip line, especially the effective dielectric constant at zero frequency $\varepsilon_{eff}(0)$, such as the two variational methods proposed in Chapter 3 which allow an evaluation of the errors in the results. This will give an indication, after the first calculations, as to whether the results obtained by applying a proposed model are in the expected range given by the proposed variational methods. Thus, a considerable amount of time can be saved;
- second, relying on accurate first-hand experimental data. This will give an indication of the accuracy of the computed results over the range of frequencies considered.

Typical experimental techniques for dispersion measurements utilize resonant structures such as:

- open- and short- circuited transmission line (Hoffmann, 1987);
- gap coupled ring resonators (York and Compton, 1990).

The methods in the first group suffer from frequency dependent effects at the open- or short-circuits terminations of the transmission line. While the ring resonator eliminates this problem, a large diameter ring may be necessary to reduce mutual coupling and radiation effects. On the other hand, resonant techniques only determine the dispersion characteristics at a set of discrete frequencies.

In contrast to resonant techniques, a sliding load method has been used at the University of Manitoba to measure directly the wavelength on the microstrip line (Forzley and Bridges, 1992). This is accomplished by sliding some type of load, such as a surface absorber, along the transmission line and measuring the variation of the input reflection coefficient, which is $\lambda/2$ periodic. The dispersion is determined through direct measurement of the voltage standing wave ratio (VSWR) on an unmatched microstrip transmission line. In this technique, the VSWR is determined by scanning a near field probe along the transmission line. The wavelength and thus $\varepsilon_{eff}(f)$ is then obtained by measuring the distance between successive voltage minima for which a 180° phase shift occurs. This method is non-invasive and transmission line termination effects do not affect the calculated $\varepsilon_{eff}(f)$. The effective relative permittivity is given by

$$\varepsilon_{eff}(f) = \left(\frac{c_0}{f\lambda_{ave}} \right)^2 \tag{4.1}$$

where c_0 is the speed of light in free space, f is the frequency, and λ_{ave} is an average of the measured values. The substrate utilized for the measurements was RT/duroid 6010 Ceramic Polytetrafluorethylene (PTFE) composite (Rogers Corporation, 2000). The relative permittivity of this material is 10.2 ± 0.25 and the dielectric thickness considered was 1.905 ± 0.1016 *mm*. The experimental data provided by Forzley and Bridges (1992) were obtained using three measurement methods: ring resonator, sliding load, and direct VSWR. For each method the error was evaluated by considering *n* test frequencies,

$$R_E^2 = \sum_{i=1}^{n}\left[\frac{\left(\varepsilon_{eff}(f)_{calc_i} - \varepsilon_{eff}(f)_{meas_i}\right)}{\varepsilon_{eff}(f)_{meas_i}}\right]^2 \tag{4.2}$$

where $\varepsilon_{eff}(f)_{calc_i}$ was obtained by using Kobayashi's formula (Kobayashi, 1988) and $\varepsilon_{eff}(f)_{meas_i}$ is the measured value, with the rms error being calculated as

$$E_{rms} = \sqrt{\frac{R_E^2}{n}} \tag{4.3}$$

The results are shown in Table 4-1.

$Z_0(\Omega)$	Measurement technique	n	E_{rms} (%)
29.0	VSWR measurement	24	2.07
	Sliding load (magnitude)	21	2.03
	Sliding load (phase)	11	1.92
48.3	VSWR measurement	25	2.30
	Sliding load (magnitude)	25	2.18
	Sliding load (phase)	16	1.41
	Ring resonator	23	0.85
61.4	VSWR measurement	27	2.64
	Sliding load (magnitude)	30	3.66
	Sliding load (phase)	25	2.02

Table 4-1. Published results in [14] showing the rms error for various experimental techniques relative to [31] for ε_r=10.2 and h=1.905 *mm*.

As seen from Table 4-1 the maximum rms error is 3.66 % for the cases considered. Taking into account that Kobayashi's formula (Kobayashi, 1988) is in error of 0.8 % when compared to the full-wave results in (Kobayashi, 1982), and that Atwater (1988) reported an average rms error of 0.73% for Kobayashi's formula, which is lower than the values in Table 4-1, we can safely conclude that, in the worst case scenario, the experimental data are in error of 3.66% + 0.8% = 4.46% when compared to the more accurate numerical methods. In addition to measurement errors, supplementary errors are due to fabrication tolerances. This can be analyzed using the sensitivity approach (Bhartia and Bahl, 1984; Gupta *et al.*, 1979) and by employing the upper and lower tolerances (Forzley and Bridges, 1992). For example, for the microstrip geometry in Fig. 4-1, the substrate RT/duroid 6010 has a relative dielectric permittivity of 10.2 ± 0.25 and a dielectric thickness of 1.905 ± 0.1016 *mm*.

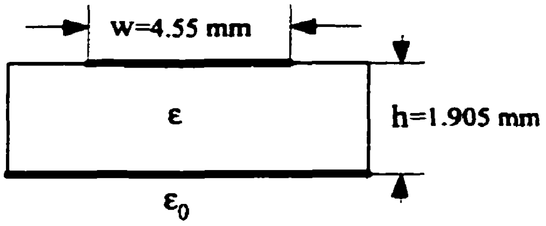

Fig. 4-1. Microstrip geometry in [14].

For $\varepsilon_r = 10.2$, h = 1.905 *mm*, and w = 4.55 *mm*, the proposed variational methods give a dielectric permittivity at zero frequency $\varepsilon_{eff}(0) = 7.446$. The value of $\varepsilon_{eff}(0)$ corresponding to the upper tolerance, calculated with $\varepsilon_r = 10.2 + 0.25 = 10.45$ and h = 1.905+0.1016=2.0066 *mm* is 7.575. For the lower tolerance, $\varepsilon_r = 10.2 - 0.25 = 9.95$ and h = 1.905-0.1016=1.8034 *mm* with the same w, the calculated value of $\varepsilon_{eff}(0)$ is 7.325. A comparison of the dispersion curves derived from a full-wave analysis (Sonnet, 1999) for the upper and lower tolerances with the experimental values corresponding to various measurement techniques is presented in Figures 4-2 to 4-4.

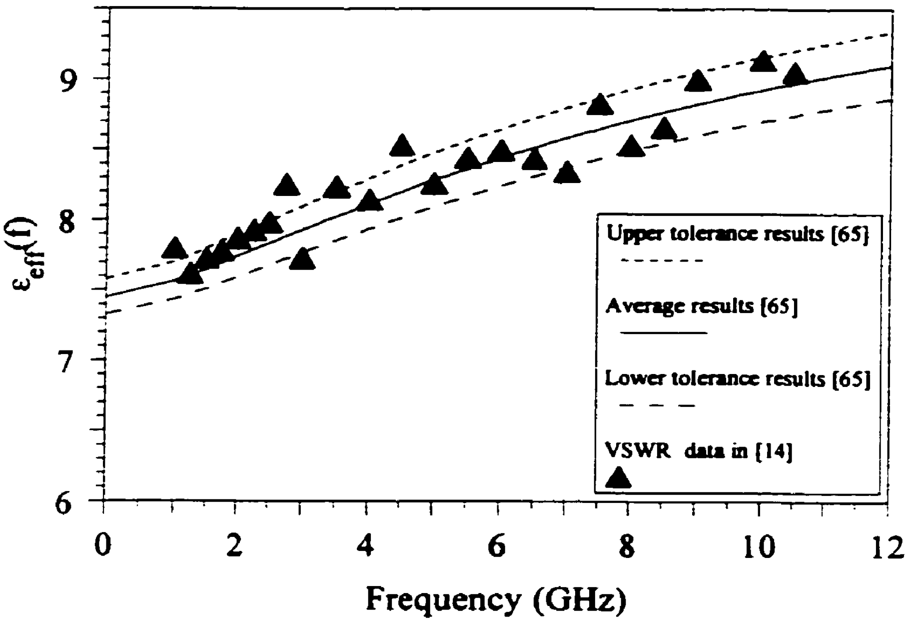

Fig. 4-2. Comparison with experimental data for the microstrip in Fig. 4-1.

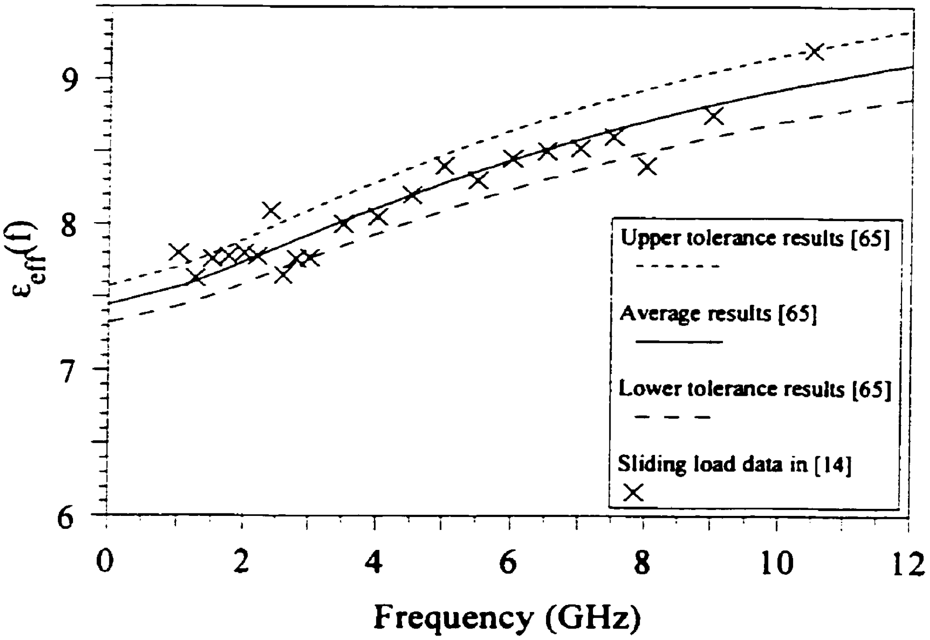

Fig. 4-3. Comparison with experimental data for the microstrip in Fig. 4-1.

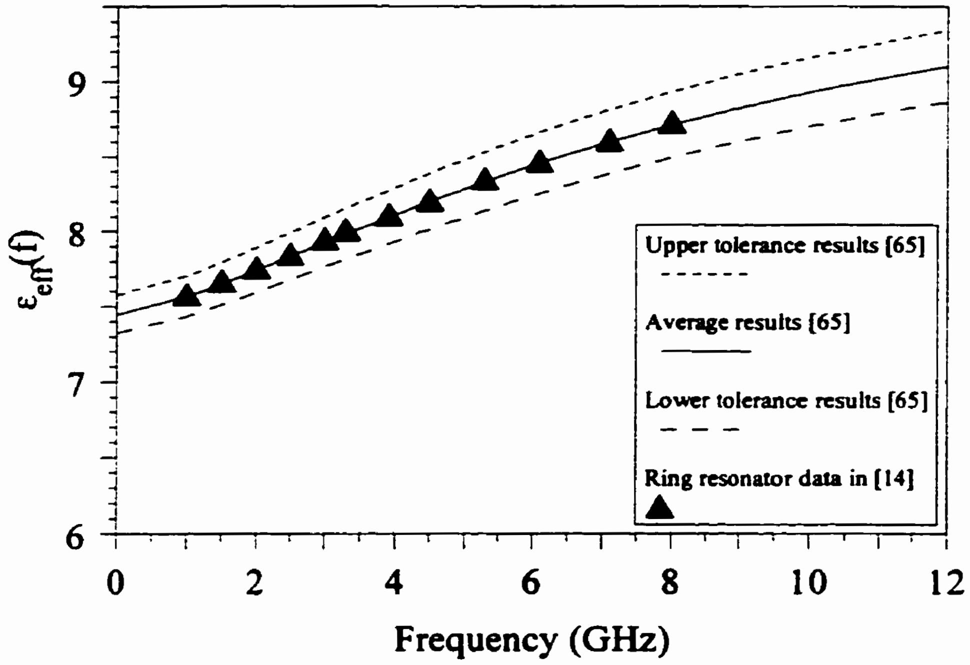

Fig. 4-4. Comparison with experimental data for the microstrip in Fig. 4-1.

Most dispersion models introduce errors of less than 5% with respect to the numerical solution based on the full-wave analysis and to experimental data (Medina *et al.*, 1993). Therefore, a new model should bring either a more simplified formulation or additional features not present in the existing models. In this thesis we construct dispersion models based on the two-dimensional telegraphists' equations. Employing these models we can calculate:

- the dispersion for the fundamental mode and the losses, simultaneously, and also
- the dispersions for the fundamental mode and for higher-order modes, simultaneously.

In order to validate the models based on the two-dimensional telegraphists' equations, the following are performed in this Chapter:

- a comparison of the dispersion obtained for the fundamental mode with that calculated using Kobayashi's formula (Kobayashi, 1988), using a full-wave solution employing the most recent Sonnet (1999), and with published experimental data in (Edwards and Owens, 1976; Forzley and Bridges, 1992; Getsinger, 1973; Yamashita *et al.*, 1981; York and Compton, 1990);

- a comparison of the losses obtained with the existing results and experimental data in (Pucel *et al*, 1968) and (Stracca, 1997);
- a comparison of the dispersion for the higher-order modes with that from solutions and data published by Gupta *et al.* (1979), Hoffmann (1987), Kompa (1973), and Kompa (1975).

4.2. Dispersion Model for Lossless Microstrips

The first order two-dimensional equations for microwave planar circuits under time-harmonic conditions (2.25), (2.26) can be written in the form

$$\begin{aligned} -\nabla U &= Z\mathbf{J}_s \\ -\nabla \cdot \mathbf{J}_s &= YU \end{aligned} \tag{4.4}$$

where U is the transverse voltage between the strip and the conducting base, $\mathbf{J}_s$ is the surface current density carried by the conducting strip, $Z = R + j\omega L$ is the longitudinal impedance per square, and $Y = G + j\omega C$ is the transverse admittance per unit area. The corresponding second order equations are

$$\begin{aligned} \nabla^2 U - \gamma^2 U &= 0 \\ \nabla^2 \mathbf{J}_s - \gamma^2 \mathbf{J}_s &= 0 \end{aligned} \tag{4.5}$$

where $\gamma^2 = ZY$. Equations (4.4), (4.5) are to be used in the computation of the microstrip dispersion on the basis of the proposed model.

The effective dielectric constant for a given microstrip structure can be expressed as

$$\varepsilon_{eff}(f) = f\left(Z_c, \frac{w}{h}, \varepsilon_r, f\right) \tag{4.6}$$

where Z_c is the characteristic impedance of the microstrip, h is the height of the substrate, w is the width of the stripline, ε_r is the relative permittivity of the substrate, and f is the operating frequency. The dispersion of a lossless microstrip can be analyzed by using a simple model in which the static parameters per unit length of the real structure, L' and C', are kept unchanged. For the microstrip shown in Figure 4-5, the model contains a parallel-plate capacitor, completed with lateral magnetic walls of $\varepsilon = 0$ and $\mu \to \infty$, such that the field exists only within the region between the plates. The model is presented in Figure 4-6, has in the central part $y \in (-a, a)$ a dielectric between the plates of same permittivity as in the original microstrip, a and b having to be determined from the condition that the corresponding propagation parameters at low frequency, $Z_c = \sqrt{L'/C'}$ and the velocity $1/\sqrt{L'C'}$, be the same as in the original microstrip.

Assuming the substrate to be non-magnetic, we have to impose only the condition that the corresponding C' remains unchanged,

$$C' = \frac{\varepsilon 2a}{h} + \frac{\varepsilon_0 2b}{h} = \varepsilon_{eff}(0) C_0 \tag{4.7}$$

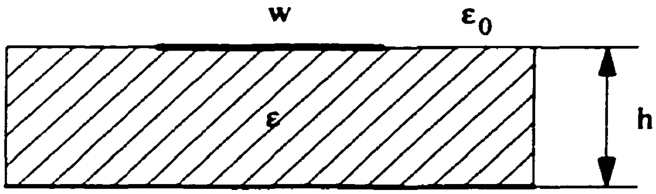

Fig. 4-5. Microstrip geometry.

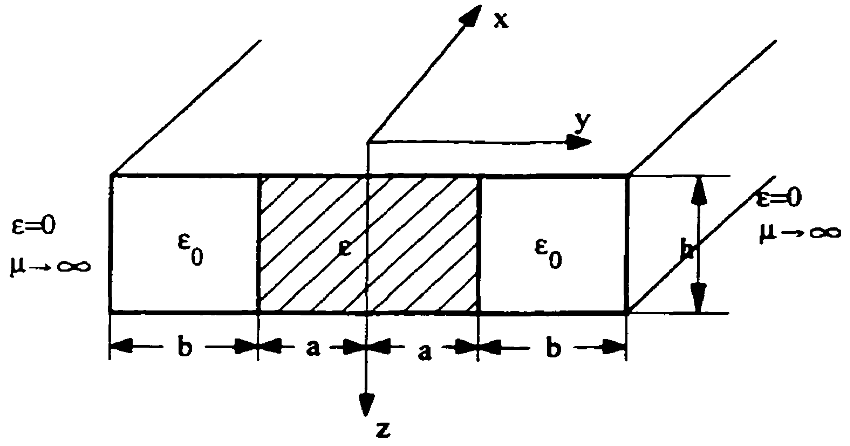

Fig. 4-6. The model.

with the capacitance of the structure filled with air

$$C_0 = \frac{2(a+b)\varepsilon_0}{h} \; . \tag{4.8}$$

The dimensions a and b are related to C_0 and $\varepsilon_{eff}(0)$ as follows:

$$a = \frac{\eta_0 h}{Z_c(m+1)\sqrt{\varepsilon_{eff}(0)}}$$

$$b = ma \tag{4.9}$$

where m is given by

$$m = \frac{\varepsilon_r - \varepsilon_{eff}(0)}{\varepsilon_{eff}(0) - 1} \tag{4.10}$$

and $\eta_0 = \sqrt{\mu_0 / \varepsilon_0}$ is the free space intrinsic impedance. This model was presented and used by Pramanick and Bhartia (1984), Tugulea (1984), and Tugulea and Ciric (1993).

Assume the line to be infinitely extended in the x-axis direction and choose the system of coordinates as shown in Figure 4-6. Denoting $U_1(x,y)$ as the voltage in the region $y \in (-a,a)$, $U_2(x,y)$ the voltage in the lateral region $y \in (a, a+b)$ and $U_3(x,y)$ the voltage in the region $y \in (-a-b, -a)$, the corresponding two-dimensional equations are

$$\frac{\partial^2 U_1}{\partial x^2} + \frac{\partial^2 U_1}{\partial y^2} + \gamma^2 U_1 = 0 \tag{4.11}$$

$$\frac{\partial^2 U_2}{\partial x^2} + \frac{\partial^2 U_2}{\partial y^2} + \beta_0^2 U_2 = 0 \tag{4.12}$$

$$\frac{\partial^2 U_3}{\partial x^2} + \frac{\partial^2 U_3}{\partial y^2} + \beta_0^2 U_3 = 0 \tag{4.13}$$

where $\gamma^2 = \omega^2 \varepsilon \mu$ for lossless structures and $\beta_0^2 = \omega^2 \varepsilon_0 \mu_0 < \gamma^2$. Assuming only the dominant mode of propagation, we look for solutions of the form

$$U_{1,2,3}(x,y) = V_{1,2,3}(y) e^{\pm j\beta x} \tag{4.14}$$

where β is real. From (4.11)-(4.13) we get

$$\begin{aligned} &V_1'' + \left(\gamma^2 - \beta^2\right) V_1 = 0 \\ &V_2'' + \left(\beta_0^2 - \beta^2\right) V_2 = 0 \\ &V_3'' + \left(\beta_0^2 - \beta^2\right) V_3 = 0 \ . \end{aligned} \tag{4.15}$$

Since $\gamma^2 > \beta^2 > \beta_0^2$, we have $\alpha_1^2 \equiv \gamma^2 - \beta^2 > 0$ and $-\alpha_2^2 \equiv \beta_0^2 - \beta^2 < 0$. Equations (4.15) yield the general solutions

$$\begin{aligned} V_1 &= A_1 \cos \alpha_1 y + B_1 \sin \alpha_1 y \\ V_2 &= A_2 \cosh \alpha_2 y + B_2 \sinh \alpha_2 y \\ V_3 &= A_3 \cosh \alpha_2 y + B_3 \sinh \alpha_2 y \end{aligned} \tag{4.16}$$

The boundary conditions are

$$U_1(x,a) = U_2(x,a) \tag{4.17}$$

$$U_1(x,-a) = U_3(x,-a) \tag{4.18}$$

$$J_{y1}(x,a) = J_{y2}(x,a) \tag{4.19}$$

$$J_{y1}(x,-a) = J_{y3}(x,-a) \tag{4.20}$$

$$J_{y2}(x,a+b) = 0 \tag{4.21}$$

$$J_{y3}(x,-a-b) = 0. \tag{4.22}$$

Imposing these conditions at $y = a$ we have:

$$A_1 \cos\alpha_1 a + B_1 \sin\alpha_1 a = A_2 \cosh\alpha_2 a + B_2 \sinh\alpha_2 a \tag{4.23}$$

$$\alpha_1 (-A_1 \sin\alpha_1 a + B_1 \cos\alpha_1 a) = \alpha_2 (A_2 \sinh\alpha_2 a + B_2 \cosh\alpha_2 a) \ ; \tag{4.24}$$

at $y = -a$

$$A_1 \cos\alpha_1 a - B_1 \sin\alpha_1 a = A_3 \cosh\alpha_2 a - B_3 \sinh\alpha_2 a \tag{4.25}$$

$$\alpha_1 (A_1 \sin\alpha_1 a + B_1 \cos\alpha_1 a) = \alpha_2 (-A_3 \sinh\alpha_2 a + B_3 \cosh\alpha_2 a) \ ; \tag{4.26}$$

at $y = a + b$

$$\alpha_2 [A_2 \sinh\alpha_2 (a+b) + B_2 \cosh\alpha_2 (a+b)] = 0 \ ; \tag{4.27}$$

and finally at $y = -a - b$

$$\alpha_2 [-A_3 \sinh\alpha_2 (a+b) + B_3 \cosh\alpha_2 (a+b)] = 0 \, . \tag{4.28}$$

From (4.27) and (4.28)

$$\frac{B_3}{A_3} = -\frac{B_2}{A_2} = \tanh\alpha_2 (a+b) \, . \tag{4.29}$$

Dividing Equations (4.23) and (4.25) gives

$$\frac{A_1 \cos\alpha_1 a + B_1 \sin\alpha_1 a}{A_1 \cos\alpha_1 a - B_1 \sin\alpha_1 a} = \frac{A_2 \cosh\alpha_2 a + B_2 \sinh\alpha_2 a}{A_3 \cosh\alpha_2 a - B_3 \sinh\alpha_2 a} = \frac{A_2}{A_3} \tag{4.30}$$

and dividing Equations (4.24) and (4.26) gives

$$\frac{-A_1 \sin \alpha_1 a + B_1 \cos \alpha_1 a}{A_1 \sin \alpha_1 a + B_1 \cos \alpha_1 a} = \frac{A_2 \sinh \alpha_2 a + B_2 \cosh \alpha_2 a}{-A_3 \sinh \alpha_2 a + B_3 \cosh \alpha_2 a} = -\frac{A_2}{A_3}. \tag{4.31}$$

A simple calculation shows that these equations are satisfied if $B_1 = 0$ and $A_2/A_3 = 1$. Hence,

$$(B_2 + B_3)\sinh \alpha_2 a = 0 \tag{4.32}$$

$$(B_2 + B_3)\cosh \alpha_2 a = 0. \tag{4.33}$$

From Equations (4.32) and (4.33) we obtain $B_2 = -B_3$. The solutions become

$$V_1(y) = A_1 \cos \alpha_1 y \tag{4.34}$$

$$V_2(y) = A_2 \cosh \alpha_2 y + B_2 \sinh \alpha_2 y \tag{4.35}$$

$$V_3(y) = A_2 \cosh \alpha_2 y - B_2 \sinh \alpha_2 y. \tag{4.36}$$

From the last two equations we observe that $V_2(y) = V_3(-y)$ and due to the symmetry we only impose the conditions for $y > 0$,

$$A_1 \cos \alpha_1 a = A_2 \cosh \alpha_2 a + B_2 \sinh \alpha_2 a \tag{4.37}$$

$$-\alpha_1 A_1 \sin \alpha_1 a = \alpha_2 (A_2 \sinh \alpha_2 a + B_2 \cosh \alpha_2 a) \tag{4.38}$$

$$\alpha_2 [A_2 \sinh \alpha_2 (a+b) + B_2 \cosh \alpha_2 (a+b)] = 0. \tag{4.39}$$

Dividing Equations (4.38) and (4.37) yields

$$-\alpha_1 \tan \alpha_1 a = \alpha_2 \frac{A_2 \sinh \alpha_2 a + B_2 \cosh \alpha_2 a}{A_2 \cosh \alpha_2 a + B_2 \sinh \alpha_2 a} \tag{4.40}$$

and from (4.39)

$$\tanh \alpha_2 (a+b) = -\frac{B_2}{A_2} \tag{4.41}$$

and

$$-\alpha_1 \tan \alpha_1 a = -\alpha_2 \tanh \alpha_2 b\,. \tag{4.42}$$

Denoting $\xi \equiv \alpha_1 a$, $k^2 \equiv \omega^2 \varepsilon_0 \mu_0 (\varepsilon_r - 1) a^2$, and $m \equiv b/a$ the following transcendental equation is derived

$$\xi \tan \xi - \sqrt{k^2 - \xi^2} \tanh\left(m\sqrt{k^2 - \xi^2}\right) = 0\,. \tag{4.43}$$

The dispersion (Gupta and Singh, 1982) of the lossless microstrip is obtained as

$$\varepsilon_{eff}(\omega) \equiv \frac{\beta^2}{\beta_0^2} = \varepsilon_r - \frac{\xi^2}{k^2}(\varepsilon_r - 1) \tag{4.44}$$

with the first root of the Equation (4.43) corresponding to the dominant mode of propagation.

At very low frequencies, $\tan \xi \approx \xi$, $\tanh\left(m\sqrt{k^2 - \xi^2}\right) \approx m\sqrt{k^2 - \xi^2}$, and (4.43) and (4.44) yield

$$\varepsilon_{eff}(0) = \varepsilon_r - \frac{m}{m+1}(\varepsilon_r - 1)\,. \tag{4.45}$$

At very high frequencies, $k^2 \to \infty$, and we check that

$$\varepsilon_{eff}(\infty) = \varepsilon_r\,. \tag{4.46}$$

To verify for accuracy, the model presented is compared with Kobayashi's model (Kobayashi, 1988) and with published experimental data. For both models $\varepsilon_{eff}(0)$ is calculated using the variational methods introduced in Chapter 3. The results are presented in the even-numbered Figures 4-8 to 4-50, with the corresponding calculated errors in the odd-numbered Tables 4-3 to 4-45. In the table header the errors are defined as follows:

- the error:

  $$e_i = \frac{\varepsilon_{effm}(f_i) - \varepsilon_{effc}(f_i)}{\varepsilon_{effm}(f_i)} \times 100 \quad (\%)$$

  where $\varepsilon_{effm}(f_i)$ is given by Equation (4.44) and $\varepsilon_{effc}(f_i)$ is given either by Kobayashi's formula (Kobayashi, 1988) or by the full-wave solution (Sonnet, 1999);

- the maximum error:

  $$e_M = Max(e_i)$$

  is the largest error in the frequency range considered;

- the mean (average) error:

  $$\bar{e} = \frac{\sum_i |e_i|}{n}$$

  is the arithmetic mean of the calculated errors with n the number of frequency points considered;

- the standard deviation (or rms error):

  $$\sigma = \sqrt{\frac{\sum_i e_i^2 - \frac{\left(\sum_i e_i\right)^2}{n}}{n}} .$$

Only the maximum error, standard deviation and mean error are given in the table header.

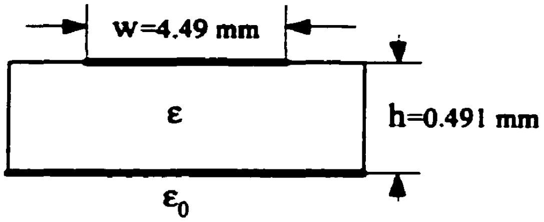

Fig. 4-7. Microstrip geometry in [11].

Substrate	w(mm)	h(mm)	w/h	ε_r	$\varepsilon_{eff}(0)$
Sapphire	4.49	0.491	9.14	11.5	9.742

Table 4-2. Data for the microstrip in Fig. 4-7.

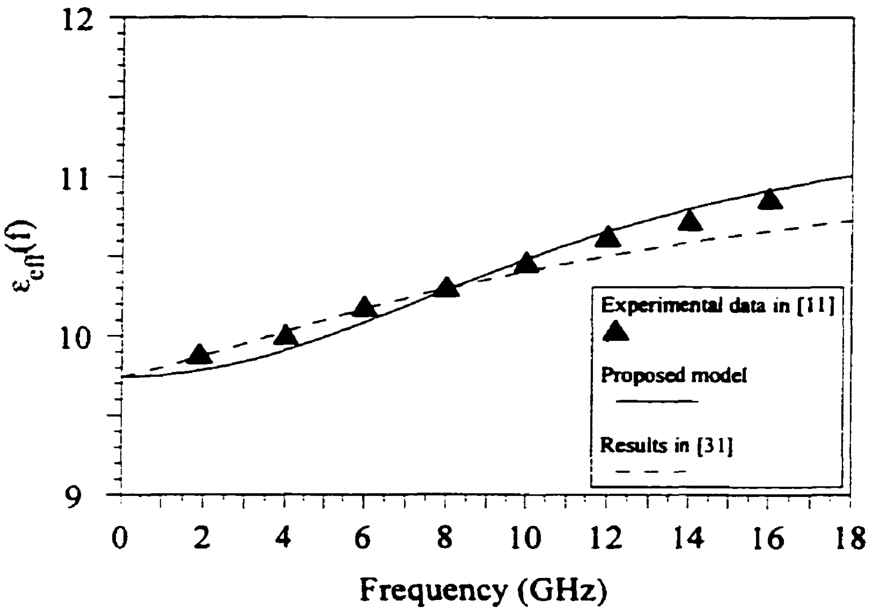

Fig. 4-8. Effective dielectric constant versus frequency for the microstrip in Fig. 4-7.

Maximum error	Standard deviation	Average error
2.63%	1.51	1.31%

Table 4-3. Comparison with Kobayashi's model [31] for the microstrip in Fig. 4-7.

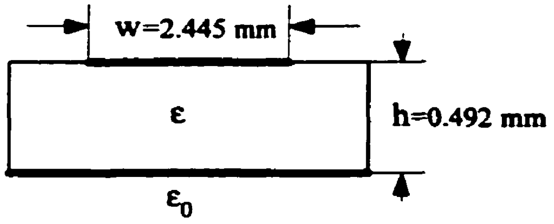

Fig. 4-9. Microstrip geometry in [11].

Substrate	w(mm)	h(mm)	w/h	ε_r	$\varepsilon_{eff}(0)$
Sapphire	2.445	0.492	4.96	11.43	9.064

Table 4-4. Data for the microstrip in Fig. 4-9.

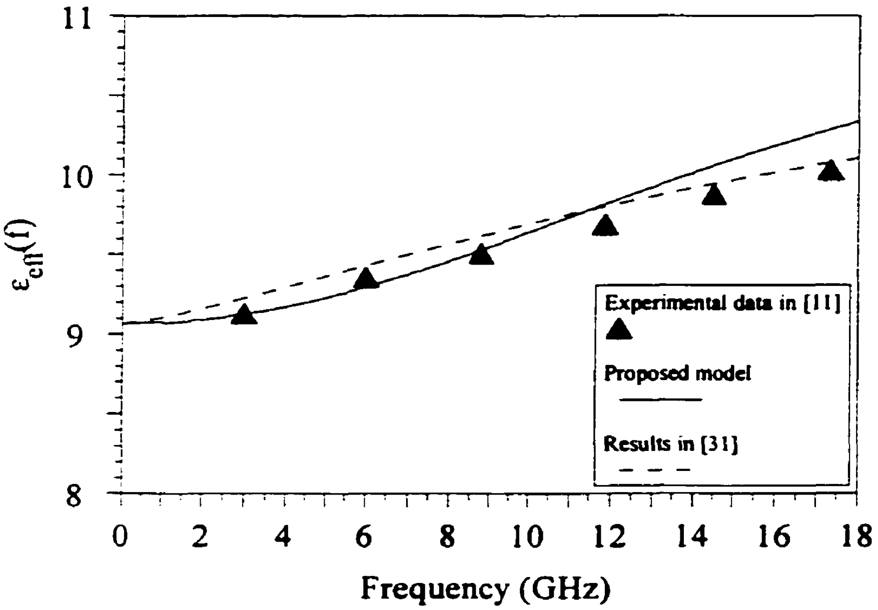

Fig. 4-10. Effective dielectric constant versus frequency for the microstrip in Fig. 4-9.

Maximum error	Standard deviation	Average error
2.42%	1.265	1.122%

Table 4-5. Comparison with Kobayashi's model [31] for the microstrip in Fig. 4-9.

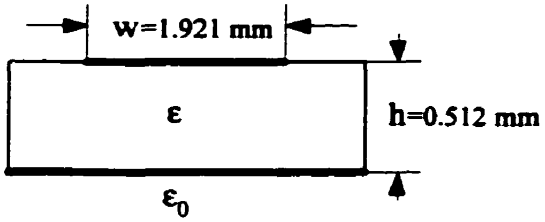

Fig. 4-11. Microstrip geometry in [11].

Substrate	w(mm)	h(mm)	w/h	ε_r	$\varepsilon_{eff}(0)$
Sapphire	1.921	0.512	3.75	11.39	8.737

Table 4-6. Data for the microstrip in Fig. 4-11.

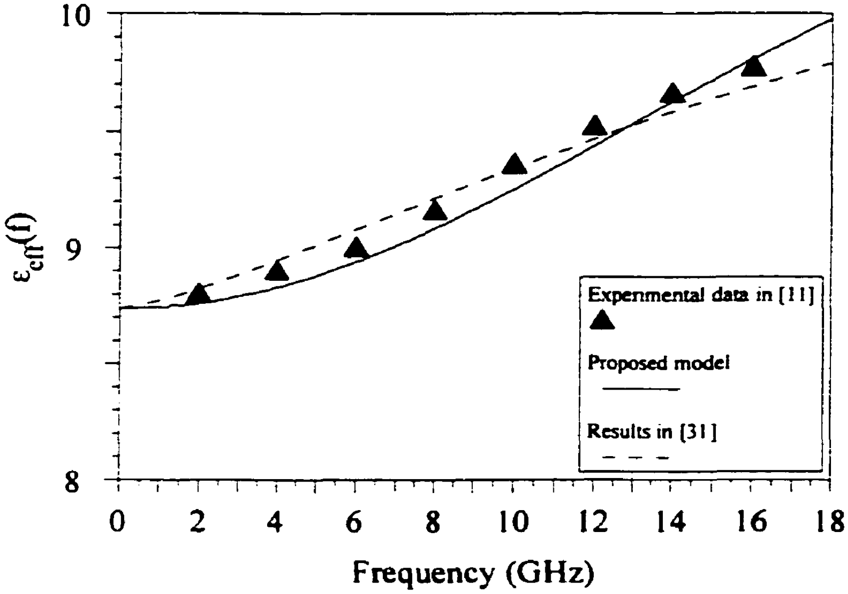

Fig. 4-12. Effective dielectric constant versus frequency for the microstrip in Fig. 4-11.

Maximum error	Standard deviation	Average error
2.121%	1.186	1.067%

Table 4-7. Comparison with Kobayashi's model [31] for the microstrip in Fig. 4-11.

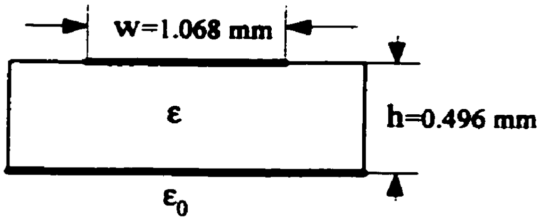

Substrate	w(mm)	h(mm)	w/h	ε_r	$\varepsilon_{eff}(0)$
Sapphire	1.068	0.496	2.15	11.29	8.108

Table 4-8. Data for the microstrip in Fig. 4-13.

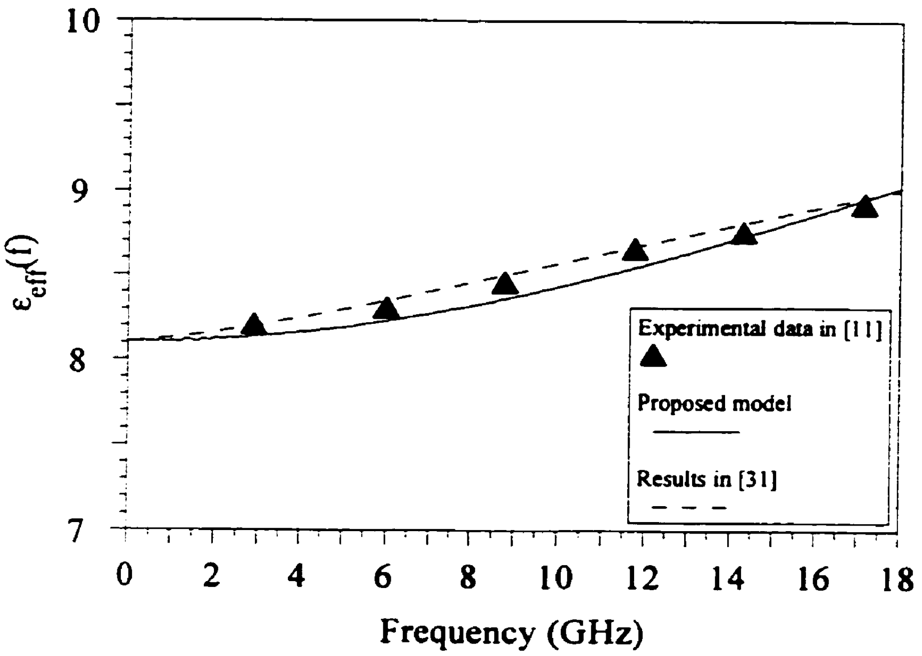

the microstrip in Fig. 4-13.

Maximum error	Standard deviation	Average error
-1.694%	1.156	1.029%

Table 4-9. Comparison with Kobayashi's model [31] for the microstrip in Fig. 4-13.

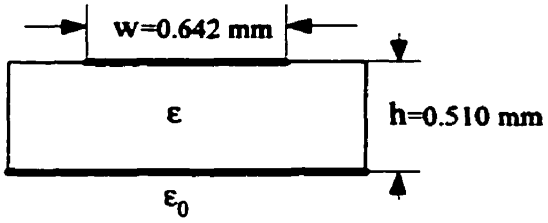

Fig. 4-15. Microstrip geometry in [11].

Substrate	w(mm)	h(mm)	w/h	ε_r	$\varepsilon_{eff}(0)$
Sapphire	0.642	0.510	1.25	11.18	7.583

Table 4-10. Data for the microstrip in Fig. 4-15.

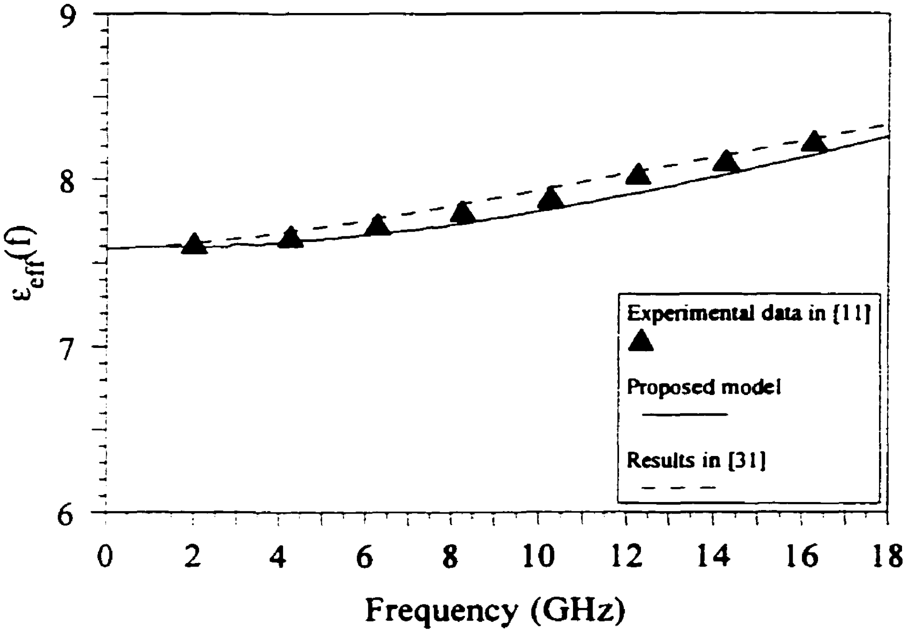

Fig. 4-16. Effective dielectric constant versus frequency for the microstrip in Fig. 4-15.

Maximum error	Standard deviation	Average error
-1.662%	1.235	1.156%

Table 4-11. Comparison with Kobayashi's model [31] for the microstrip in Fig. 4-15.

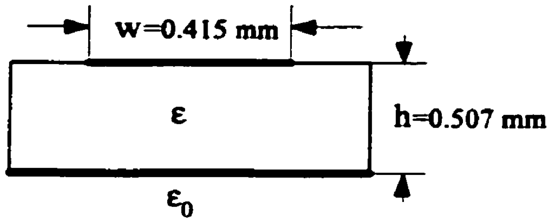

Fig. 4-17. Microstrip geometry in [11].

Substrate	w(mm)	h(mm)	w/h	ε_r	$\varepsilon_{eff}(0)$
Sapphire	0.415	0.507	0.81	11.08	7.245

Table 4-12. Data for the microstrip in Fig. 4-17.

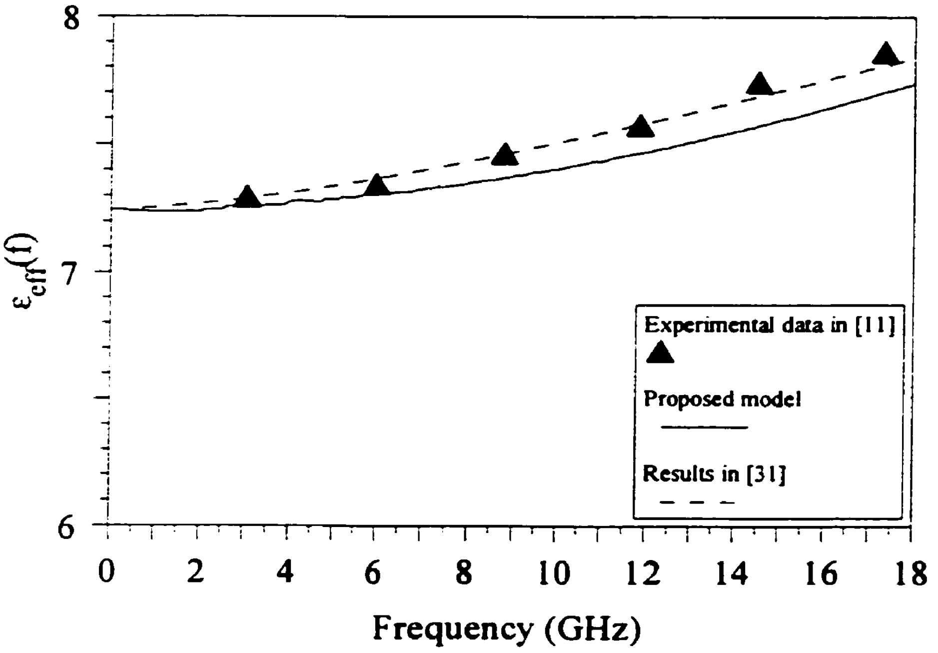

Fig. 4-18. Effective dielectric constant versus frequency for the microstrip in Fig. 4-17.

Maximum error	Standard deviation	Average error
-1.558%	1.185	1.102%

Table 4-13. Comparison with Kobayashi's model [31] for the microstrip in Fig. 4-17.

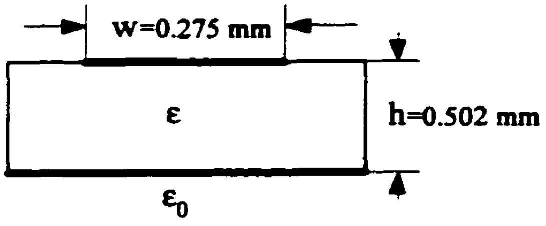

Fig. 4-19. Microstrip geometry in [11].

Substrate	w(mm)	h(mm)	w/h	ε_r	$\varepsilon_{eff}(0)$
Sapphire	0.275	0.502	0.54	10.99	7.005

Table 4-14. Data for the microstrip in Fig. 4-19.

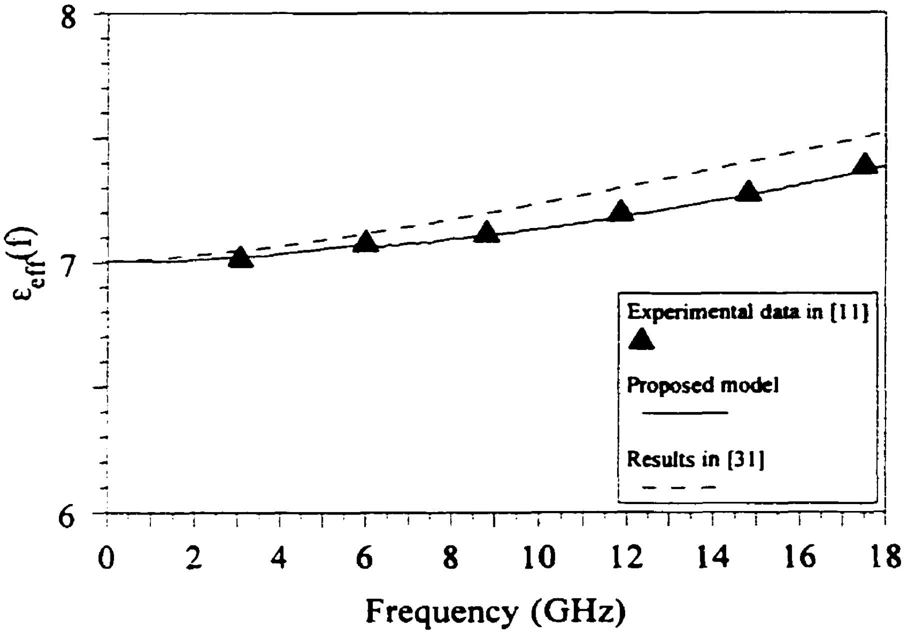

Fig. 4-20. Effective dielectric constant versus frequency for the microstrip in Fig. 4-19.

Maximum error	Standard deviation	Average error
-1.892%	1.360	1.218%

Table 4-15. Comparison with Kobayashi's model [31] for the microstrip in Fig. 4-19.

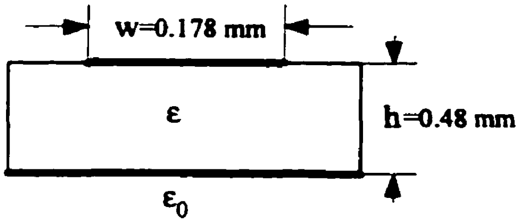

Fig. 4-21. Microstrip geometry in [11].

Substrate	w(mm)	h(mm)	w/h	ε_r	$\varepsilon_{eff}(0)$
Sapphire	0.178	0.480	0.37	10.91	6.821

Table 4-16. Data for the microstrip in Fig. 4-21.

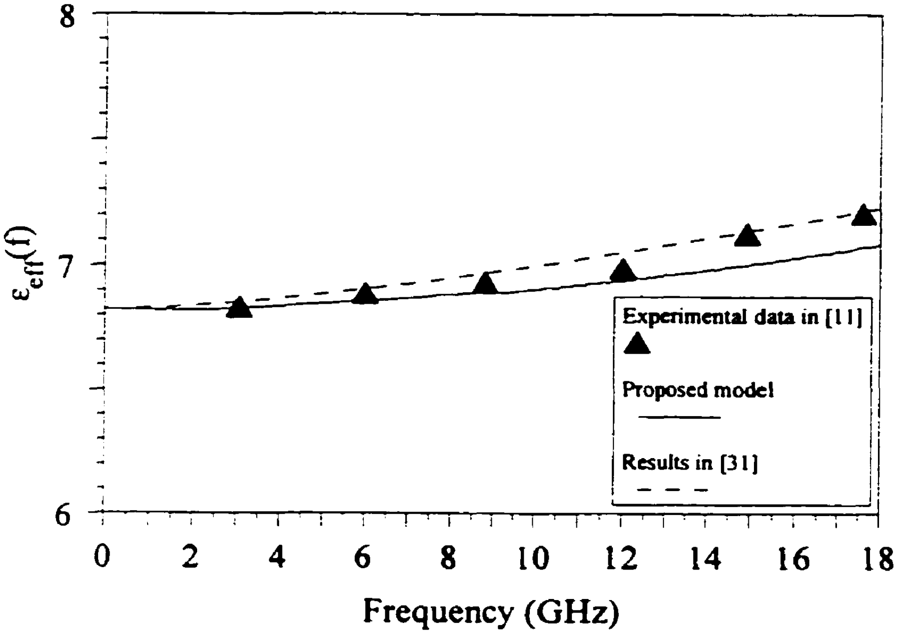

Fig. 4-22. Effective dielectric constant versus frequency for the microstrip in Fig. 4-21.

Maximum error	Standard deviation	Average error
-2.1%	1.394	1.232%

Table 4-17. Comparison with Kobayashi's model [31] for the microstrip in Fig. 4-21.

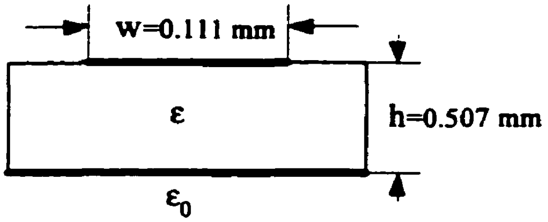

Fig. 4-23. Microstrip geometry in [11].

Substrate	w(mm)	h(mm)	w/h	ε_r	$\varepsilon_{eff}(0)$
Sapphire	0.111	0.507	0.21	10.82	6.632

Table 4-18. Data for the microstrip in Fig. 4-23.

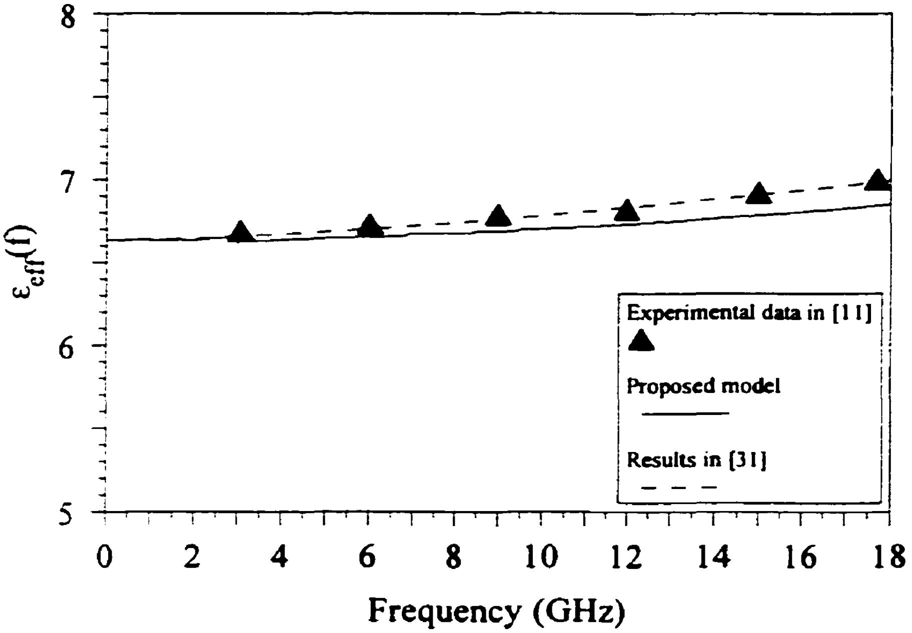

Fig. 4-24. Effective dielectric constant versus frequency for the microstrip in Fig. 4-23.

Maximum error	Standard deviation	Average error
-2.159%	1.337	1.18%

Table 4-19. Comparison with Kobayashi's model [31] for the microstrip in Fig. 4-23.

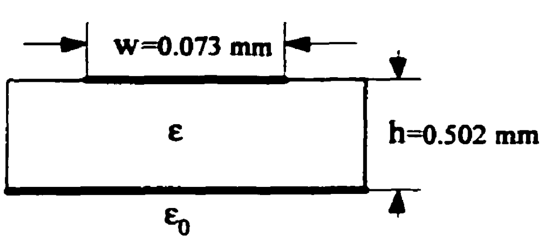

Fig. 4-25. Microstrip geometry in [11].

Substrate	w(mm)	h(mm)	w/h	ε_r	$\varepsilon_{eff}(0)$
Sapphire	0.073	0.502	0.14	10.76	6.519

Table 4-20. Data for the microstrip in Fig. 4-25.

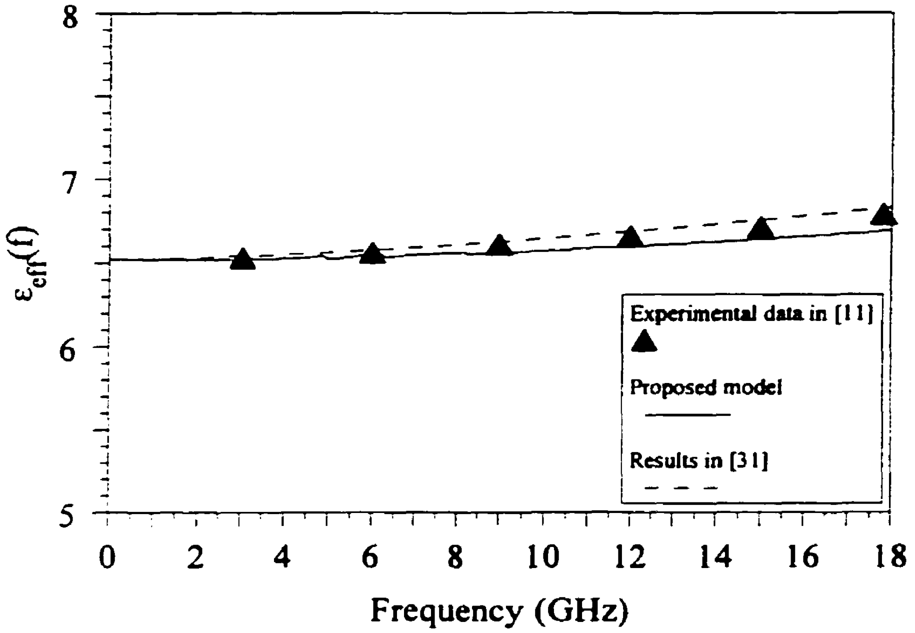

Fig. 4-26. Effective dielectric constant versus frequency for the microstrip in Fig. 4-25.

Maximum error	Standard deviation	Average error
-2.138%	1.251	1.087%

Table 4-21. Comparison with Kobayashi's model [31] for the microstrip in Fig. 4-25.

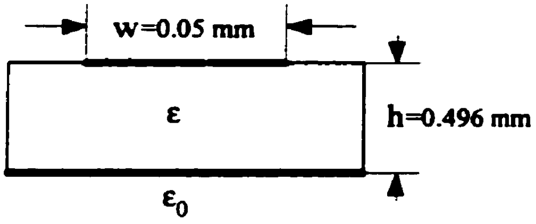

Fig. 4-27. Microstrip geometry in [11].

Substrate	w(mm)	h(mm)	w/h	ε_r	$\varepsilon_{eff}(0)$
Sapphire	0.05	0.496	0.1008	10.73	6.446

Table 4-22. Data for the microstrip in Fig. 4-27.

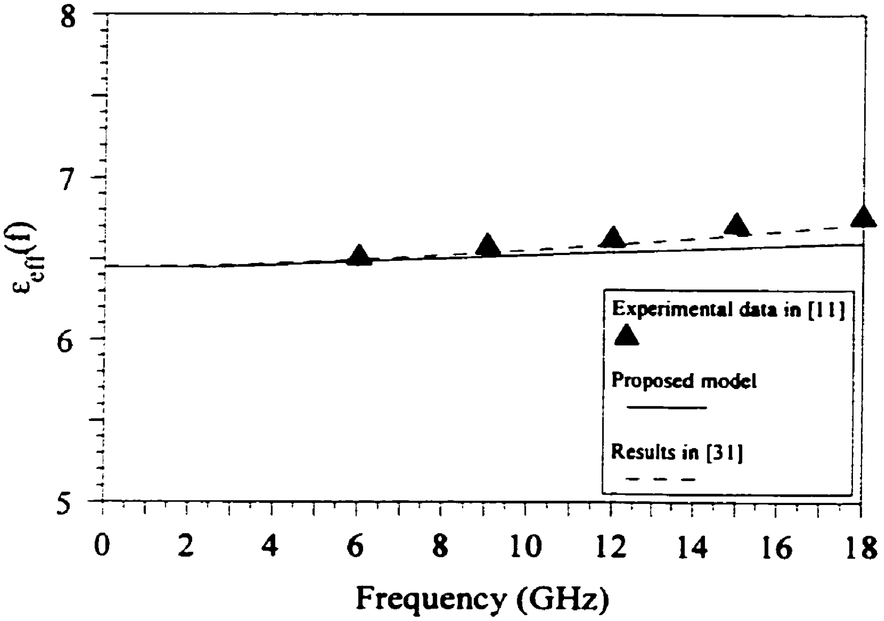

Fig. 4-28. Effective dielectric constant versus frequency for the microstrip in Fig. 4-27.

Maximum error	Standard deviation	Average error
-2.14%	1.177	1.01%

Table 4-23. Comparison with Kobayashi's model [31] for the microstrip in Fig. 4-27.

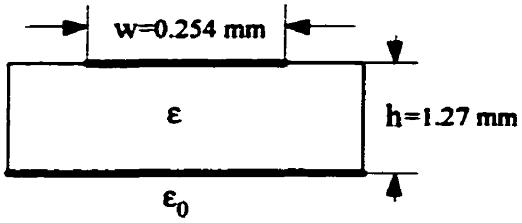

Fig. 4-29. Microstrip geometry in [16].

Substrate	w(mm)	h(mm)	w/h	ε_r	$\varepsilon_{eff}(0)$
Alumina	0.254	1.27	0.2	10.185	6.251

Table 4-24. Data for the microstrip in Fig. 4-29.

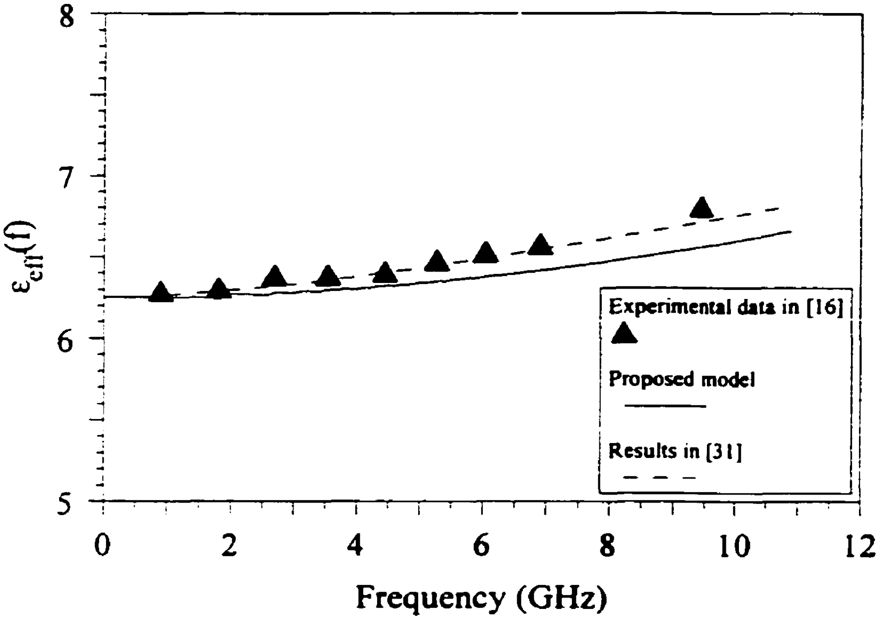

Fig. 4-30. Effective dielectric constant versus frequency for the microstrip in Fig. 4-29.

Maximum error	Standard deviation	Average error
-1.26%	1.359	0.93%

Table 4-25. Comparison with Kobayashi's model [31] for the microstrip in Fig. 4-29.

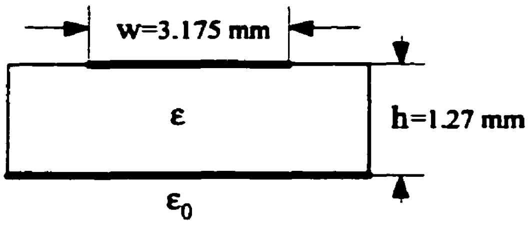

Fig. 4-31. Microstrip geometry in [16].

Substrate	w(mm)	h(mm)	w/h	ε_r	$\varepsilon_{eff}(0)$
Alumina	3.175	1.27	2.5	10.1	7.416

Table 4-26. Data for the microstrip in Fig. 4-31.

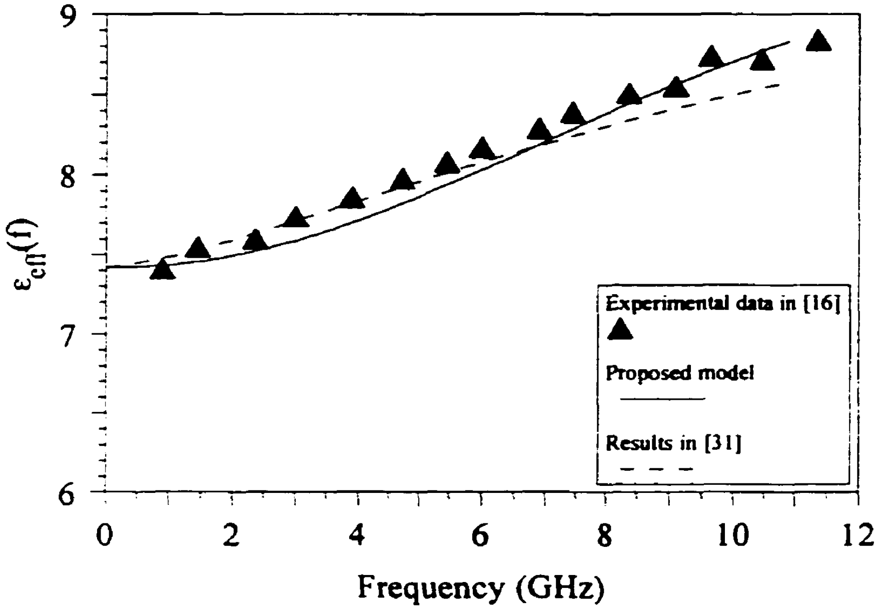

Fig. 4-32. Effective dielectric constant versus frequency for the microstrip in Fig. 4-31.

Maximum error	Standard deviation	Average error
2.35%	1.32	1.12%

Table 4-27. Comparison with Kobayashi's model [31] for the microstrip in Fig. 4-31.

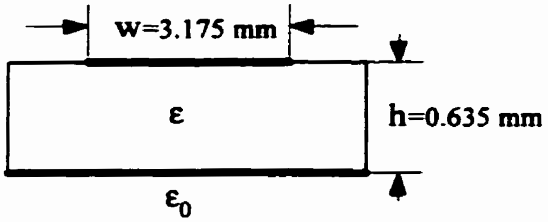

Fig. 4-33. Microstrip geometry in [16].

Substrate	w(mm)	h(mm)	w/h	ε_r	$\varepsilon_{eff}(0)$
Alumina	3.175	0.635	5	10.51	8.361

Table 4-28. Data for the microstrip in Fig. 4-33.

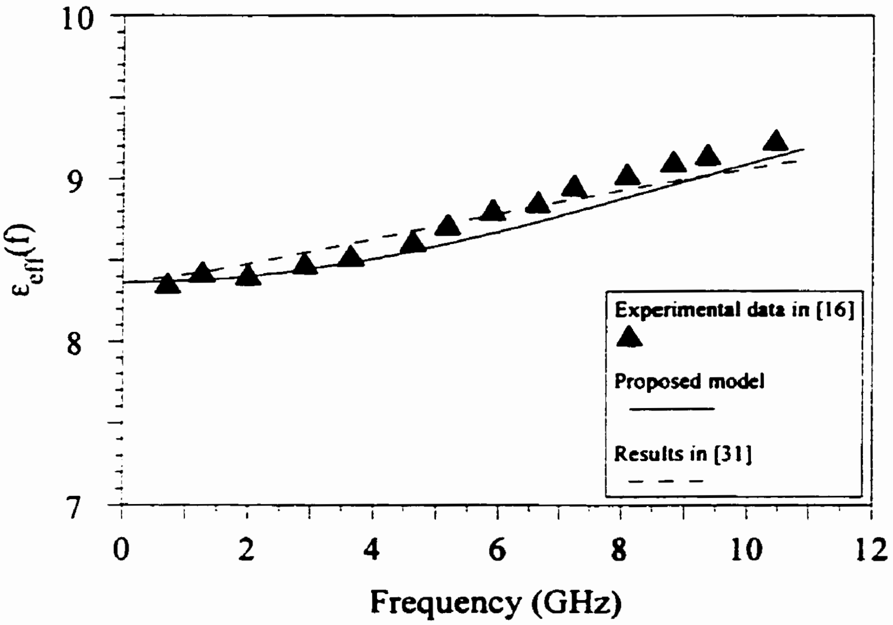

Fig. 4-34. Effective dielectric constant versus frequency for the microstrip in Fig. 4-33.

Maximum error	Standard deviation	Average error
-1.46%	0.745	0.497%

Table 4-29. Comparison with Kobayashi's model [31] for the microstrip in Fig. 4-33.

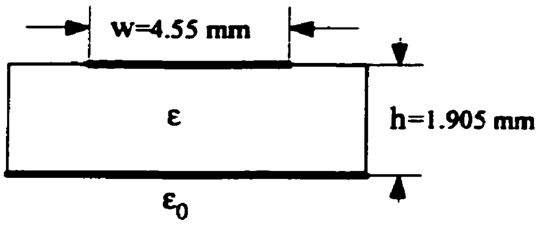

Fig. 4-35. Microstrip geometry in [14].

Substrate	w(mm)	h(mm)	w/h	ε_r	$\varepsilon_{eff}(0)$
RT/duroid	4.55	1.905	2.38	10.2	7.447

Table 4-30. Data for the microstrip in Fig. 4-35.

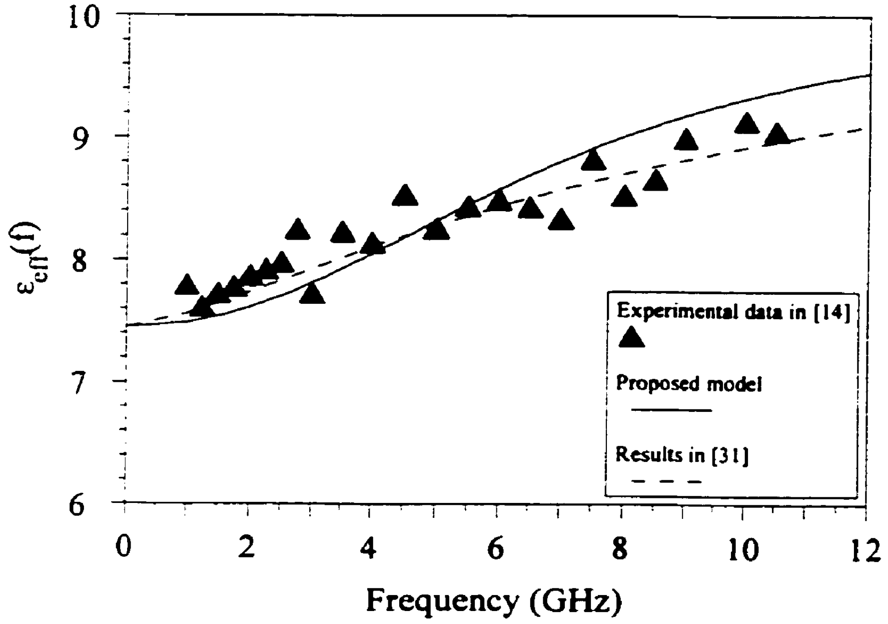

Fig. 4-36. Effective dielectric constant versus frequency for the microstrip in Fig. 4-35.

Maximum error	Standard deviation	Average error
4.60%	2.459	1.735%

Table 4-31. Comparison with Kobayashi's model [31] for the microstrip in Fig. 4-35.

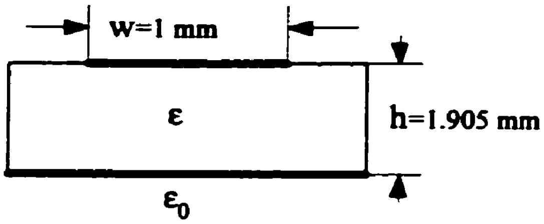

Fig. 4-37. Microstrip geometry in [14].

Substrate	w(mm)	h(mm)	w/h	ε_r	$\varepsilon_{eff}(0)$
RT/duroid	1.0	1.905	0.52	10.2	6.514

Table 4-32. Data for the microstrip in Fig. 4-37.

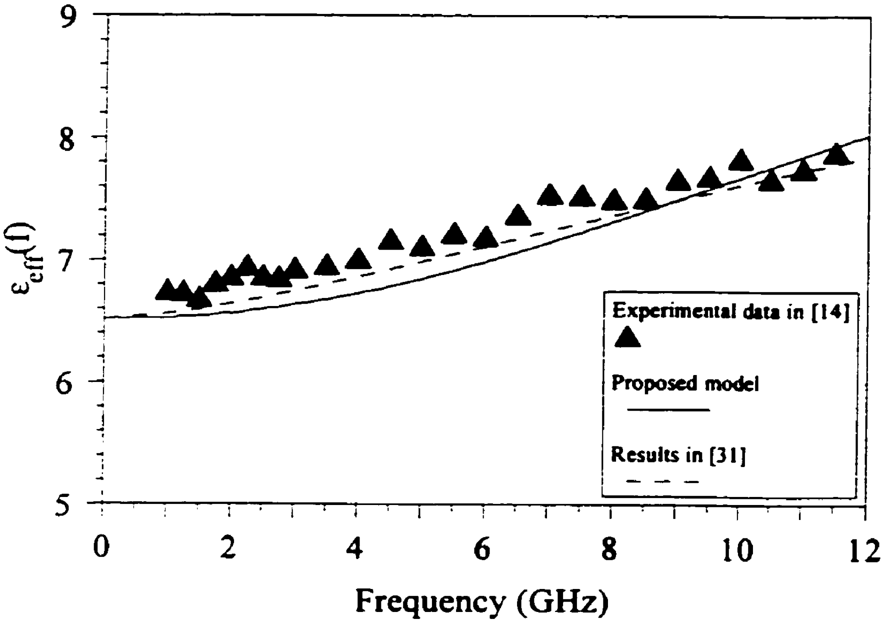

Fig. 4-38. Effective dielectric constant versus frequency for the microstrip in Fig. 4-37.

Maximum error	Standard deviation	Average error
-2.74%	1.264	0.931%

Table 4-33. Comparison with Kobayashi's model [31] for the microstrip in Fig. 4-37.

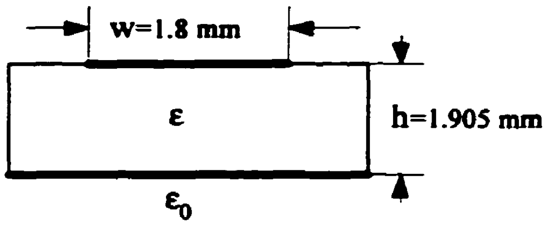

Fig. 4-39. Microstrip geometry in [14].

Substrate	w(mm)	h(mm)	w/h	ε_r	$\varepsilon_{eff}(0)$
RT/duroid	1.8	1.905	0.94	10.2	6.777

Table 4-34. Data for the microstrip in Fig. 4-39.

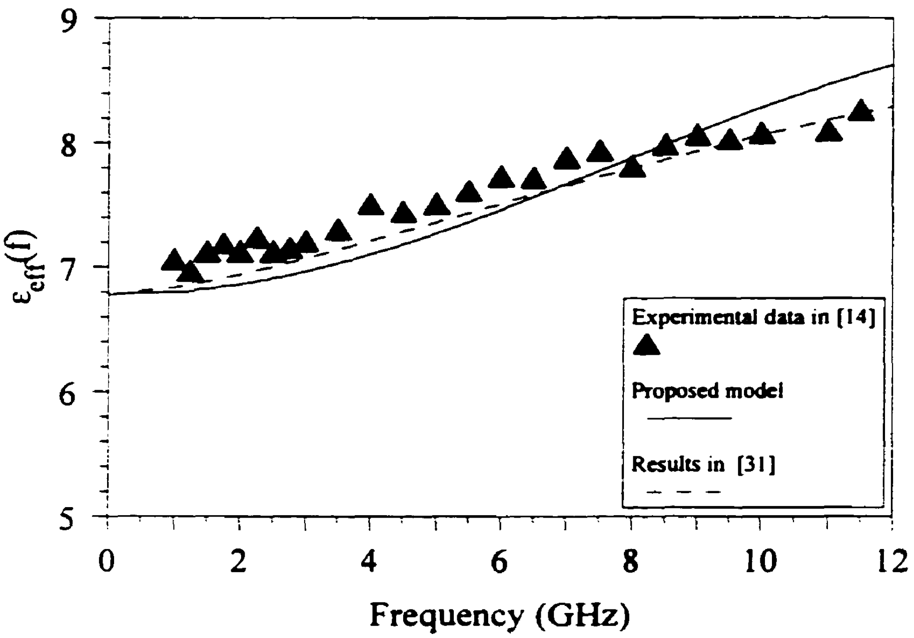

Fig. 4-40. Effective dielectric constant versus frequency for the microstrip in Fig. 4-39.

Maximum error	Standard deviation	Average error
4.28%	1.724	1.17%

Table 4-35. Comparison with Kobayashi's model [31] for the microstrip in Fig. 4-39.

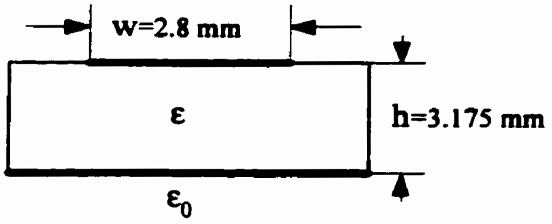

Fig. 4-41. Microstrip geometry in [14].

Substrate	w(mm)	h(mm)	w/h	ε_r	$\varepsilon_{eff}(0)$
RT/duroid	2.8	3.175	0.88	10.5	6.925

Table 4-36. Data for the microstrip in Fig. 4-41.

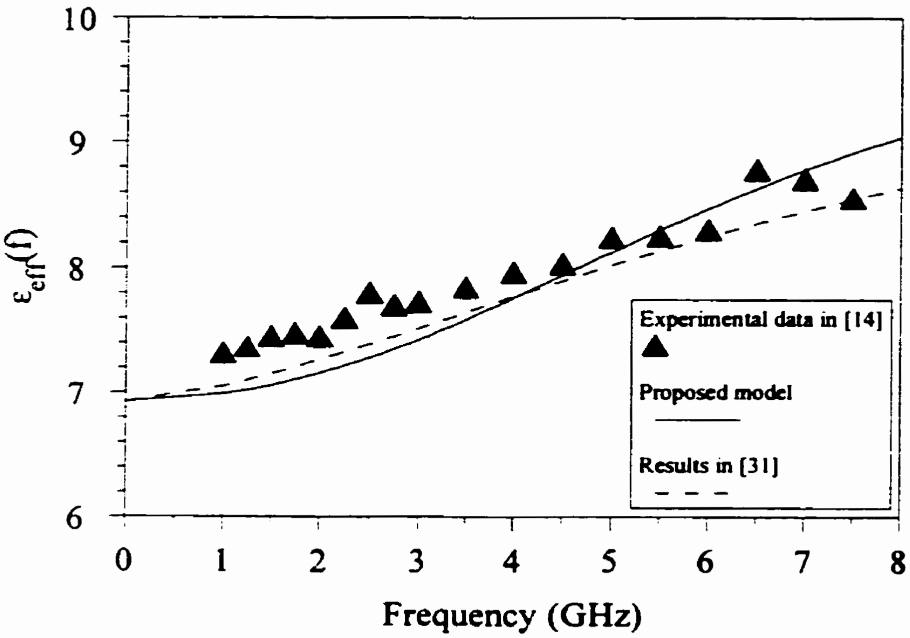

Fig. 4-42. Effective dielectric constant versus frequency for the microstrip in Fig. 4-41.

Maximum error	Standard deviation	Average error
5.21%	2.985	2.109%

Table 4-37. Comparison with Kobayashi's model [31] for the microstrip in Fig. 4-41.

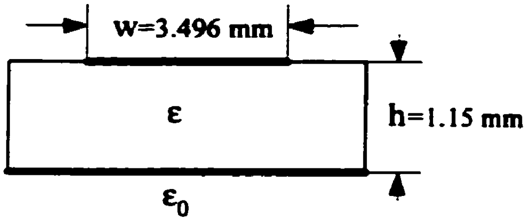

Fig. 4-43. Microstrip geometry in [83].

Substrate	w(mm)	h(mm)	w/h	ε_r	$\varepsilon_{eff}(0)$
Fluorglas	3.496	1.15	3.04	2.5	2.099

Table 4-38. Data for the microstrip in Fig. 4-43.

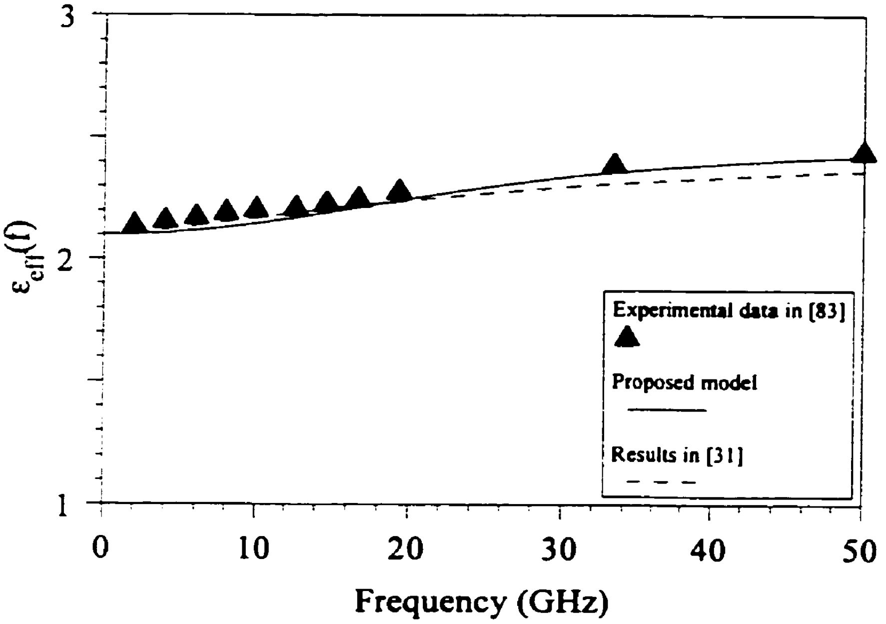

Fig. 4-44. Effective dielectric constant versus frequency for the microstrip in Fig. 4-43.

Maximum error	Standard deviation	Average error
-1.09%	0.773	0.722%

Table 4-39. Comparison with Kobayashi's model [31] for the microstrip in Fig. 4-43.

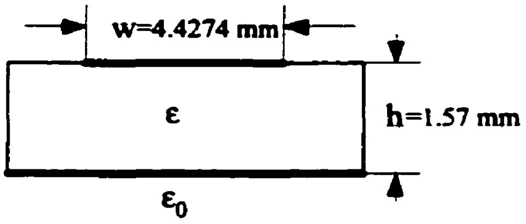

Fig. 4-45. Microstrip geometry in [83].

Substrate	w(mm)	h(mm)	w/h	ε_r	$\varepsilon_{eff}(0)$
Rexolite	4.4274	1.57	2.81	2.62	2.175

Table 4-40. Data for the microstrip in Fig. 4-45.

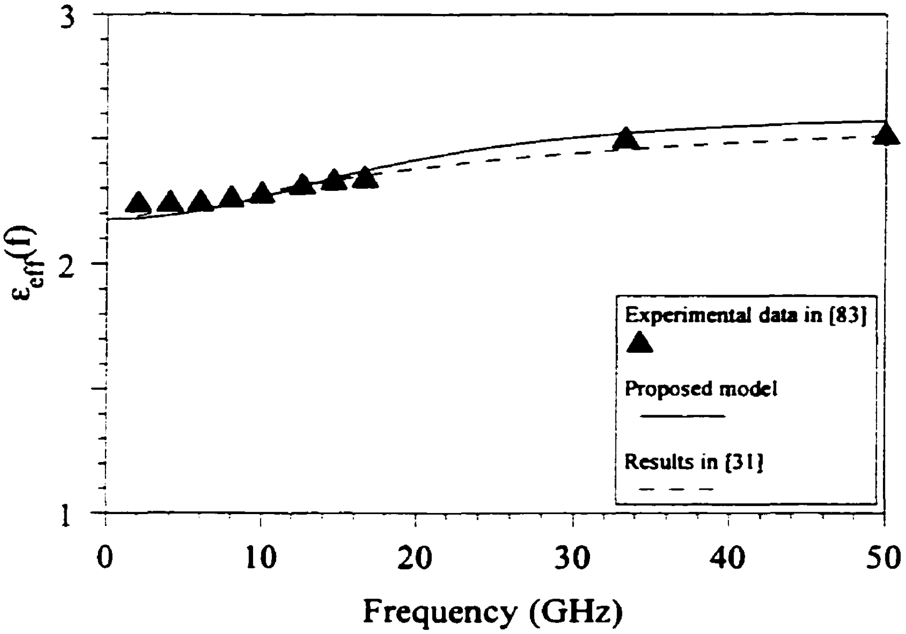

Fig. 4-46. Effective dielectric constant versus frequency for the microstrip in Fig. 4-45.

Maximum error	Standard deviation	Average error
1.646%	0.953	0.901%

Table 4-41. Comparison with Kobayashi's model [31] for the microstrip in Fig. 4-45.

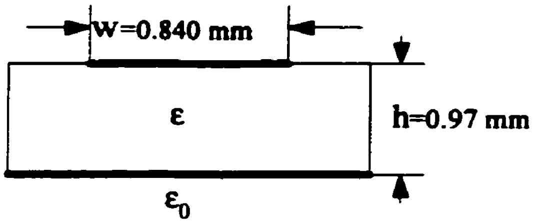

Fig. 4-47. Microstrip geometry in [83].

Substrate	w(mm)	h(mm)	w/h	ε_r	$\varepsilon_{eff}(0)$
Alumina	0.840	0.97	0.865	9.0	5.987

Table 4-42. Data for the microstrip in Fig. 4-47.

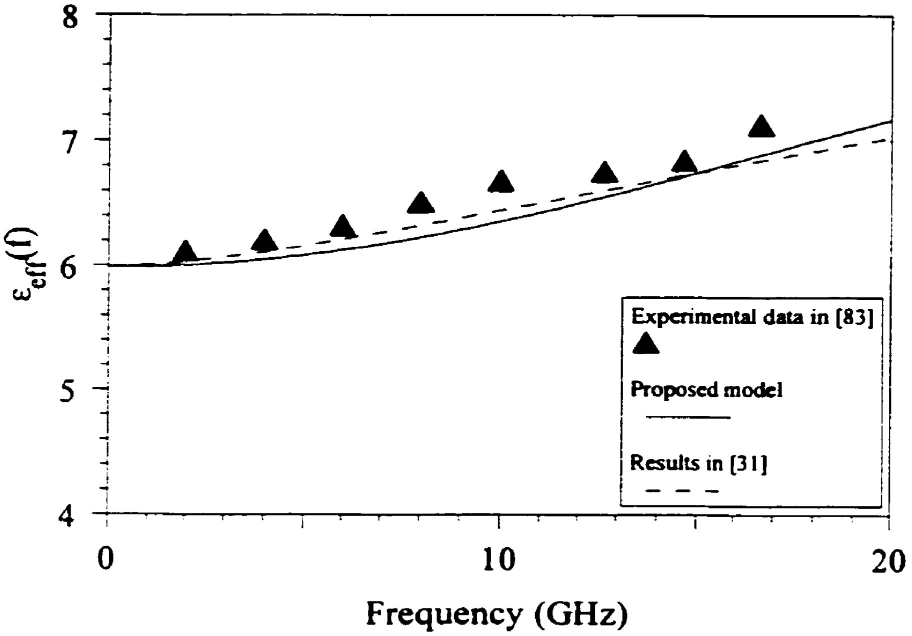

Fig. 4-48. Effective dielectric constant versus frequency for the microstrip in Fig. 4-47.

Maximum error	Standard deviation	Average error
1.882%	1.141	1.054%

Table 4-43. Comparison with Kobayashi's model [31] for the microstrip in Fig. 4-47.

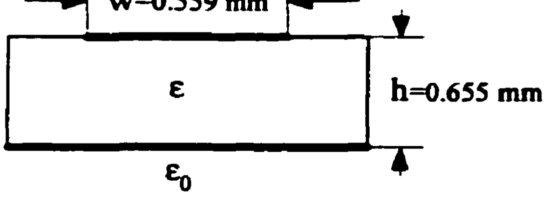

Fig. 4-49. Microstrip geometry in [84].

Substrate	w(mm)	h(mm)	w/h	ε_r	$\varepsilon_{eff}(0)$
Alumina	0.559	0.655	0.853	9.8	6.476

Table 4-44. Data for the microstrip in Fig. 4-49.

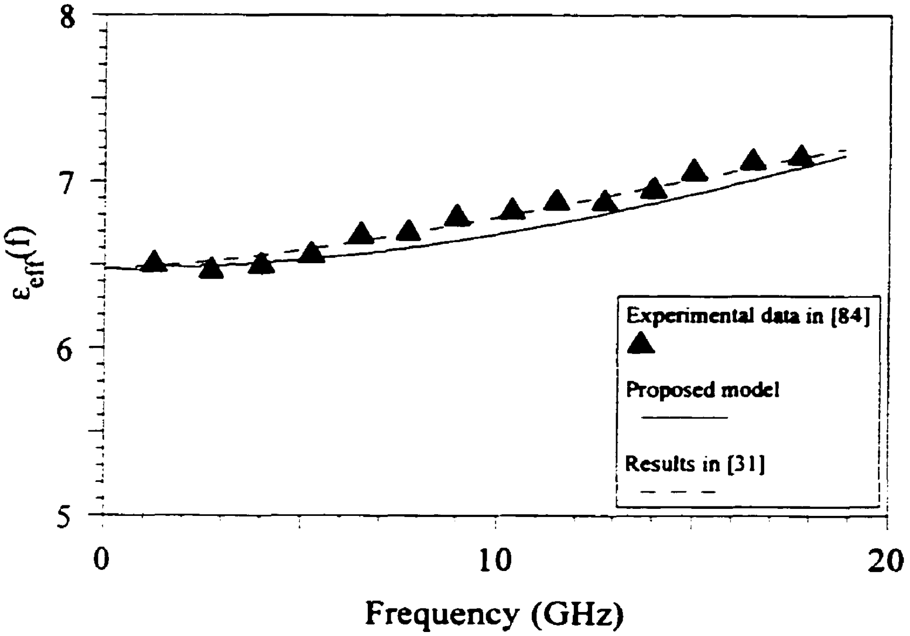

Fig. 4-50. Effective dielectric constant versus frequency for the microstrip in Fig. 4-49.

Maximum error	Standard deviation	Average error
-1.575%	1.157	1.080%

Table 4-45. Comparison with Kobayashi's model [31] for the microstrip in Fig. 4-49.

As it can be seen from the results presented, the best accuracy is obtained for $w/h > 1$ where the proposed model gives results closer to the experimental data than those from Kobayashi (1988). In order to minimize the errors in calculating the dispersion, it is also important to have an accurate value for $\varepsilon_{eff}(0)$. For the microstrip geometry in Figure 4-51 and Table 4-46, the variational methods give the upper bound of the effective permittivity at zero frequency as $\varepsilon^{s}_{eff}(0) = 6.875$ and the lower bound as $\varepsilon^{l}_{eff}(0) = 6.873$. Wheeler's formula (Wheeler, 1965; Hoffmann, 1987) gives $\varepsilon_{eff}(0) = 6.868$ which is lower than $\varepsilon^{l}_{eff}(0)$ and Hammerstad and Jensen's formula (Hammerstad and Jensen, 1980) gives $\varepsilon_{eff}(0) = 6.900$, which is higher than $\varepsilon^{s}_{eff}(0)$. The dispersion curves based on these results are presented in Figure 4-52.

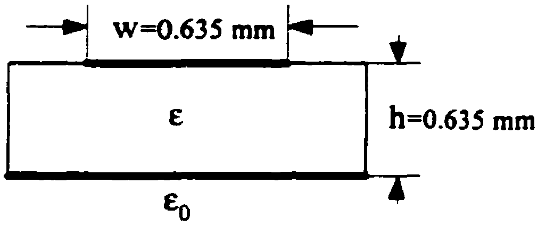

Fig. 4-51. Microstrip geometry in [16].

Substrate	w(mm)	h(mm)	w/h	ε_r	$\varepsilon_{eff}(0)$
Alumina	0.635	0.635	1.0	10.31	6.875

Table 4-46. Data for the microstrip in Fig. 4-51.

For the microstrip geometry in Figure 4-51, a comparison with the results from the full-wave solution (Sonnet, 1999) is also performed for the results from Kobayashi's formula (Kobayashi, 1988) and from the proposed model, and the respective errors are presented in Tables 4-47 and 4-48, respectively, and in Figure 4-52. The CPU time on a HP Vectra 300 *MHz* personal computer is about 1 s for Kobayashi's formula, 13 s for the proposed model and 48 min and 31 s for the full-wave solution.

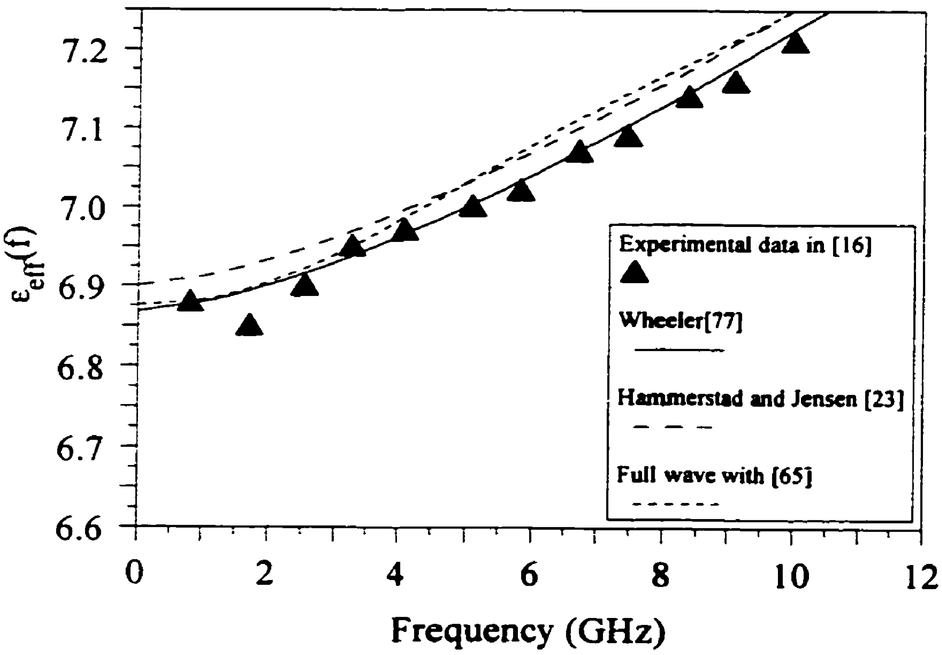

Fig. 4-52. Effective dielectric constant versus frequency for the microstrip in Fig. 4-51.

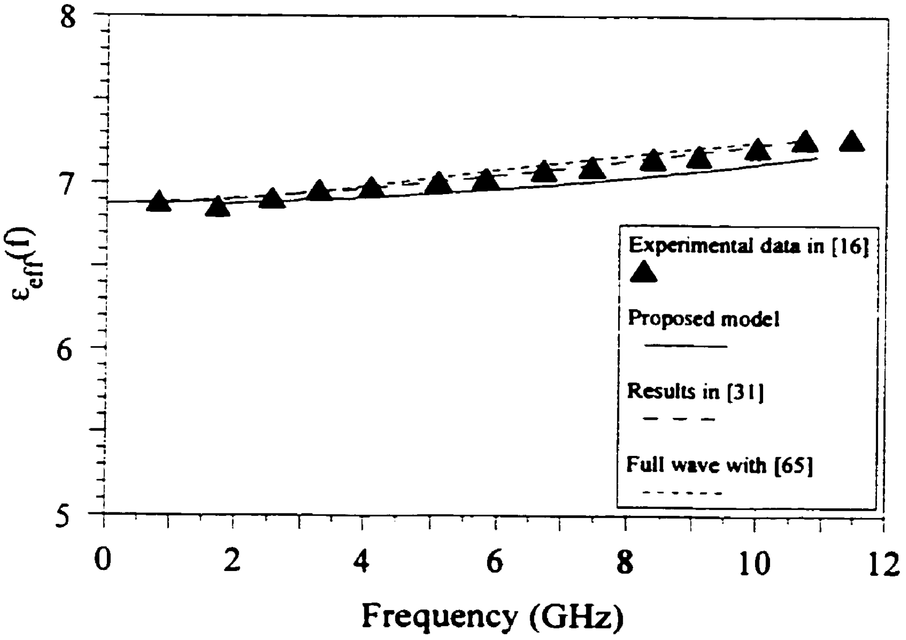

Fig. 4-53. Effective dielectric constant versus frequency for the microstrip in Fig. 4-51.

Maximum error	Standard deviation	Average error
0.428%	0.195	0.119%

Table 4-47. Comparison of Kobayashi's formula and the full-wave solution [65] for the microstrip in Fig. 4-51.

Maximum error	Standard deviation	Average error
1.869%	0.951	0.597%

Table 4-48. Comparison of the proposed method and the full-wave solution [65] for the microstrip in Fig. 4-51.

The range of applicability of the proposed model is determined by that of the two-dimensional equations, which can be used as long as the thickness of the substrate is much less than the wavelength $h << \lambda$. If, for example, h is taken to be ten times less than the wavelength, then

$$h = \frac{\lambda}{10} = \frac{c}{f_{\max}} \frac{1}{10} = \frac{c_0}{f_{\max}} \frac{1}{10\sqrt{\varepsilon_r}} \tag{4.47}$$

where c is the velocity of the wave in the substrate. Hence, the maximum operating frequency is

$$f_{\max} = \frac{2.99 \times 10^7}{h\sqrt{\varepsilon_r}} \ . \tag{4.48}$$

For the structure in Figure 4-7, $h = 0.491\,mm$, $\varepsilon_r = 11.5$ and from (4.48) $f_{\max} = 17.95$ *GHz*. This condition is quite restrictive considering that at 50 *GHz* the dispersion given by the model is less then 2% different from that given by Kobayashi's model (Kobayashi, 1988).

Same general conclusions can be drawn from all the cases considered in this Chapter. The results in Figures 4-7 to 4-42 and Figures 4-47 to 4-53 are computed up to only 18, 12, 8, or 20 *GHz*, respectively, since the experimental results in the literature are available only for these ranges. It should be noted that Kobayashi's formula (Kobayashi, 1988) is an empirical/fitting formula. This is why its agreement with the available experimental data cannot be related logically to various ranges of frequencies. On the other hand, the two-dimensional equations method based on the quasistationary approximation gives in general, as a rule of thumb, better results at low frequencies than at higher frequencies. The advantage of the method presented in the thesis for evaluating the microstrip line dispersion consists in the fact that it can be extended to lossy lines and to the analysis of dispersion of the higher-order modes. This is shown in the next section and in Chapter 5.

The purpose of the study presented in this Section is to show the range of validity and the accuracy of the two-dimensional equations model. This will justify the construction of similar models for lossy structures (Section 4.3) for which the theoretical results presented in the literature are rather limited. Also, the results obtained here will be exploited in Section 5.7 where the higher-order modes of propagation on microstrip lines are investigated. The analysis based on the models presented in the next Section allows an accurate determination of dispersion, attenuation and of the higher order modes at the same time, which cannot be done using existing models.

4.3. Dispersion Model for Lossy Structures

Analysis of attenuation and dispersion along transmission lines is important particularly at high frequencies. In the case of microstrip lines the wave attenuation is caused by the conductor loss, the substrate loss, and the radiation loss. The conductor loss is due to the finite conductivity of the strip material (Itoh, 1987) and is related to the skin depth of the conductor. As well, the current density near the edges of the microstrip is much higher and this also contributes to the wave attenuation. In (Pucel *et al.*, 1968) the conductor loss calculations are based on the incremental inductance rule described by Wheeler (1965). The change in strip inductance due to the skin depth is used in this method for calculating the series resistance in the microstrip model, necessary for the evaluation of the attenuation constant.

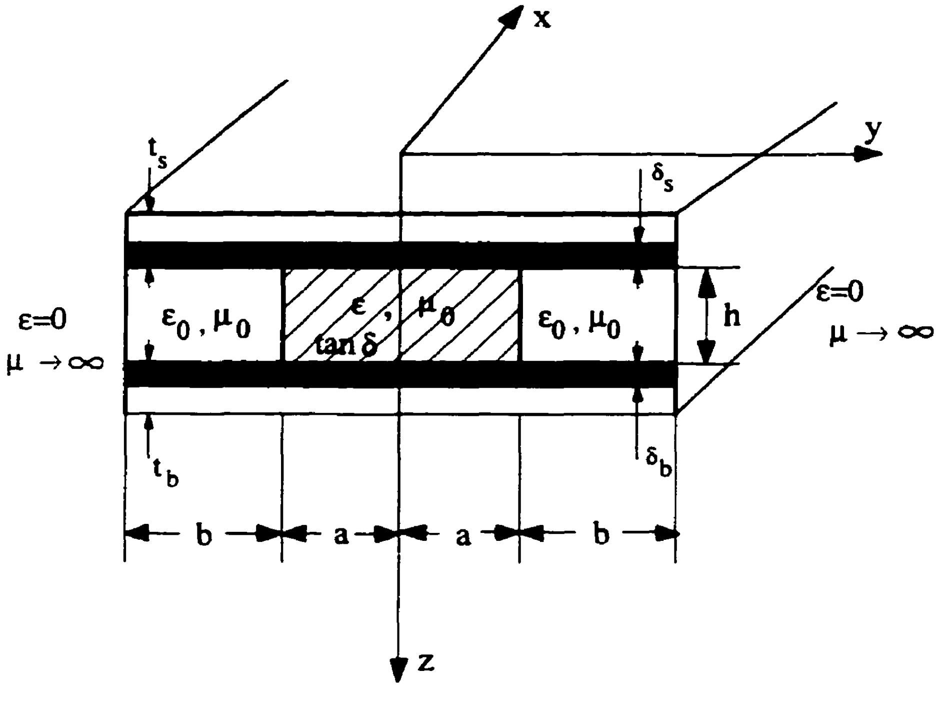

Fig. 4-54. Proposed Model.

For the lossy microstrip geometry shown in Figure 4-5, the proposed model (Tugulea, 1998; Tugulea and Ciric, 1999) has two vertical magnetic walls ($\mu \rightarrow \infty$) and two horizontal walls assumed to be made from the same material as the original microstrip conductors, with the same longitudinal impedance per square. It is also assumed that the thickness of the strip and of the base ground is $t_s > \delta_s$ and $t_b > \delta_b$, where δ_s and δ_b are the skin depths of the strip line and the ground base, respectively. The model (shown in Figure 4-54) has a dielectric between the plates of same permittivity in its central part $y \in (-a, a)$ as in the original microstrip, with a and b determined as in (4.9). The capacitances per unit area for the three regions in the model are

$$C_{s1} = \varepsilon_0 \varepsilon_r \frac{1 - j \tan\delta}{h}, \qquad y \in (-a, a) \tag{4.49}$$

$$C_2 = \frac{\varepsilon_0}{h}, \qquad y \in (a, a+b) \tag{4.50}$$

$$C_3 = \frac{\varepsilon_0}{h}, \qquad y \in (-a-b, -a) \tag{4.51}$$

where $\tan\delta$ is the loss angle.

We choose the system of coordinates as shown in Figure 4-54 and assume the line to be infinitely extended in the x-axis direction. Denoting $U_1(x, y)$ the voltage in region $y \in (-a, a)$, $U_2(x, y)$ the voltage in region $y \in (a, a+b)$ and $U_3(x, y)$ the voltage in $y \in (-a-b, -a)$, the corresponding two-dimensional second order equations are

$$\begin{aligned}
&\frac{\partial^2 U_1}{\partial x^2} + \frac{\partial^2 U_1}{\partial y^2} + \gamma_1^2 U_1 = 0 \\
&\frac{\partial^2 U_2}{\partial x^2} + \frac{\partial^2 U_2}{\partial y^2} + \gamma_2^2 U_2 = 0 \\
&\frac{\partial^2 U_3}{\partial x^2} + \frac{\partial^2 U_3}{\partial y^2} + \gamma_3^2 U_3 = 0
\end{aligned} \tag{4.52}$$

where $-\gamma_1^2 = (R + j\omega L) j\omega C_{s1}$ and $-\gamma_2^2 = -\gamma_3^2 = (R + j\omega L) j\omega C_2$. The attenuated voltages have the following form:

$$U_{1,2,3}(x, y) = V_{1,2,3}(y) e^{\pm\gamma x} \tag{4.53}$$

with $\gamma = \alpha + j\beta$ to be determined. Substituting (4.53) in (4.52) yields

$$
\begin{aligned}
&V_1 + \left(\gamma_1^2 + \gamma^2\right)V_1 = 0 \\
&V_2 + \left(\gamma_2^2 + \gamma^2\right)V_2 = 0 \\
&V_3 + \left(\gamma_2^2 + \gamma^2\right)V_3 = 0
\end{aligned}
\tag{4.54}
$$

whose solutions are

$$
\begin{aligned}
&V_1 = A\cos\alpha_1 y + B\sin\alpha_1 y \\
&V_2 = C\cos\alpha_2 y + D\sin\alpha_2 y \\
&V_3 = E\cos\alpha_2 y + F\sin\alpha_2 y
\end{aligned}
\tag{4.55}
$$

where $\alpha_1^2 = \left(\gamma_1^2 + \gamma^2\right)$ and $\alpha_2^2 = \left(\gamma_2^2 + \gamma^2\right)$ are complex quantities. Imposing the boundary conditions

$$
\begin{aligned}
&U_1(x,a) = U_2(x,a) \\
&U_1(x,-a) = U_3(x,-a) \\
&J_{y1}(x,a) = J_{y2}(x,a) \\
&J_{y1}(x,-a) = J_{y3}(x,-a) \\
&J_{y2}(x,a+b) = 0 \\
&J_{y3}(x,-a-b) = 0\ ,
\end{aligned}
\tag{4.56}
$$

the following transcendental equation is finally derived

$$
\alpha_1 \tan\alpha_1 a + \alpha_2 \tan\alpha_2 b = 0 \tag{4.57}
$$

where α_1 and α_2 are unknown. With C_{x1} and C_2 from (4.49) and (4.50), and the total inductance $L = \mu_0 h + \Delta L$, where (Pucel *et al*, 1968) the additional inductance due to the skin effect $\Delta L = R/\omega$, with $R = 1/\sigma_s \delta_s = \sqrt{\omega\mu_0/(2\sigma_s)}$, σ_s being the conductivity of the strip conductor, we obtain

$$\begin{aligned} \gamma_1^2 &= -j\omega C_1 \left[(R + \omega L \tan\delta) - j(R \tan\delta - \omega L) \right] \\ \gamma_2^2 &= -j\omega C_2 (R + j\omega L) \end{aligned} \tag{4.58}$$

with $C_1 = \varepsilon_0 \varepsilon_r / h$. For a given frequency, equation (4.57) now gives both α and β. The effective relative permittivity $\varepsilon'_{eff}(\omega)$ which characterizes the microstrip dispersion is given by

$$\varepsilon'_{eff}(\omega) = \beta^2 / \beta_0^2 \tag{4.59}$$

where $\beta_0 = \omega / c_0$ with c_0 the speed of light in free space. For the microstrip in Figure 4-55, the dispersion and attenuation determined from (4.57) are presented in Figures 4-56 and 4-57.

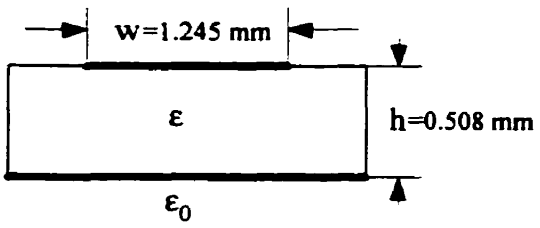

Fig. 4-55. Microstrip geometry in [54].

Substrate	w(mm)	h(mm)	w/h	ε_r	$\varepsilon_{eff}(0)$
Alumina	1.245	0.508	2.45	9.35	6.715

Table 4-49. Data for the microstrip in Fig. 4-55.

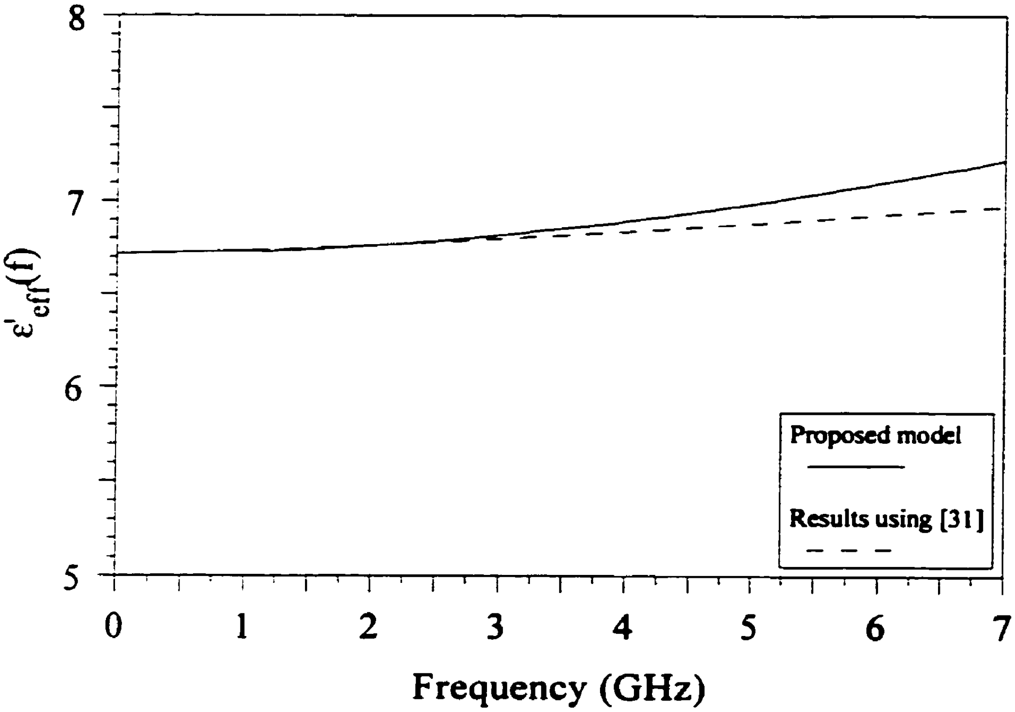

Fig. 4-56. Effective dielectric constant versus frequency for the microstrip in Fig. 4-55.

Maximum error	Standard deviation	Average error
3.31%	0.866	0.361%

Table 4-50. Comparison with Kobayashi's model [31] for the lossy microstrip in Fig. 4-55.

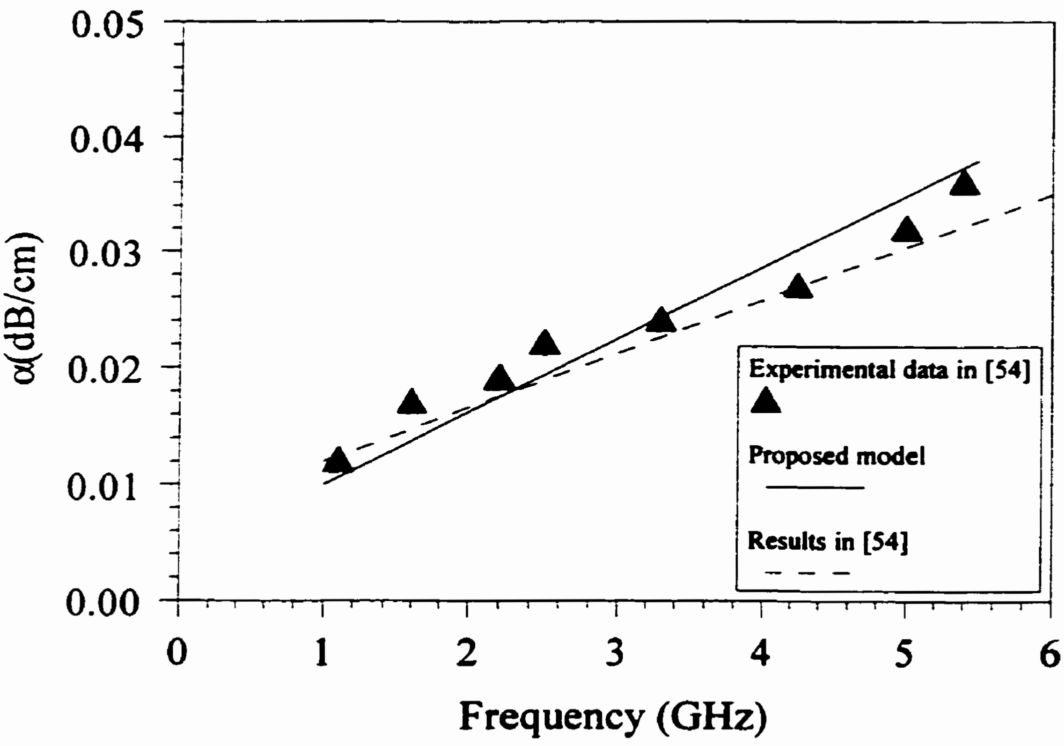

Fig. 4-57. Attenuation constant versus frequency for the microstrip in Fig. 4-55.

For the microstrip in Figure 4-58, the dispersion and attenuation derived from (4.57) are presented in Figures 4-59 and 4-60.

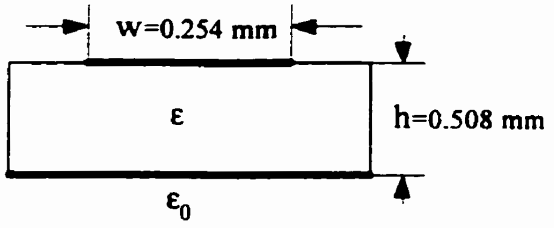

Fig. 4-58. Microstrip geometry in [54].

Substrate	w(mm)	h(mm)	w/h	ε_r	$\varepsilon_{eff}(0)$
Alumina	0.254	0.508	0.5	9.35	5.965

Table 4-51. Data for the microstrip in Fig. 4-58.

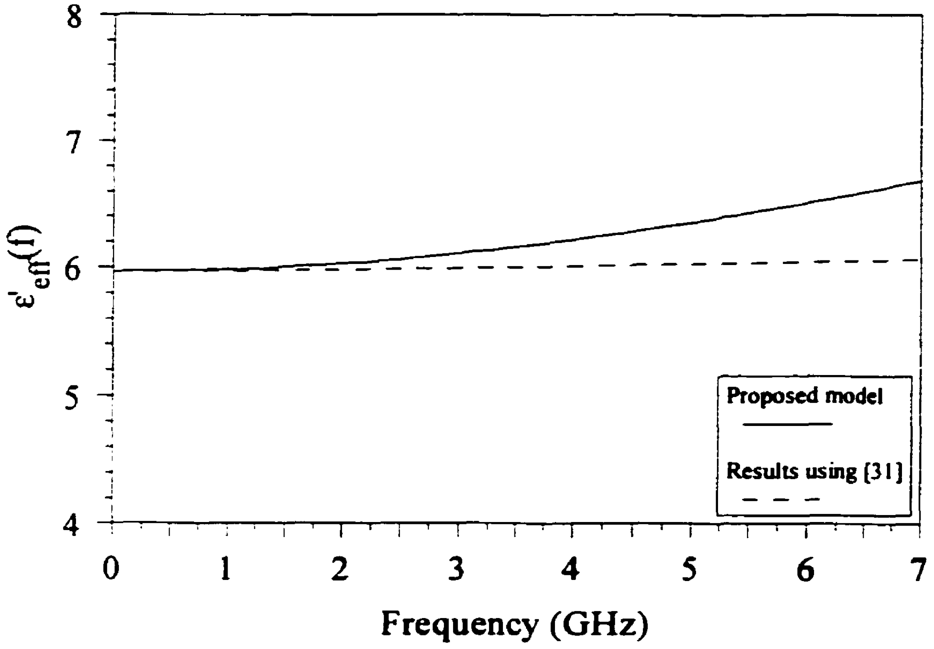

Fig. 4-59. Effective dielectric constant versus frequency for the microstrip in Fig. 4-58.

Maximum error	Standard deviation	Average error
9.066%	2.670	1.248%

Table 4-52. Comparison with Kobayashi's model [31] for the lossy microstrip in Fig. 4-58.

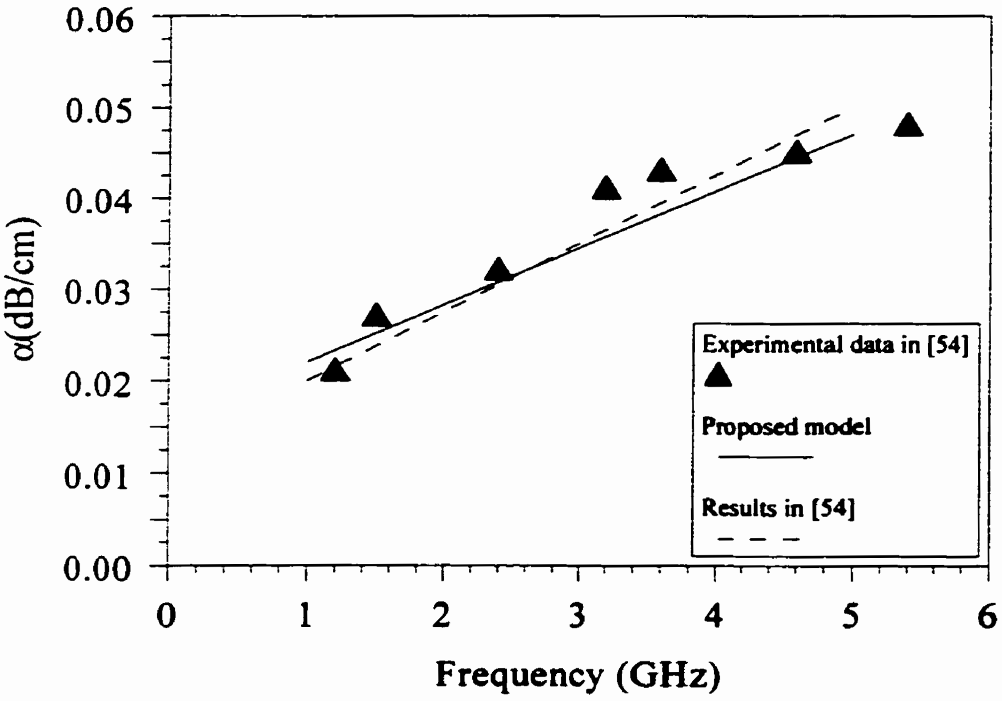

Fig. 4-60. Attenuation constant versus frequency for the microstrip in Fig. 4-58.

The dispersion and attenuation from (4.57) for the microstrip in Figure 4-61 are presented in Figures 4-62 and 4-63.

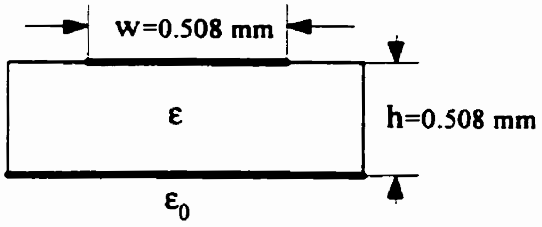

Fig. 4-61. Microstrip geometry in [54].

Substrate	w(mm)	h(mm)	w/h	ε_r	$\varepsilon_{eff}(0)$
Rutile	0.508	0.508	1	105	66.619

Table 4-53. Data for the microstrip in Fig. 4-61.

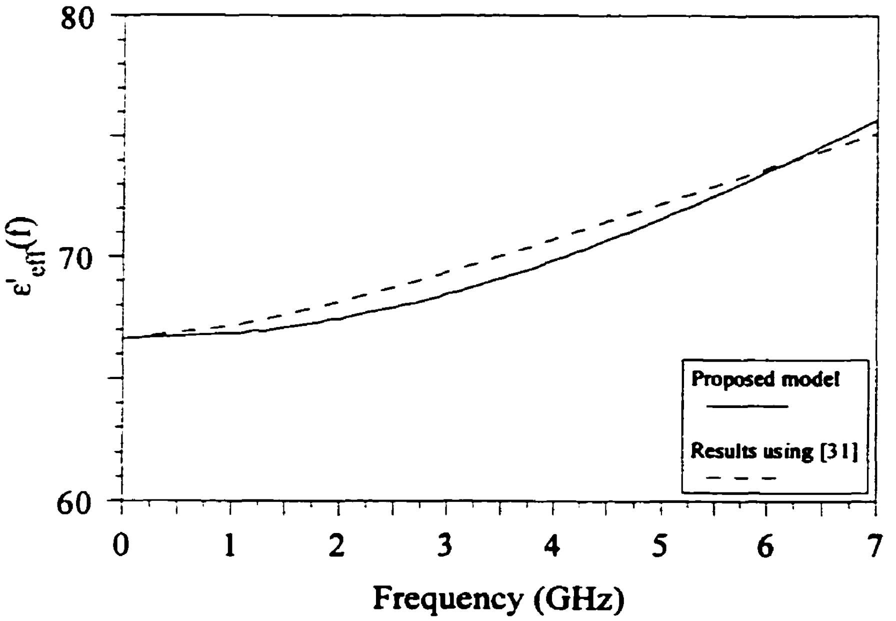

Fig. 4-62. Effective dielectric constant versus frequency for the microstrip in Fig. 4-61.

Maximum error	Standard deviation	Average error
-1.356%	0.551	0.2893%

Table 4-54. Comparison with Kobayashi's model [31] for the lossy microstrip in Fig. 4-61.

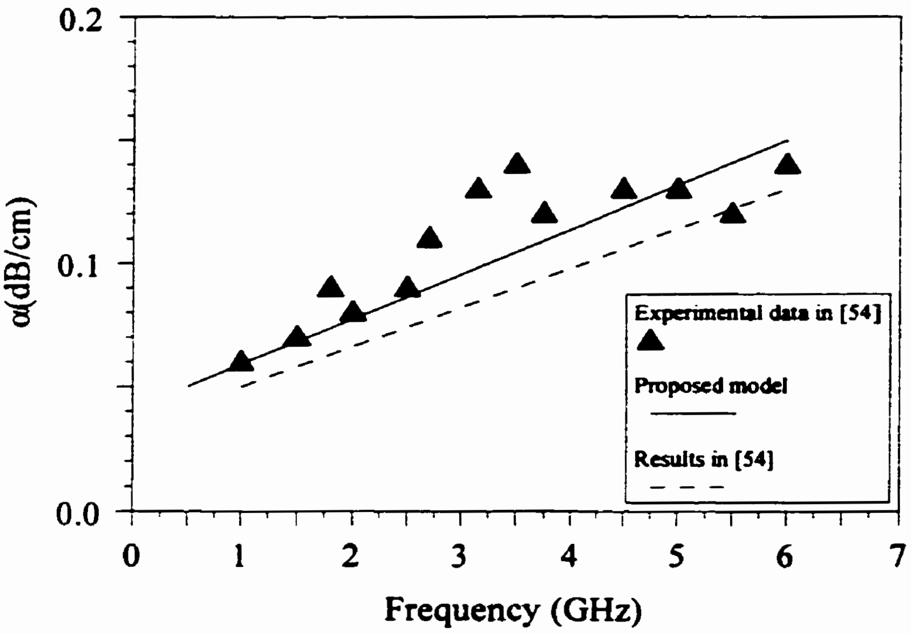

Fig. 4-63. Attenuation constant versus frequency for the microstrip in Fig. 4-61.

For the microstrip geometry in Figure 4-64, the dispersion and attenuation calculated from the proposed model (Equation 4.57) are presented in Figures 4-65 and 4-66.

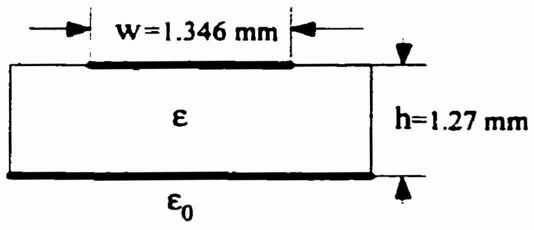

Fig. 4-64. Microstrip geometry in [54].

Substrate	w(mm)	h(mm)	w/h	ε_r	$\varepsilon_{eff}(0)$
Rutile	1.346	1.27	1.059	105	65.835

Table 4-55. Data for the microstrip in Fig. 4-64.

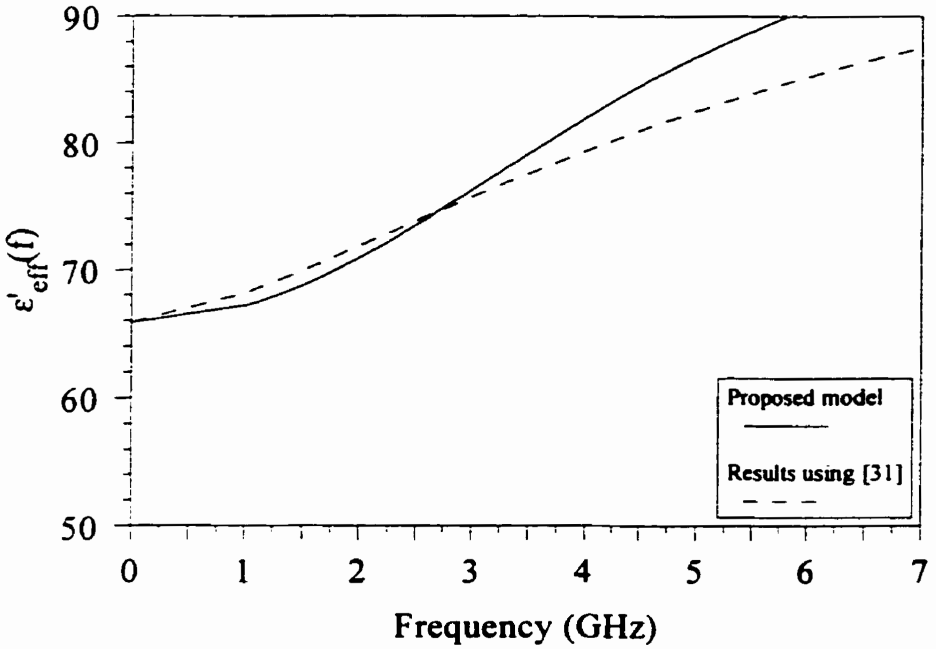

Fig. 4-65. Effective dielectric constant versus frequency for the microstrip in Fig. 4-64.

Maximum error	Standard deviation	Average error
6.32%	2.254	1.097%

Table 4-56. Comparison with Kobayashi's model [31] for the lossy microstrip in Fig. 4-64.

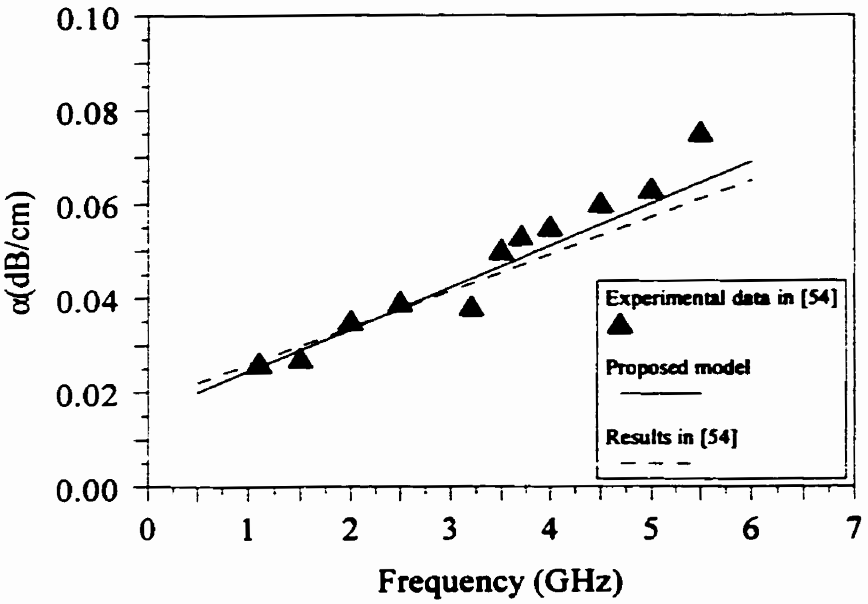

Fig. 4-66. Attenuation constant versus frequency for the microstrip in Fig. 4-64.

The average difference between the attenuation constant calculated with the formula in (Pucel *et al.*, 1968) and that determined using our model is under 3%. The loss angle for Alumina is $\tan\delta = 2.1 \times 10^{-4}$ and it is assumed to be constant over the frequency range considered (Pucel *et al.*, 1968). For Rutile, the loss angle varies with frequency and measurements have to be made in order to calculate the attenuation (Pucel *et al.*, 1968). Pucel *et al.* (1968) indicate that the dielectric losses account for less than 20% of the total attenuation, therefore assuming a constant value for the loss tangent should not affect significantly the final result. The copper conductivity used in calculations is $\sigma_s = 5.81 \times 10^7 S/m$. The attenuation measurements were made with a resonance-Q technique on open-circuit terminated lines. This method is described by Pucel *et al.* (1968) to be "very sensitive to low losses". However, no numerical indication of the accuracy of the method is given by these authors.

In this Section the model presented for the lossless lines in Section 4.2 was extended to the general case of lossy lines. The main advantages of the two-dimensional equations over previously published models consist in the fact that the losses can be easily accounted for in the initial formulation of the problem. The model presented in the thesis has a more rigorous basis than other presentations in the literature and can be applied to all practical microstrips.

CHAPTER 5. HIGHER-ORDER MODES ON MICROSTRIP LINES

5.1. Introduction

The two-dimensional equations for planar structures can also be used in the calculation of the higher-order modes of propagation along microstrip lines. A planar circuit (Okoshi and Miyoshi, 1972) is defined as an electric circuit having dimensions comparable to the wavelength in two directions but a much smaller dimension in the third direction. Microwave integrated circuits, which have replaced the conventional microwave circuits (Hoffmann, 1987), are constructed in a planar form. The transmission systems contain striplines, the most common being the microstrips. As any electrical transmission line, the microstrip is a waveguide where the waves are propagating in an inhomogeneous medium consisting of substrate, conductor, and air.

The exact formulation of the problems relative to planar structures is based on the Maxwell's equations. In a correct formulation, the integration of these equations assumes:

- the existence of the solutions;
- the uniqueness of the existent solutions.

The last two conditions depend on:

- the geometric structure of the conductors and dielectrics;
- the materials characteristics of the conductor and dielectric;
- the excitation modalities of the electromagnetic field;
- the mathematical method used to construct the solution.

A most complete formulation is difficult and not efficient from an engineering viewpoint. Even in the full-wave approach one assumes perfect conductors, piecewise homogeneous dielectrics, and so on, which are in fact approximations. The following simultaneous phenomena should be considered in the formulation of the problem:

- propagation of electromagnetic waves with dispersion;
- standing electromagnetic waves, therefore the resonance;
- loss of energy in conductors and dielectrics, hence the attenuation;

- electromagnetic radiation.

These phenomena bear different weights which finally determine the functionality and the role of the structure:

- in microstrips and striplines the analysis of the wave propagation is the main objective;
- in microwave resonators the filter effects are investigated;
- in microwave antennas the study of radiation is most important.

The geometry of these three categories of devices is different accordingly. For example, the microstrips have longitudinal dimensions much larger than their transverse dimensions, and the resonators and antennas have dimensions which are of the same order of magnitude.

Until microstrip lines were invented, only two systems of transmission of electromagnetic waves existed: transmission lines, based on the theory of telegraphists' equations (for example the coaxial cable), and waveguides (for example the hollow single conductor waveguide) whose theory is based directly on Maxwell's equations. As expected, the theoretical investigations of the new structures started by applying these two acknowledged theories.

The classical waveguide theory, which considers the guide with all the side walls to be perfect conductors ($\sigma \to \infty$) was excluded from the very beginning because it does not admit *TEM* waves (not even at low frequencies).

The transmission line theory based on the existence of *TEM* modes was appealing due to its simplicity, but finally it proved unable to explain the high frequency behavior of the microstrips, for instance the dispersion on a lossless line or the propagation of higher-order modes.

Dispersion, i.e. the dependence of the propagation velocity on frequency, has been accounted for in a simplified manner by considering that the capacitance per unit length varies with the effective dielectric constant $\varepsilon_{eff}(\omega)$. Various quasi-*TEM* models use the inductance per unit length at zero frequency (for non-magnetic substrates) and correct only the capacitance per unit length in terms of frequency. These are approximate theories, which prove their limitations at higher frequencies, being not able to characterize the higher-order modes.

Even the two-dimensional equations for the microwave planar circuits as presented by Radulet and Tugulea (1983) were derived by considering quasistationary conditions, with the

TEM mode as the fundamental mode of propagation. In this Chapter we show that the two-dimensional equations can be used not only to analyze the fundamental mode but also higher-order modes of propagation (Tugulea and Ciric, 1998) and the range of validity of these equations in terms of the operating frequency is determined.

Consider a rectangular waveguide with magnetic vertical walls ($\mu \to \infty$) and perfectly conducting horizontal walls ($\sigma \to \infty$) filled with a lossless homogeneous dielectric as indicated in Figure 5-1. A guide with all the walls considered to be perfect conductors walls admits only *TE* and *TM* modes. The difference between the guide with hybrid walls and the one with only perfectly conducting walls is in the existence in the former of a *TEM* mode as fundamental mode, with *TE* and *TM* modes as higher-order modes. In what follows we assume all the fields to be time-harmonic of same frequency.

5.2. The TEM Mode

The electric and magnetic field intensities for this mode are expressed in the form

$$\begin{aligned} \mathbf{E}(z) &= \mathbf{a}_y E_0 \, \mathrm{e}^{\pm j\beta_0 z} \\ \mathbf{H}(z) &= -\mathbf{a}_x H_0 \, \mathrm{e}^{\pm j\beta_0 z} \end{aligned} \tag{5.1}$$

with the corresponding voltage and current

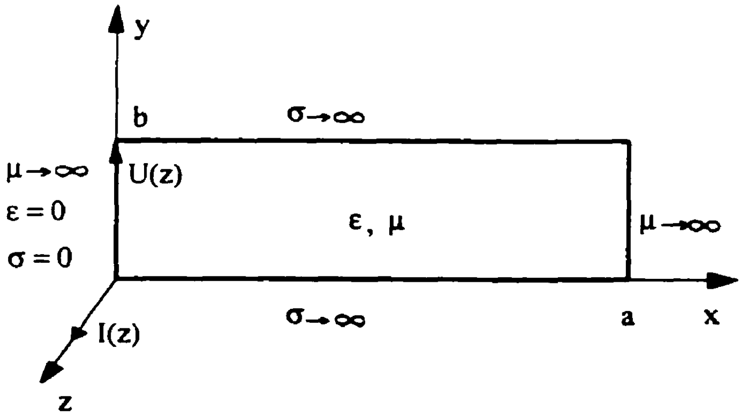

Fig. 5-1. Cross section of a rectangular waveguide with hybrid walls.

$$U(z) = E_0 b\, e^{\pm j\beta_0 z}$$
$$I(z) = H_0 a\, e^{\pm j\beta_0 z} \ . \tag{5.2}$$

The capacitance and the inductance per unit length are defined as

$$C' = \varepsilon \frac{a}{b} \ , \qquad\qquad L' = \mu \frac{b}{a} \ . \tag{5.3}$$

The phase constant β_0 and the characteristic impedance Z_0 are obtained as

$$\beta_0 = \omega \sqrt{L'C'} = \omega \sqrt{\varepsilon\mu} \tag{5.4}$$

$$Z_0 = \sqrt{\frac{L'}{C'}} = \sqrt{\frac{\mu}{\varepsilon}} \left(\frac{b}{a} \right) = \frac{U(z)}{I(z)} \ . \tag{5.5}$$

It can be seen that the Maxwell equations and the transmission line equations, as well as the boundary conditions, are verified by using these expressions.

5.2. TE Modes

The *TE* or *H* modes associated with the model can be derived from a Hertzian magnetic potential (Collin, 1992)

$$\Pi_h = \mathbf{a}_z \psi_h(x, y) e^{\pm j\beta z} \ . \tag{5.6}$$

The field expressions are

$$\mathbf{E} = -j\omega\mu \nabla \times \Pi_h = -j\omega\mu \nabla \left[\psi_h(x, y) e^{\pm j\beta z} \right] \times \mathbf{a}_z$$

$$\mathbf{H} = \nabla \times (\nabla \times \Pi_h) \tag{5.7}$$

where ψ_h satisfies the Helmholtz equation

$$\frac{\partial^2 \psi_h}{\partial x^2} + \frac{\partial^2 \psi_h}{\partial y^2} + k_c^2 \psi_h = 0$$

$$k_c^2 = \omega^2 \varepsilon \mu - \beta^2 = \beta_0^2 - \beta^2 \ . \tag{5.8}$$

The field components are

$$E_x = -j\omega\mu \, \mathrm{e}^{\pm j\beta z} \frac{\partial \psi_h}{\partial y}$$

$$E_y = j\omega\mu \, \mathrm{e}^{\pm j\beta z} \frac{\partial \psi_h}{\partial x}$$

$$H_x = \pm j\beta \, \mathrm{e}^{\pm j\beta z} \frac{\partial \psi_h}{\partial x}$$

$$H_y = \pm j\beta \, \mathrm{e}^{\pm j\beta z} \frac{\partial \psi_h}{\partial y}$$

$$H_z = k_c^2 \, \mathrm{e}^{\pm j\beta z} \, \psi_h(x, y) \tag{5.9}$$

with the boundary conditions

$$E_x(x,0) = E_x(x,b) = 0 \ ; \ x \in (0,a)$$

$$H_y(0,y) = H_y(a,y) = 0 \ ; \ y \in (0,b)$$

$$H_z(0,y) = H_z(a,y) = 0 \ ; \ y \in (0,b) \ . \tag{5.10}$$

The eigenvalue solutions of the equation in ψ_h are all possible products

$$\psi_h(x, y) = \begin{Bmatrix} \sin \gamma x \\ \cos \gamma x \end{Bmatrix} \times \begin{Bmatrix} \sin \delta y \\ \cos \delta y \end{Bmatrix} \tag{5.11}$$

with

$$\gamma^2 + \delta^2 = k_c^2 \tag{5.12}$$

and according to the boundary conditions

$$\begin{gathered}\psi_h(0,y) = \psi_h(a,y) = 0 \\ \frac{\partial\psi_h}{\partial y}(x,0) = \frac{\partial\psi_h}{\partial y}(x,b) = 0\ .\end{gathered} \tag{5.13}$$

We observe that only the combination

$$\psi_h(x,y) = \sin\gamma x\cos\delta y \tag{5.14}$$

verifies the above conditions, therefore

$$\psi_{hm,n} = \sin\frac{m\pi}{a}x\cos\frac{n\pi}{b}y,\qquad m = 1,2,\ldots\ ,\quad n = 0,1,2\ldots\ . \tag{5.15}$$

There is an infinity of solutions defined by the parameters m,n, which satisfy the equation (5.12). Each pair of values defines a $TE_{m,n}$ propagation mode also denoted $H_{m,n}$. From (5.8) the acceptable values of β are

$$\beta_{m,n}^2 = \beta_0^2 - \left[\left(\frac{m\pi}{a}\right)^2 + \left(\frac{n\pi}{b}\right)^2\right]. \tag{5.16}$$

We observe that:

- if $\beta_0^2 > k_c^2$ then $\beta_{m,n}^2 > 0$ and there is a propagation mode;
- if $\beta_0^2 < k_c^2$ then $\beta_{m,n}^2 < 0$ and there is an evanescent mode;

- if $\beta_0^2 = k_c^2$ then $\beta_{m,n} = 0$ and the corresponding ω is a cutoff frequency.

The cutoff frequencies are therefore

$$f_c^{m,n} = \frac{c}{2}\left[\left(\frac{m}{a}\right)^2 + \left(\frac{n}{b}\right)^2\right]^{\frac{1}{2}} , \quad m = 1,2,\ldots \quad , \quad n = 0,1,2\ldots \tag{5.16}$$

where $c = 1/\sqrt{\varepsilon\mu}$. The lowest cutoff frequency for the first propagation mode $H_{1,0}$ corresponds to $m = 1$ and $n = 0$ (for $a \geq b$),

$$f_c^{1,0} = \frac{c}{2a} \tag{5.18}$$

and then

$$\psi_{h1,0} = \sin\frac{\pi x}{a} \ . \tag{5.19}$$

The fields for this mode do not depend on y, no matter what the ratio b/a is. If

$$N = \frac{a}{b} >> 1 \tag{5.20}$$

the guide modeled becomes a planar circuit and we can write

$$f_c^{m,n} = \frac{c}{2a}\left(m^2 + n^2N^2\right)^{\frac{1}{2}} \ . \tag{5.21}$$

For each $m \leq N$ and $n = 0$ we have $f_c^{m,0} \leq f_c^{1,1}$. Thus, these are $N - 1$ $TE_{m,0}$ or $H_{m,0}$ modes defined by the functions

$$\psi_h^{m,0} = \sin\frac{m\pi}{a}x \;, \qquad m = 1,2,\ldots,N-1 \tag{5.22}$$

for which the fields are independent of y,

$$\begin{aligned}
E_x^{m,0} &= 0 \\
H_y^{m,0} &= 0 \\
E_y^{m,0} &= j\omega\mu\, \mathrm{e}^{\pm j\beta z}\frac{m\pi}{a}\cos\frac{m\pi x}{a} \\
H_x^{m,0} &= \pm j\beta\, \mathrm{e}^{\pm j\beta z}\frac{m\pi}{a}\cos\frac{m\pi x}{a} \\
H_z^{m,0} &= k_c^2\, \mathrm{e}^{\pm j\beta z}\sin\frac{m\pi x}{a} \;.
\end{aligned} \tag{5.23}$$

These fields satisfy the Maxwell equations

$$\frac{\partial E_y}{\partial x} = -j\omega\mu H_z \tag{5.24}$$

$$\frac{\partial E_y}{\partial z} = j\omega\mu H_x \tag{5.25}$$

$$-\left(\frac{\partial H_z}{\partial x} - \frac{\partial H_x}{\partial z}\right) = j\omega\varepsilon E_y \tag{5.26}$$

and observing that on the perfectly conducting walls

$$H_x = -J_{sz} \tag{5.27}$$

$$H_z = J_{sx} \;, \tag{5.28}$$

we have

$$\frac{\partial E_y}{\partial x} = -j\omega\mu J_{sx} \tag{5.29}$$

$$\frac{\partial E_y}{\partial z} = -j\omega\mu J_{sz} \tag{5.30}$$

$$\frac{\partial J_{sx}}{\partial x} + \frac{\partial J_{sz}}{\partial z} = -j\omega\varepsilon E_y \ . \tag{5.31}$$

Multiplying the equations (5.29)-(5.31) with b, the height of the waveguide, and denoting

$$bE_y = U(x,z) \tag{5.32}$$

$$\mu b = L \tag{5.33}$$

$$\frac{\varepsilon}{b} = C \tag{5.34}$$

we obtain

$$-\frac{\partial U}{\partial x} = j\omega L J_{sx} \tag{5.35}$$

$$-\frac{\partial U}{\partial z} = j\omega L J_{sz} \tag{5.36}$$

$$-\left(\frac{\partial J_{sx}}{\partial x} + \frac{\partial J_{sz}}{\partial z}\right) = j\omega C U \ . \tag{5.37}$$

These are just the two-dimensional equations which are valid for the first $N-1$ $TE_{m,0}$ modes $(m \le N-1)$. If, for example, $a/b = N = 5$ then the fundamental TEM mode and four higher-order $TE_{m,0}$ modes, $m = 1,2,3,4$, can be sufficiently rigorously treated with the two-dimensional equations, L and C being the inductance per square and the capacitance per unit area, respectively, defined at zero frequency.

5.4. TM Modes

Consider the Hertzian electric potential (Collin, 1992)

$$\mathbf{\Pi}_e = \mathbf{a}_z \psi_e(x,y)\,\mathrm{e}^{\pm j\beta z} \tag{5.38}$$

The expressions of the fields are

$$\begin{aligned} &\mathbf{E} = \nabla \times (\nabla \times \mathbf{\Pi}_e) \\ &\mathbf{H} = j\omega\varepsilon \nabla \times \mathbf{\Pi}_e = j\omega\varepsilon(\nabla \psi_e \times \mathbf{a}_z) \end{aligned} \tag{5.39}$$

where $\psi_e(x,y)$ satisfies the Helmholtz equation

$$\frac{\partial \psi_e^2}{\partial x^2} + \frac{\partial \psi_e^2}{\partial y^2} + k_c^2 \psi_e = 0 \tag{5.40}$$

with

$$k_c^2 = \omega^2 \varepsilon\mu - \beta^2 = \beta_0^2 - \beta^2 . \tag{5.41}$$

The field components are

$$\begin{aligned} E_x &= \pm j\beta\,\mathrm{e}^{\pm j\beta z} \frac{\partial \psi_e}{\partial x} \\ E_y &= \pm j\beta\,\mathrm{e}^{\pm j\beta z} \frac{\partial \psi_e}{\partial y} \\ E_z &= k_c^2\,\mathrm{e}^{\pm j\beta z}\,\psi_e(x,y) \\ H_x &= +j\omega\varepsilon\,\mathrm{e}^{\pm j\beta z} \frac{\partial \psi_e}{\partial y} \end{aligned}$$

$$H_y = -j\omega\varepsilon\, e^{\pm j\beta z} \frac{\partial \psi_e}{\partial x} \tag{5.42}$$

with the same boundary conditions as for the *TE* modes,

$$\psi_e(x,0) = \psi_e(x,b) = 0 \ , \qquad x \in (0,a) \tag{5.43}$$

$$\frac{\partial \psi_e}{\partial x}(0,y) = \frac{\partial \psi_e}{\partial x}(a,y) = 0 \ , \quad y \in (0,b) \,. \tag{5.44}$$

The only combination that satisfies these conditions is

$$\psi_e(x,y) = \cos\gamma x \sin\delta y \tag{5.45}$$

with

$$\gamma = \frac{m\pi}{a} \ , \qquad \delta = \frac{n\pi}{b} \tag{5.46}$$

or

$$\psi_e = \cos\frac{m\pi x}{a}\sin\frac{n\pi y}{b} \ , \quad m = 0,1,2,\ldots \ , \ n = 1,2,\ldots \tag{5.47}$$

Following the same reasoning as in the *TE* case we obtain again the cutoff frequencies

$$f_c^{m,n} = \frac{c}{2a}\left[m^2 + \left(\frac{a}{b}\right)^2 n^2\right]^{\frac{1}{2}} \equiv \frac{c}{2a}\left(m^2 + n^2 N^2\right)^{\frac{1}{2}}$$

$$m = 0,1,2,\ldots \ , \ n = 1,2,\ldots \tag{5.48}$$

The lowest cutoff frequency is

$$\left(f_c^{0,1}\right)_{TM} = \frac{c}{2a}\left(\frac{a}{b}\right) = N\frac{c}{2a} = N\left(f_c^{1,0}\right)_{TE} . \tag{5.49}$$

Therefore, the cutoff frequencies of the first $N-1$ TE modes are lower than the cutoff frequency of the first TM mode. In conclusion, the two-dimensional theory can be applied to and the cutoff frequencies can be obtained for the first $N-1$ TE modes. The TM modes can not be described by the two-dimensional equations, but these modes appear at much higher frequencies for planar circuits.

5.5. Definition of the Effective Dielectric Constant

For the TEM mode the effective dielectric constant ε_{eff} is simply the relative permittivity ε_r of the material filling the waveguide and

$$\beta_0 = \frac{\omega}{c} = 2\pi f\sqrt{\varepsilon\mu} . \tag{5.50}$$

For the higher-order modes the phase constant is

$$\beta_{m,n} = \frac{\omega}{c_{m,n}} \tag{5.51}$$

with the phase velocity

$$c_{m,n} = \frac{\omega}{\beta_{m,n}} = \frac{2\pi f}{\left(\beta_0{}^2 - k_{cm,n}^2\right)^{1/2}} . \tag{5.52}$$

Therefore

$$\beta_{m,n} = \left\{ \frac{\omega^2}{c^2} - \left[\left(\frac{m\pi}{a} \right)^2 + \left(\frac{n\pi}{b} \right)^2 \right] \right\}^{1/2} = \frac{\omega}{c} \left[1 - \left(\frac{f_c^{m,n}}{f} \right)^2 \right]^{1/2} \tag{5.53}$$

for $f > f_c^{m,n}$. With

$$c_{m,n} = 1 \Big/ \sqrt{\varepsilon_0 \varepsilon_{eff}(f) \mu} \tag{5.54}$$

the effective dielectric constant for a mode of cutoff frequency f_c^{mn} is defined as

$$\varepsilon_{eff}^{m,n}(f) = \varepsilon_r \left[1 - \left(\frac{f_c}{f} \right)^2 \right] \tag{5.55}$$

i.e. for higher-order modes $\varepsilon_{eff}(f) < \varepsilon_r$.

In conclusion, only for the *TEM* mode $\varepsilon_{eff}(f) > \varepsilon_{eff}(0) > 1$. For the higher-order modes $\varepsilon_{eff}(f)$ can be greater or smaller than $\varepsilon_{eff}(0)$, and even negative (for evanescent modes).

5.6. Rectangular Waveguide with Hybrid Walls and Inhomogeneous Dielectric

The dispersion model presented in Chapter 4 uses a rectangular waveguide with hybrid walls and different dielectrics. Consider the cross-section of such a waveguide, as shown in Figure 5-2. A *TEM* wave can not propagate in this structure due to the presence of two dielectrics of different permittivities. The analysis of the higher-order modes of propagation in this case is performed in a similar way.

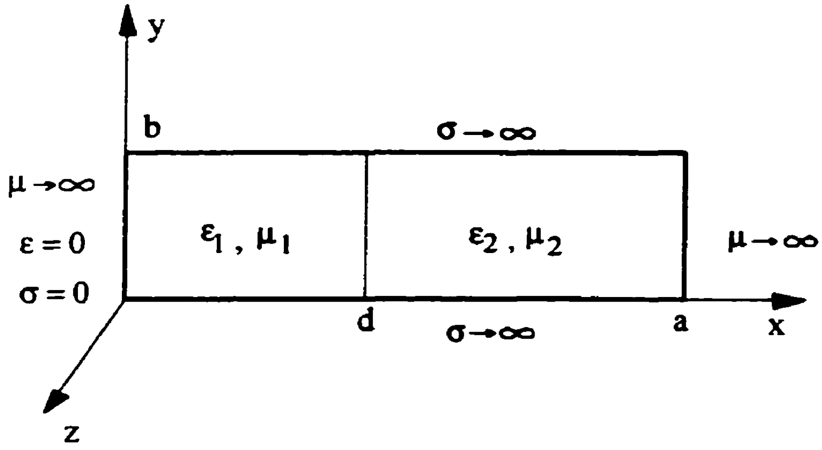

Fig. 5-2. Rectangular waveguide with hybrid walls filled with inhomogeneous dielectric.

The TE Mode

Consider the Hertzian magnetic vector potential

$$\Pi_{1h} = \mathbf{a}_z \psi_1(x,y) e^{\Gamma z}, \qquad x \in (0,d)$$
$$\Pi_{2h} = \mathbf{a}_z \psi_2(x,y) e^{\Gamma z}, \qquad x \in (d,a). \tag{5.56}$$

The fields in the two regions are

$$\mathbf{E}_{1,2} = -j\omega\mu_{1,2} \nabla \times \Pi_{1,2h}$$

$$\mathbf{H}_{1,2} = \nabla \times \left(\nabla \times \Pi_{1,2h} \right) \tag{5.57}$$

where the subscripts 1 and 2 denote the two regions, and the respective functions ψ_1 and ψ_2 satisfy the equations

$$\frac{\partial^2 \psi_1}{\partial x^2} + \frac{\partial^2 \psi_1}{\partial y^2} + k_{c1}^2 \psi_1 = 0$$

$$\frac{\partial^2 \psi_2}{\partial x^2} + \frac{\partial^2 \psi_2}{\partial y^2} + k_{c2}^2 \psi_2 = 0 \tag{5.58}$$

where

$$k_{c1}^2 = \Gamma^2 + \frac{\omega^2}{c_1^2} \;,\quad c_1^2 = \frac{1}{\varepsilon_1 \mu_1}$$

$$k_{c2}^2 = \Gamma^2 + \frac{\omega^2}{c_2^2} \;,\quad c_2^2 = \frac{1}{\varepsilon_2 \mu_2}\,. \tag{5.59}$$

The corresponding field components are

$$E_{x1,2} = -j\omega\mu_{1,2}\, \mathrm{e}^{\Gamma z} \frac{\partial \psi_{1,2}}{\partial y}$$

$$E_{y1,2} = j\omega\mu_{1,2}\, \mathrm{e}^{\Gamma z} \frac{\partial \psi_{1,2}}{\partial x}$$

$$H_{x1,2} = \Gamma \mathrm{e}^{\Gamma z} \frac{\partial \psi_{1,2}}{\partial x}$$

$$H_{y1,2} = \Gamma \mathrm{e}^{\Gamma z} \frac{\partial \psi_{1,2}}{\partial y}$$

$$H_{z1,2} = k_{c1,2}^2 \psi_{1,2}\, \mathrm{e}^{\Gamma z} \tag{5.60}$$

with the boundary conditions

$$
\begin{aligned}
&E_{z1,2}(x,0) = E_{z1,2}(x,b) = 0 && \text{for electric walls} \\
&H_{y1}(0,y) = H_{z1}(0,y) = 0 && \text{for magnetic walls} \\
&H_{y2}(a,y) = H_{z2}(a,y) = 0 && \text{for magnetic walls}
\end{aligned}
\qquad (5.61)
$$

and with the interface conditions at $x = d$

$$
\begin{aligned}
&\varepsilon_1 E_{x1}(d,y) = \varepsilon_2 E_{x2}(d,y) \\
&E_{y1}(d,y) = E_{y2}(d,y) \\
&\mu_1 H_{x1}(d,y) = \mu_2 H_{x2}(d,y) \\
&H_{y1}(d,y) = H_{y2}(d,y) \\
&H_{z1}(d,y) = H_{z2}(d,y) \ .
\end{aligned}
\qquad (5.62)
$$

The solutions of the equations (5.58), which satisfies the boundary conditions in (5.61), have the form

$$
\begin{aligned}
&\psi_1(x,y) = A\sin\alpha x\cos\frac{n\pi}{b}y \\
&\psi_2(x,y) = B\sin\beta(a-x)\cos\frac{n\pi}{b}y\ , \quad n = 0,1,\ldots
\end{aligned}
\qquad (5.63)
$$

where α and β are parameters resulting from equations (5.58),

$$
\begin{aligned}
&-\alpha^2 - \frac{n^2\pi^2}{b^2} + k_{c1}^2 = 0 \\
&-\beta^2 - \frac{n^2\pi^2}{b^2} + k_{c2}^2 = 0 \ .
\end{aligned}
\qquad (5.64)
$$

Imposing the second and the last conditions in (5.62) gives

$$A\alpha\mu_1 \cos\alpha d = -B\beta\mu_2 \cos\beta(a-d)$$
$$Ak_{c1}^2 \sin\alpha d = Bk_{c2}^2 \sin\beta(a-d)\,. \tag{5.65}$$

Dividing the last two equations yields the following eigenvalue transcendental equation

$$\frac{k_{c1}^2}{\alpha\mu_1}\tan\alpha d + \frac{k_{c2}^2}{\beta\mu_2}\tan\beta(a-d) = 0\ . \tag{5.66}$$

The first and fourth conditions in (5.62) would give the condition

$$\varepsilon_1\mu_1 = \varepsilon_2\mu_2 \tag{5.67}$$

which is, generally, not satisfied, for example when $\mu_1 = \mu_2 = \mu_0$ and $\varepsilon_1 \neq \varepsilon_2$. All the conditions from (5.62) can be satisfied if the functions $\psi_{1,2}$ do not depend on y i.e. for $n = 0$, when

$$\psi_1(x,y) = A\sin\alpha x$$
$$\psi_2(x,y) = B\sin\beta(a-x)\,.$$

Therefore the only admissible solution is that of a field with one vertical electric component and two magnetic components H_x and H_z, parallel to the electric walls. This is exactly the structure of the field used in the definition of the two-dimensional equations (as shown in Chapter 2). In a homogeneous guide Equation (5.67) is identically satisfied and this is why higher-order modes with $n \neq 0$ exist. As well, Equation (5.66) is the eigenvalue equation which results directly from applying the two-dimensional equations. Indeed, from (5.64) with $n = 0$, the only possible solution is $\alpha^2 = k_{c1}^2$, $\beta^2 = k_{c2}^2$, and (5.66) becomes

$$\frac{\alpha d}{\mu_1}\tan\alpha d + \frac{\beta d}{\mu_2}\tan\beta(a-d) = 0\,. \tag{5.68}$$

Since $\alpha^2 = \Gamma^2 + \omega^2/c_1^2$ and $\beta^2 = \Gamma^2 + \omega^2/c_2^2$ we have

$$\beta^2 = \alpha^2 + \omega^2\left(\frac{1}{c_2^2} - \frac{1}{c_1^2}\right). \tag{5.69}$$

If $\Gamma^2 = -\omega^2/c^2$ and $\Gamma = -j\omega/c$ there is propagation, and if $c_2 > c_1$, for instance, then $c_2 > c > c_1$ and

$$\begin{aligned} \alpha^2 &= -\frac{\omega^2}{c^2} + \frac{\omega^2}{c_1^2} > 0 \\ \beta^2 &= -\frac{\omega^2}{c^2} + \frac{\omega^2}{c_2^2} < 0 \quad ; \end{aligned} \tag{5.70}$$

with

$$-\beta^2 \equiv k^2 - \alpha^2, \quad \alpha d \equiv \xi \ , \quad (a-d)/d \equiv m \tag{5.71}$$

the following equation is obtained from (5.68)

$$\xi \tan\xi - \frac{\mu_1}{\mu_2}\sqrt{\nu^2 - \xi^2}\tanh m\sqrt{\nu^2 - \xi^2} = 0 \tag{5.72}$$

where $\nu \equiv kd$. Equation (5.72) is identical with the one obtained for the lossless dispersion model if $\mu_1 = \mu_2$. The corresponding field solution is given by

$$\begin{aligned} E_{y1} &= Aj\omega\mu_1 \mathrm{e}^{\Gamma z}\alpha\cos\alpha x \\ E_{y2} &= -Bj\omega\mu_2 \mathrm{e}^{\Gamma z}\beta\cos\beta(a-x) \\ H_{x1} &= \Gamma e^{\Gamma z}\alpha A\cos\alpha x \end{aligned}$$

$$H_{x2} = -\Gamma e^{\Gamma z} \alpha B\beta \cos\beta(a-x)$$
$$H_{z1} = k_{c1}^2 A\sin\alpha x$$
$$H_{z2} = k_{c2}^2 B\sin\beta(a-x)\,. \tag{5.73}$$

When Equation (5.67) is satisfied, the two waves have the same speed in the two dielectrics and higher-order *TE* modes with $n \neq 0$ can propagate. In this case, also a *TEM* can be supported by the structure. Indeed, if $c_1 = c_2 = c$ then $k_{c1}^2 = k_{c2}^2 = 0$ and the solutions are

$$\psi_1 = Ae^{\Gamma z}x + \text{constant}\,; \qquad \psi_2 = Be^{\Gamma z}x + \text{constant} \tag{5.74}$$

with only the field components

$$E_{y1} = E_{y2} = E_0 e^{\Gamma z}\ ;\ \ E_0 = -j\omega\mu_1 A = -j\omega\mu_2 B \Rightarrow \ \mu_1 A = \mu_2 B$$
$$H_{x1} = A\Gamma e^{\Gamma z} \neq H_{x2} = B\Gamma e^{\Gamma z}\,. \tag{5.75}$$

A similar analysis of the guide in Figure 5-2 using the LSE mode (Collin, 1992) leads to the same Equation (5.72).

Since (5.72) is a transcendental equation, one cannot have directly the higher-order modes arranged in the order of increase of their cutoff frequencies. To determine the lowest higher-order mode and its cutoff frequency we use the following procedure. Since the phase velocity of the wave c satisfies the condition $c_2 > c > c_1$, we consider initially the case when the waveguide is filled only with the first dielectric (ε_{r1}) and the speed of the wave is c_1. The corresponding cutoff frequency, with $m = 1$ and $n = 0$, is from (5.21)

$$\left(f_c^{1,0}\right)_1 = \frac{c_1}{2a}\,.$$

Consider then the waveguide filled with the second dielectric (ε_{r2}) and the speed of the wave is now c_2. The corresponding cutoff frequency, with $m = 1$ and $n = 0$ is

$$\left(f_c^{1,0}\right)_2 = \frac{c_2}{2a}.$$

If $\varepsilon_{r1} > \varepsilon_{eff}(f) > \varepsilon_{r2}$ $(c_2 > c > c_1)$ then

$$\left(f_c^{1,0}\right)_2 > \left(f_c^{1,0}\right)_1$$

and the waveguide filled with ε_{r1} has the lowest cutoff frequency.

5.7. Higher-Order Modes

In this Section we show how the model presented in Section 4.2, used for the calculation of the dispersion characteristic of the fundamental mode, can also be employed to find the higher-order modes of propagation and the evanescent modes on microstrip lines.

Equation (4.43) has been applied to determine $\varepsilon_{eff}(f)$ in (4.44), for the fundamental mode of propagation, by using its first root ξ_1. The same Equation (4.43) can be employed to find the higher-order modes of propagation and the evanescent modes from its next roots ξ_k.

The following procedure has been implemented and illustrated considering the example in Figure 5-3. For given values of frequency, starting from $f = 0$, we find solutions of Equation (4.43). As seen in Figures 5-4 to 5-6, the first root ξ_1 is found always in the interval $0 < \xi_1 < \pi/2$. This corresponds to a *TEM* mode with zero cutoff frequency, which is the fundamental mode of propagation. If no other root (intersection) occurs for which $\xi \tan\xi > 0$, then all the other intersections ($\xi_2, \xi_{3,...}$) correspond to evanescent modes (as in Figure 5-4).

On the other hand, if there are two or more roots of Equation (4.43) for which $\xi \tan\xi > 0$, then the first solution ξ_1, corresponds to the fundamental mode and the others to the higher-order propagation modes; the subsequent roots, for which $\xi \tan\xi < 0$, correspond to evanescent modes (see Figures 5-5, 5-6).

For a given f a set $\xi_1, \xi_{2,..}$ is determined. The first root ξ_1 substituted in (4.44) gives $\varepsilon_{eff}(f)$ for the fundamental mode. The second root ξ_2 when substituted in (4.44) gives $\varepsilon_{eff}(f)$ for the first higher-order mode (if $\xi \tan\xi > 0$). Thus, by repeating the procedure described, the curves in Figure 5-7 are obtained for the frequency range considered.

One can distinguish two cases. In the first case, when the quantity under the square root in (4.43) is positive or zero, $k^2 - \xi^2 \geq 0$, the first solution will give the fundamental mode, all the others will give higher-order propagation modes. In the second case, when $k^2 - \xi^2 < 0$ the square root (4.43) becomes imaginary and with

$$\sqrt{k^2 - \xi^2} \tanh\left(m\sqrt{k^2 - \xi^2}\right) = -\sqrt{\xi^2 - k^2} \tan\left(m\sqrt{\xi^2 - k^2}\right)$$

the equation becomes

$$\xi \tan\xi + \sqrt{\xi^2 - k^2} \tan\left(m\sqrt{\xi^2 - k^2}\right) = 0 \ . \tag{5.76}$$

All solutions of (5.76) correspond to evanescent modes. Equations (4.43) and (5.76) admit as a solution $\xi = \pi$ which corresponds to the cutoff frequency of the first higher-order mode, as illustrated for $f = 14.15\ GHz$ in Figure 5-5. With $k = \omega a\sqrt{\varepsilon_0 \mu_0 (\varepsilon_r - 1)}$ (from Section 4.2), we obtain for $\xi = \pi$ the cutoff frequency for the first higher-order mode, *TE₁,₀*, as

$$f_{TE_{1,0}} = \frac{1}{2a\sqrt{\varepsilon_0 \mu_0}\sqrt{(\varepsilon_r - 1)}} \tag{5.77}$$

where $a = \eta_0 h / \left(Z_c (m+1)\sqrt{\varepsilon_{eff}(0)}\right)$ as calculated from (4.9). The cutoff frequency for the *m* higher-order mode, $TE_{m,0}$ is

$$f_{TE_{m,0}} = m f_{TE_{1,0}} \tag{5.78}$$

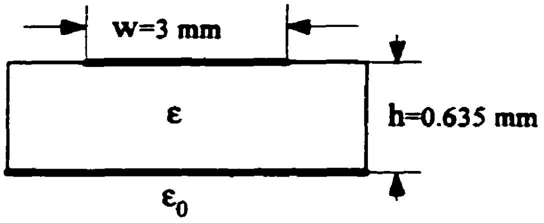

Fig. 5-3. Microstrip geometry in [12].

Substrate	w(mm)	h(mm)	w/h	ε_r	$\varepsilon_{eff}(0)$
Alumina	3	0.635	4.72	9.8	7.753

Table 5-1. Data for the microstrip in Fig. 5-3.

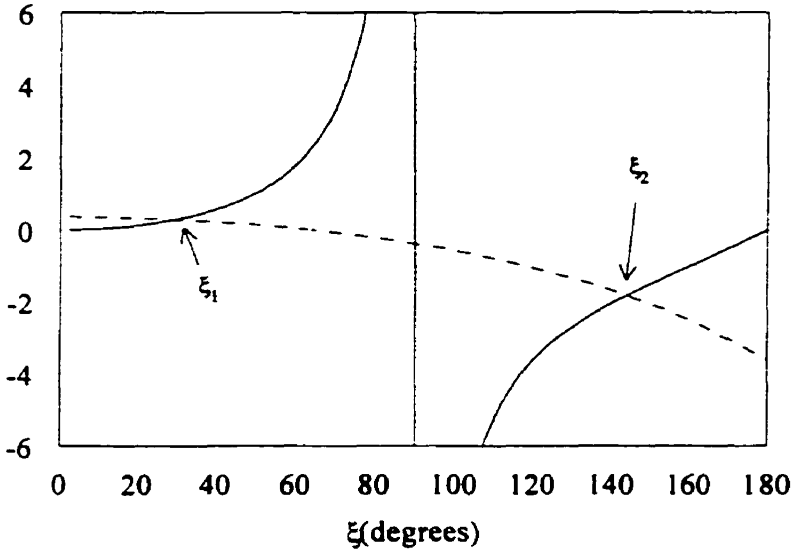

Fig. 5-4. Solving the transcendental equation (4.43) at 5 GHz for the structure in Fig. 5-3 gives ξ for the fundamental mode and evanescent modes:

$\xi \tan\xi$:— ; $\sqrt{k^2-\xi^2}\tanh\left(m\sqrt{k^2-\xi^2}\right)$: - - - ; k=0.173 ; m=0.303.

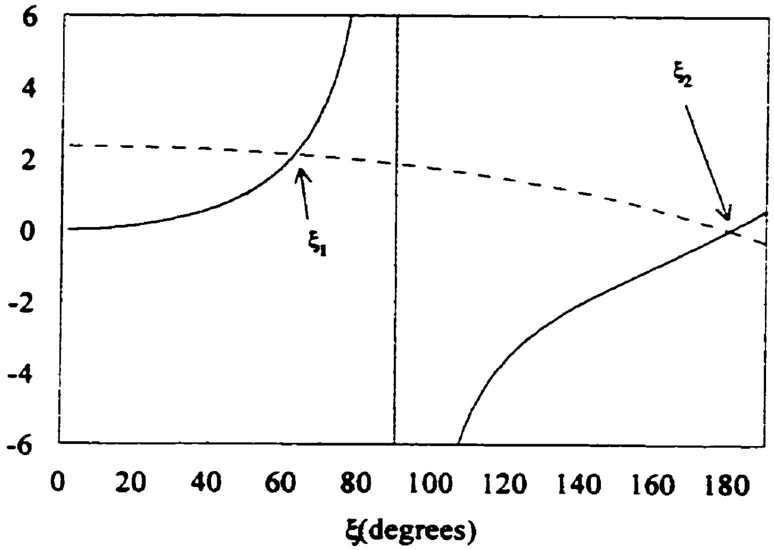

Fig. 5-5. Solving the transcendental equation (4.43) at 14.15 GHz for the structure in Fig. 5-3 gives ξ for the fundamental mode and for the cutoff frequency of the first higher-order mode:

$\xi \tan\xi$: — ; $\sqrt{k^2-\xi^2}\tanh\left(m\sqrt{k^2-\xi^2}\right)$: - - - ; k=0.489; m=0.303.

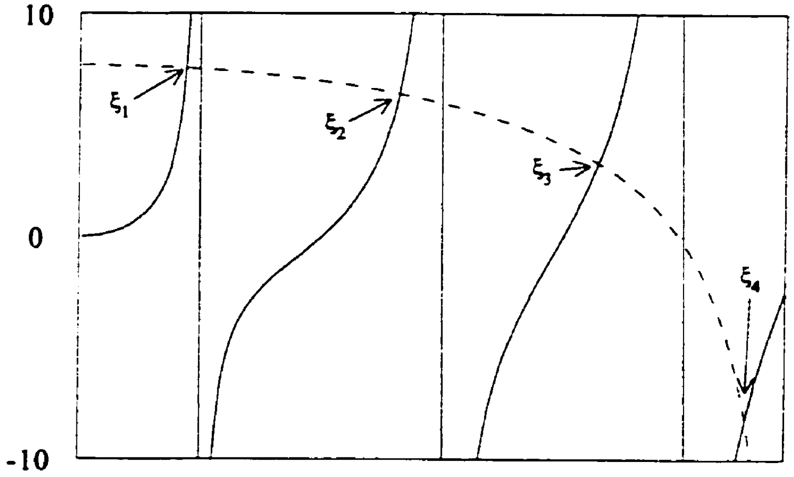

Fig. 5-6. Solving the transcendental equation (4.43) at 35 GHz for the structure in Fig. 5-3 gives ξ for the fundamental mode, for the first two higher -order modes, and for evanescent modes:

$\xi \tan\xi$: — ; $\sqrt{k^2-\xi^2}\tanh\left(m\sqrt{k^2-\xi^2}\right)$: - - - ; k=1.211; m=0.303

For the structure in Figure 5-3, the formula (5.77) gives $f_{TE_{1,0}} = 14.09$ GHz. The formula given by Hoffmann (1987) for "a quick, rough estimate of $f_{TE_{1,0}}$" is

$$f_{TE_{1,0}} = \frac{c_0 Z_c}{2\eta_0 h} \tag{5.79}$$

where c_0 is the speed of light in free space, η_0 is the free-space impedance, and $Z_c = 18.47\ \Omega$ the characteristic impedance. From (5.79) $f_{TE_{1,0}} = 11.57$ GHz and the difference with respect to the result from the proposed formula (5.77) is

$$error = \frac{11.57 - 14.09}{14.09} \times 100 = -17.8\% \ .$$

The cutoff frequency $f_{TE_{1,0}}$ based on the planar waveguide model (Hoffmann, 1987) is given by

$$f_{TE_{1,0}} = \frac{c_0}{2w\sqrt{\varepsilon_r}} = 15.96 \text{ GHz} \tag{5.80}$$

This time the error is

$$error = \frac{15.96 - 14.09}{14.09} \times 100 = 13.2\% \ .$$

Finally, the cutoff frequency $f_{TE_{1,0}}$ obtained by full-wave analysis (Ermert, 1976) of the structure in Figure 5-3 is $f_{TE_{1,0}} = 14.20$ GHz and the error of our formula with respect to this value is

$$error = \frac{14.09 - 14.20}{14.20} \times 100 = -0.77\% \ .$$

- In Figure 5-7, the dispersion curves for the fundamental and the first two higher-order modes are represented. Only the results obtained from the proposed theory are represented, since they are very close to those from the full-wave solution (Ermert, 1976).

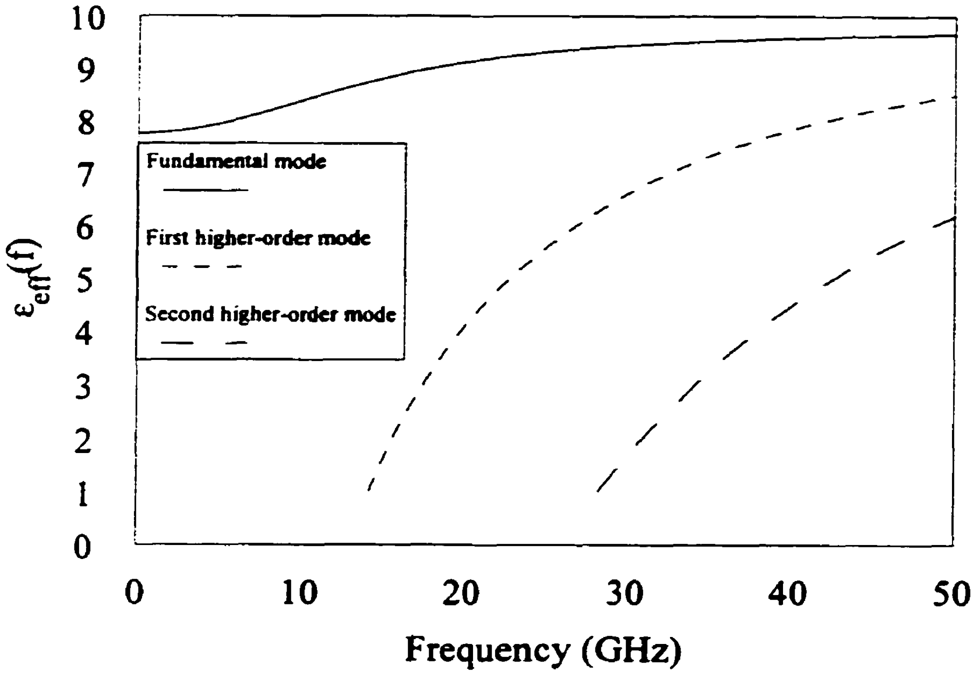

Fig. 5-7. Dispersion characteristics for the fundamental and higher-order modes for the structure in Fig. 5-3.

In order to further validate the proposed model, comparisons with experimental data have been performed. The dispersion measurements for the fundamental and the first two higher-order modes published by Kompa (1975) were made using both the resonator and the sliding-load techniques. Kompa (1975) concluded that utilizing the sliding-load technique, dispersion measurements are possible up to near the cutoff frequencies of the higher-order modes. No indication on the accuracy of measurements is given, but based on the investigation published by Forzley and Bridges (1992), a 3-5 % error is expected when compared to the full-wave solution. Two examples are given in Figures 5-8 and 5-10.

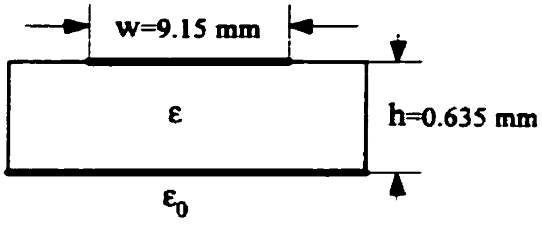

Fig. 5-8. Microstrip geometry in [33].

Substrate	w(mm)	h(mm)	w/h	ε_r	$\varepsilon_{eff}(0)$
Alumina	9.15	0.635	14.40	9.7	8.566

Table 5-2. Data for the microstrip in Fig. 5-8.

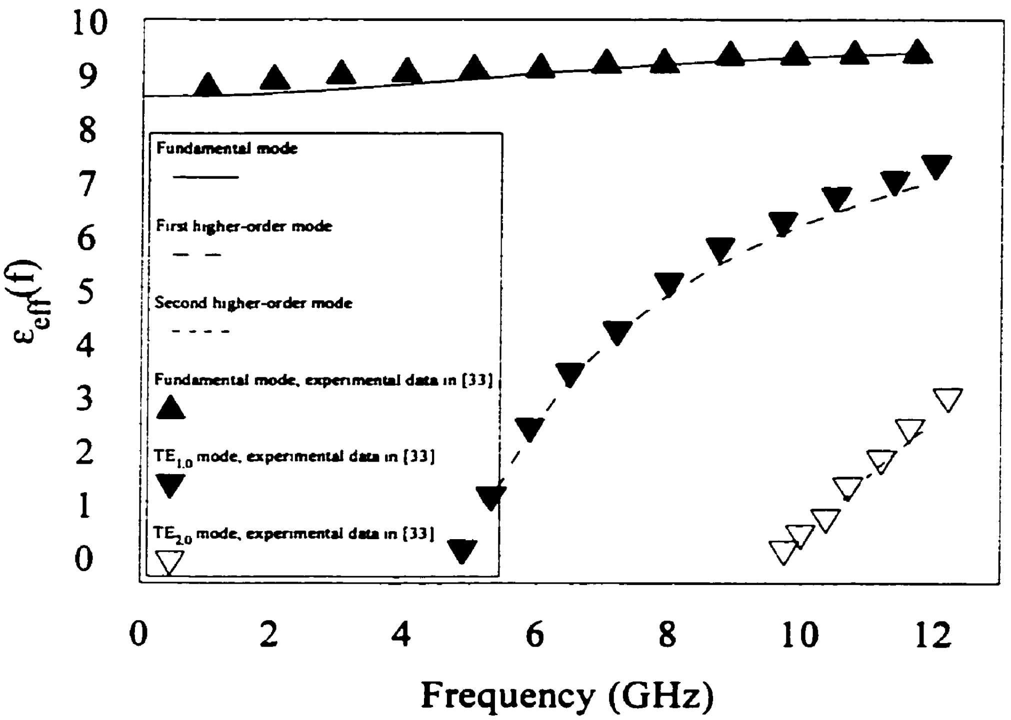

Fig. 5-9. Dispersion curves for the fundamental and higher-order modes for the structure in Fig. 5-8.

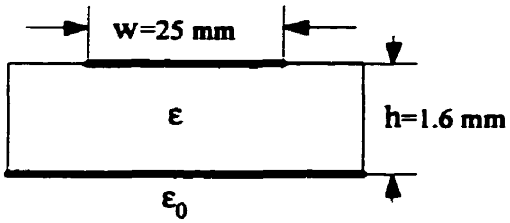

Fig. 5-10. Microstrip geometry in [12].

Substrate	w(mm)	h(mm)	w/h	ε_r	$\varepsilon_{eff}(0)$
Polyguide	25.0	1.6	15.62	2.32	2.163

Table 5-3. Data for the microstrip in Fig. 5-10.

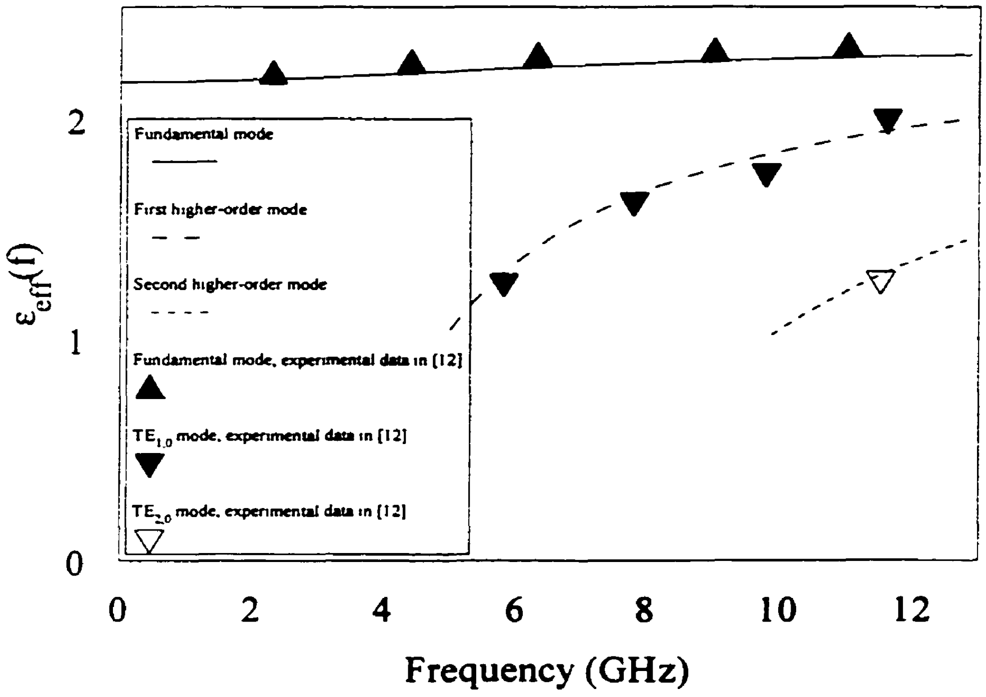

Fig. 5-11. Comparison of the results by the proposed model with experimental data for the structure in Fig. 5-10.

The present model does not allow the analysis of radiation from microstrip lines (Oliner and Lee, 1986). Also the leaky modes can not be obtained from the two-dimensional equations. To analyze leaky modes, full-wave analysis (Mesa *et al.*, 1999; Nghiem *et al.*,1996) has to be used.

The following main conclusions can be finally drawn.

- The two-dimensional equations, derived from the exact Maxwell's equations can be used for the analysis of higher-order $TE_{m,0}$ modes giving faster results than the existing methods (Ermert, 1976) (CPU time on a HP Vectra 300 *MHz* personal computer necessary to calculate the dispersions characteristics of the fundamental and of the first two higher-order modes is 16 seconds).
- The frequency range of applicability of the method presented extends up to the cutoff frequency of the first *TM* mode, which covers the entire technical operating range for practical microstrips (fundamental mode and higher-order $TE_{m,0}$ modes).

CHAPTER 6. MICROSTRIP STEP DISCONTINUITIES

6.1. Excitation of the Higher-Order Modes

Stepped microstrip components are often found in microstrip integrated circuits. They act as impedance transformer, as compensating elements in microstrip power dividers, or are used in LC ladder structures with filtering properties. Thus, knowledge of the scattering matrix of these configurations is of great interest for their design and for the performance analysis of the respective circuits. Earlier authors tackled the discontinuity problem under the assumption of stationary or quasistationary conditions. For this reason the derived results are only valid in the lower frequency range. Another approach was to use a parallel-plate waveguide model and a mode-matching procedure in order to determine the scattering parameters (Koster and Jansen, 1986) employing a method of moments solution (Xu *et al.*, 1989). Computer-aided design software such as Sonnet (1999) utilizes a modified method of moments based on Maxwell's equations to perform a three dimensional analysis of planar structures. These methods require a substantial computer time. In this chapter, simple formulas for the scattering parameters of a microstrip step discontinuity, are derived from the two-dimensional telegraphists' equations (Tugulea and Ciric, 2000).

Consider a symmetrical step discontinuity in a microstrip line as shown in Figure 6-1, where $2a$ is the width of the wide microstrip line and $2b$ is the width of the narrow microstrip line. In the case of a lossless, isotropic microstrip, the inductance per square and capacitance per unit area L and C, are constant and the resistance per square and the conductance per unit area, R and G, are zero. In the case $b << a$, let us consider first the surface current density, of frequency ω, injected at the origin, with the corresponding surface density injected at the origin in the form

$$J_{sy}(x,0) = I\delta(x) \tag{6.1}$$

where I is the total current and $\delta(x)$ is the Dirac function.

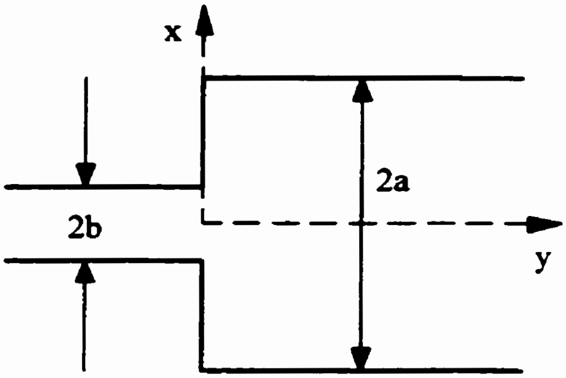

Fig. 6-1. Symmetric step discontinuity.

The voltage and the current will depend on both x and y coordinates, as does the current density (sketched in Figure 6-2). The first order two-dimensional scalar equations are

$$-\frac{\partial U}{\partial x} = j\omega L J_{sx} \tag{6.2}$$

$$-\frac{\partial U}{\partial y} = j\omega L J_{sy} \tag{6.3}$$

$$-\frac{\partial J_{sx}}{\partial x} - \frac{\partial J_{sy}}{\partial y} = j\omega C U \ . \tag{6.4}$$

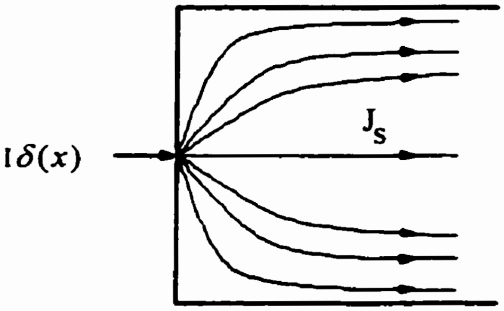

Fig. 6-2. The current density distribution on the wide strip.

The second order two-dimensional equations are

$$\frac{\partial^2 U}{\partial x^2}+\frac{\partial^2 U}{\partial y^2}+\beta^2 U=0 \tag{6.5}$$

$$\frac{\partial^2 J_{sx}}{\partial x^2}+\frac{\partial^2 J_{sx}}{\partial y^2}+\beta^2 J_{sx}=0 \tag{6.6}$$

$$\frac{\partial^2 J_{sy}}{\partial x^2}+\frac{\partial^2 J_{sy}}{\partial y^2}+\beta^2 J_{sy}=0 \tag{6.7}$$

where $\beta=\omega\sqrt{LC}$. The boundary conditions are

$$\begin{gathered} J_{sx}(-a,y)=J_{sx}(a,y)=0 \\ J_{sy}(x,0)=I\delta(x) \end{gathered} \tag{6.8}$$

and we also assume that no inverse waves are present. Using the separation of variables for (6.5) the voltage U, is derived in the form

$$U(x,y)=U_0\,\mathrm{e}^{-j\beta y}+\sum_{k=1}^{\infty}U_k\cos(\nu_k x)\mathrm{e}^{\pm j\gamma_k y} \tag{6.9}$$

where $\gamma_k=\sqrt{\beta^2-\nu_k^2}$. From the first boundary condition in (6.8) the transverse eigenvalue equation is $\sin\nu_k a=0$, hence $\nu_k=k\pi/a$ with $k=1,2,\ldots$. Using the cosine series expansion for $\delta(x)$ and imposing the second boundary condition leads to

$$U(x,y)=I\frac{\omega L}{2a}\left(\frac{\mathrm{e}^{-j\beta y}}{\beta}\mp 2\sum_{k=1}^{\infty}\frac{\mathrm{e}^{\pm j\gamma_k y}}{\gamma_k}\cos\nu_k x\right) \tag{6.10}$$

and from the first order equations

$$J_{sx}(x,y) = \pm j\frac{I}{a}\sum_{k=1}^{\infty} \mathrm{e}^{\pm j\gamma_k y}\frac{\nu_k}{\gamma_k}\sin \nu_k x \tag{6.11}$$

$$J_{sy}(x,y) = \frac{I}{2a}\left(\mathrm{e}^{-j\beta y} + 2\sum_{k=1}^{\infty} \mathrm{e}^{\pm j\gamma_k y}\cos \nu_k x\right). \tag{6.12}$$

To decide on the sign of the exponentials, the nature of the propagation constant γ_k must be studied and the third boundary condition (no inverse waves) must be imposed. The propagation constant is

$$\gamma_k = j\frac{2\pi}{\lambda}\sqrt{\left(\frac{k\lambda}{2a}\right)^2 - 1} \tag{6.13}$$

with λ being the wavelength. The wavelength is assumed to be much greater than the transverse dimensions of the microstrip line (Denlinger, 1971). If $\lambda > 2a$, then $k\lambda/(2a) > 1$. In this case γ_k is imaginary, $\gamma_k \equiv j\beta_k$ and

$$\mathrm{e}^{\pm j(j\beta_k)y} = \mathrm{e}^{\mp\beta_k y} .$$

The plus sign must be considered, otherwise unbounded solutions are obtained for $y \to \infty$. With this observation, the equations (6.10)-(6.12) are now

$$U(x,y) = I\frac{\omega L}{2a}\left(\frac{\mathrm{e}^{-j\beta y}}{\beta} + 2j\sum_{k=1}^{\infty}\frac{\mathrm{e}^{-\beta_k y}}{\beta_k}\cos \nu_k x\right) \tag{6.14}$$

$$J_{sx}(x,y) = \frac{I}{a}\sum_{k=1}^{\infty}\frac{\nu_k}{\beta_k}\mathrm{e}^{-\beta_k y}\sin \nu_k x \tag{6.15}$$

$$J_{sy}(x,y) = \frac{I}{2a}\left(\mathrm{e}^{-j\beta y} + 2\sum_{k=1}^{\infty}\mathrm{e}^{-\beta_k y}\cos \nu_k x\right) \tag{6.16}$$

Only the dominant mode will propagate along the microstrip since the higher-order modes are attenuated exponentially. The less attenuated mode is obtained for $k = 1$. Let y_m be the distance at which the exponent has the value of m (for $m = 3$, the exponential is ≈ 0.05)

$$m = y_m \frac{2\pi}{\lambda}\sqrt{\left(\frac{\lambda}{2a}\right)^2 - 1} \qquad \Rightarrow$$

$$y_m = \frac{m\lambda}{2\pi}\frac{1}{\sqrt{(\lambda/2a)^2 - 1}} = \frac{ma}{\pi}\left[1-\left(\frac{2a}{\lambda}\right)^2\right]^{-\frac{1}{2}} \approx \frac{ma}{\pi}\left[1+\frac{1}{2}\left(\frac{2a}{\lambda}\right)^2 + \ldots\right]$$

For $m = 3$, $y_m \approx a$, therefore at distances equal to the half width of the microstrip the higher-order modes practically vanish. The reference planes are chosen at this distance. For the geometry in Figure 6-1 the reference planes, T-T, are shown in Figure 6-3.

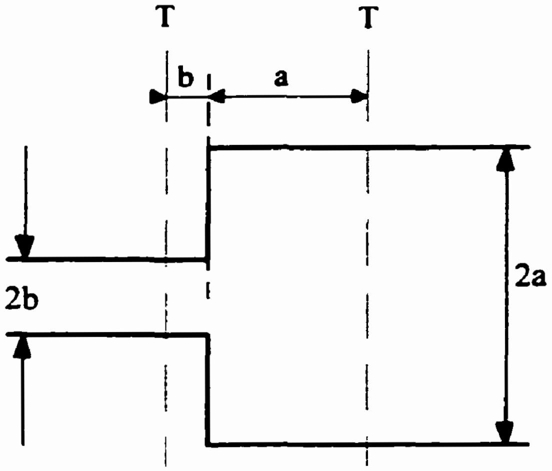

Fig. 6-3. Showing the reference planes for a microstrip step discontinuity.

For $y > y_m$ we have

$$J_{sx} \approx 0 \tag{6.17}$$

$$J_{sy} \approx \frac{I}{2a} e^{-j\beta y} \tag{6.18}$$

$$U(x,y) \approx I \frac{\omega L}{2a\beta} e^{-j\beta y} = \sqrt{\frac{L}{C}} J_{sy} \tag{6.19}$$

6.2. Characterization of the Discontinuity Region

Consider the case in Figure 6-1, where $\lambda >> 2a$ and $b < a$, in which the fundamental mode of propagation is the only one not attenuated. The two-dimensional equations are to be integrated under the following boundary conditions

$$J_{sy}^{(1)}(x,0) = J_{sy}^{(2)}(x,0) \ , \ \ x \in [-b,b] \tag{6.20}$$

$$U^{(1)}(x,0) = U^{(2)}(x,0) \tag{6.21}$$

where the superscripts are *(1)* for the narrow line and *(2)* for the wide line. There is no closed-form analytical solution for this problem because of the transverse eigenfunctions which are different for the two lines

$$\nu_k^{(1)} = \frac{k\pi}{b} \neq \nu_k^{(2)} = \frac{k\pi}{a} \ .$$

An approximate solution can be obtained by considering the current density to be uniformly distributed on the narrow line (see Figure 6-4)

$$J_{sy}^{(1)}(x,y) = J_{sy}^{(2)}(x,0) = \frac{I}{2b} \ , \ \ x \in [-b,b] \ . \tag{6.22}$$

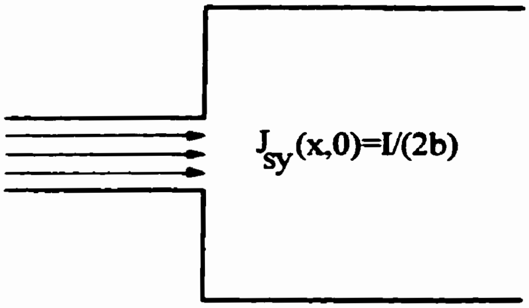

Fig. 6-4. Uniform current density distribution on the narrow microstrip.

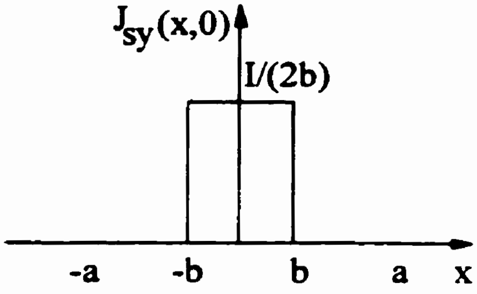

Fig. 6-5. Current density on the narrow microstrip line.

With this assumption, it is now possible to solve the problem analytically, on the wide line, by developing the current distribution shown in Figure 6-5 in a Fourier series as

$$J_{sy}(x,0)=\frac{I}{2a}\left(1+\sum_{k=1}^{\infty}d_k\cos\nu_k x\right) \tag{6.23}$$

where

$$\frac{Id_k}{2a}=\frac{1}{a}\int_{-b}^{b}\frac{I}{2b}\cos\nu_k x dx=\frac{I}{ab\nu_k}\sin\nu_k b\ , \tag{6.24}$$

hence

$$d_k=\frac{2}{b}\frac{\sin\nu_k b}{\nu_k}\ . \tag{6.25}$$

Finally, we have

$$J_{sy}(x,0) = \frac{I}{2a}\left(1 + \frac{2}{b}\sum_{k=1}^{\infty}\frac{\sin \nu_k b}{\nu_k}\cos \nu_k x\right). \tag{6.26}$$

Using again equation (6.9) for U and the first order equation for J_{sy}, we obtain for $y = 0$

$$\frac{I}{2a}\left(1 + \frac{2}{b}\sum_{k=1}^{\infty}\frac{\sin \nu_k b}{\nu_k}\cos \nu_k x\right) = -\frac{1}{j\omega L}\left(-j\beta U_0 - \sum_{k=1}^{\infty}\beta_k U_k \cos \nu_k x\right). \tag{6.27}$$

From the identification of the coefficients we have

$$\frac{I}{2a} = \frac{\beta}{\omega L}U_0 \tag{6.28}$$

and

$$\frac{I}{ab}\frac{\sin \nu_k b}{\nu_k} = \frac{\beta_k}{j\omega L}U_k \ . \tag{6.29}$$

Thus, U_0 and U_k are

$$U_0 = \frac{\omega L I}{2a\beta} \tag{6.30}$$

$$U_k = j\omega L \frac{I}{ab}\frac{\sin \nu_k b}{\beta_k \nu_k} \tag{6.31}$$

and the expression for the voltage is

$$U(x,y) = \frac{\omega L I}{2a\beta}\left(e^{-j\beta y} + \frac{2j\beta}{b}\sum_{k=1}^{\infty}\frac{\sin \nu_k b}{\beta_k \nu_k}e^{-\beta_k y}\cos \nu_k x\right) \tag{6.32}$$

where $\beta_k = \sqrt{\nu_k^2 - \beta^2}$, $\beta = \omega\sqrt{LC}$, and $\nu_k \equiv k\pi/a$. Because in the discontinuity region the voltage is not constant on the whole width of the microstrip, it is necessary to use the complex power in the attempt to find the input impedance seen at the microstrip junction

$$\begin{aligned} S(x,0) &= \int_{-b}^{b} U(x,0) J_{sy}^{*}(x,0) dx = \int_{-b}^{b} U(x,0) \frac{I^{*}}{2b} dx \\ &= \frac{I^{*}}{2b} \frac{\omega L I}{2a\beta} \int_{-b}^{b} \left(1 + \frac{2j\beta}{b} \sum_{k=1}^{\infty} \frac{\sin \nu_k b}{\beta_k \nu_k} \cos \nu_k x \right) dx \\ &= \frac{\omega L I^2}{4ab\beta} \left(2b + \frac{4j\beta}{b} \sum_{k=1}^{\infty} \frac{\sin^2 \nu_k b}{\beta_k \nu_k^2} \right) = Z_i I^2 \ . \end{aligned} \tag{6.33}$$

With

$$\frac{\omega L}{2a\beta} = \frac{\omega L}{2a\omega\sqrt{LC}} = \sqrt{\frac{L/(2a)}{C2a}} = \sqrt{\frac{L'}{C'}} = R_{ca} \tag{6.34}$$

where L' and C' are the parameters per unit length, and R_{ca} is the characteristic resistance of the corresponding one-dimensional transmission line, the input impedance can be written in the form

$$Z_i = R_{ca} \left(1 + j \frac{2\beta}{b^2} \sum_{k=1}^{\infty} \frac{\sin^2 \nu_k b}{\beta_k \nu_k^2} \right) = R_{ca} + jX \tag{6.35}$$

where X is the reactance due to the discontinuity. We observe that

$$X = R_{ca} \frac{2\beta}{b^2} \sum_{k=1}^{\infty} \frac{\sin^2 \nu_k b}{\beta_k \nu_k^2} > 0 \tag{6.36}$$

and therefore X is inductive (Kompa, 1978). By replacing ν_k , β , and β_k , we obtain

$$X = \sqrt{\frac{L}{C}} \frac{2}{2ab^2} \sum_{k=1}^{\infty} \frac{\omega\sqrt{LC}}{\sqrt{k^2\pi^2/a^2 - \omega^2 LC}} \frac{1}{k^2\pi^2/a^2} \sin^2 \frac{k\pi}{a} b \tag{6.37}$$

or

$$X = \frac{\omega La}{\pi^2 b^2} \sum_{k=1}^{\infty} \frac{\sin^2 k\pi b/a}{k^2 \sqrt{k^2\pi^2/a^2 - \omega^2 LC}} \tag{6.38}$$

for $k\pi/a > \omega\sqrt{LC}$. In the case β_k in equation (6.33) becomes imaginary, then the respective terms in the series do not contribute to X, but to the input resistance.

6.3. Asymmetric Step Discontinuity

Consider the asymmetric step discontinuity in Figure 6-6.

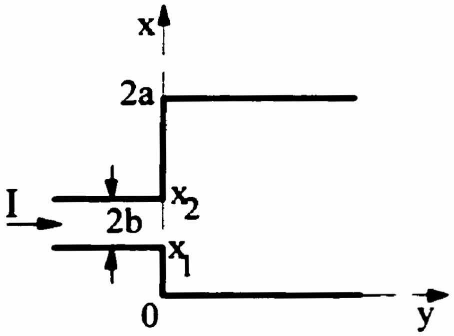

Fig. 6-6. Asymmetric step discontinuity in microstrip line.

The first-order two-dimensional equations are (6.2) and (6.3) and the second-order two-dimensional equation for the voltage is (6.5). We look for a solution of the form

$$U(x,y)=U_0\,e^{-j\beta y}+\sum_{k=1}^{\infty}U_k\,e^{-\beta_k y}\cos\nu_k x \tag{6.39}$$

where $\beta=\omega\sqrt{LC}$, $\beta_k=\sqrt{\nu_k^2-\beta^2}$ and $\nu_k\equiv k\pi/(2a)$. Whenever the ratio b/a is small, we assume that the current is uniformly distributed over the width $2b$ of the narrow line. With the system of Cartesian coordinates chosen as shown in Figure 6-6, the boundary conditions for the region $x\in[0,2a]$, $y\in[0,\infty)$ are expressed as

$$J_{sx}(0,y)=J_{sx}(2a,y)=0 \tag{6.40}$$

$$J_{sy}(x,0)=\begin{vmatrix}\dfrac{I}{2b} & \text{for} & x\in(x_1,x_2)\\ & & \\ 0 & \text{elsewhere} & \end{vmatrix}\;. \tag{6.41}$$

Applying the method of separation of variables to the voltage Equation (6.5) and taking into account the Equations (6.2)-(6.3) yields

$$U(x,y)=\frac{\omega LI}{2a\beta}\left(e^{-j\beta y}+j\frac{4a\beta}{\pi b}\sum_{k=1}^{\infty}\frac{\sin\nu_k b\;\cos\nu_k x_m}{\beta_k k}e^{-\beta_k y}\cos\nu_k x\right) \tag{6.42}$$

where $x_m\equiv(x_1+x_2)/2$. To obtain the impedance Z_t seen at the microstrip junction, we calculate the complex power transferred into the section of width $2a$ as

$$S(x,0)=\int_{x_1}^{x_2}U(x,0)J_{sy}^{*}(x,0)dx=\frac{\omega LI^2}{2a\beta}\left(1+j\frac{2\beta}{b^2}\sum_{k=1}^{\infty}\frac{\sin^2\nu_k b\;\cos^2\nu_k x_m}{\beta_k\nu_k^2}\right)=Z_t I^2 \tag{6.43}$$

with I being the rms value of the current. The input impedance is derived in the form

$$Z_t=R_{ca}+jX \tag{6.44}$$

where R_{ca} is given in (6.34) and X is the reactance due to the discontinuity

$$X = \frac{\omega L}{ab^2}\sum_{k=1}^{\infty}\frac{\sin^2 v_k b\ \cos^2 v_k x_m}{v_k^2 \beta_k}. \tag{6.45}$$

For the special case of a symmetric step discontinuity $x_m = a$ and the reactance expression becomes

$$X = \frac{\omega La}{\pi^2 b^2}\sum_{n=1}^{\infty}\frac{\sin^2 n\pi b/a}{n^2\beta_n}\ , \quad \beta_n \equiv \sqrt{\left(\frac{n\pi}{a}\right)^2 - \omega^2 LC}\ . \tag{6.46}$$

In the case β_k in (6.43) becomes imaginary, then the respective terms in the series do not contribute to X, but to the input resistance. It should be remarked that the series in (6.45) is rapidly convergent. For example, retaining only the first 15 terms in equation (6.45) evaluates the series with an accuracy of 10^{-3}, for a microstrip step (Xu *et al.*, 1989) with $\varepsilon_r = 2.32$, the height of the dielectric substrate $h = 1.58\ mm$, $2a = 16.65\ mm$ and $2b = 4.5\ mm$.

6.4. Numerical Results

In order to validate the formulation presented and the formulas derived in this Chapter, we compare results for the scattering matrix of the equivalent circuit of the step discontinuity with available published data. The equivalent circuit for a step discontinuity is shown in Figure 6-7. The scattering matrix for this circuit is (Feldstein *et al.*, 1967)

$$[S] = \begin{bmatrix} S_{11} & S_{12} \\ S_{21} & S_{22} \end{bmatrix} \tag{6.47}$$

with

$$
\begin{aligned}
S_{11} &= \frac{Z+r-1}{Z+r+1} \\
S_{12} = S_{21} &= \frac{2\sqrt{r}}{Z+r+1} \\
S_{22} &= \frac{Z-r+1}{Z+r+1}
\end{aligned}
\tag{6.48}
$$

with $r = R_{ca}/R_{cb}$ and $Z = jX/R_{cb}$, where R_{cb} is the characteristic resistance of the narrow microstrip section, or

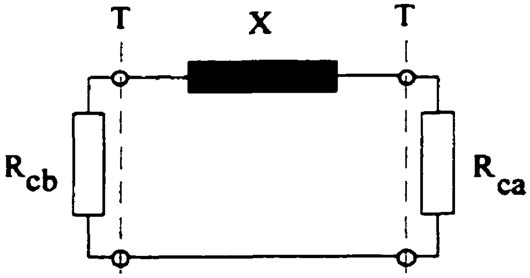

Fig. 6-7. Equivalent circuit for the step discontinuity.

$$
\begin{aligned}
S_{11} &= \frac{R_{ca}^2 - R_{cb}^2 + X^2 + 2jXR_{cb}}{(R_{ca}+R_{cb})^2 + X^2} \\
S_{12} = S_{21} &= \frac{2\sqrt{R_{ca}R_{cb}}\,(R_{ca}+R_{cb}) - j2X\sqrt{R_{ca}R_{cb}}}{(R_{ca}+R_{cb})^2 + X^2} \\
S_{22} &= \frac{R_{cb}^2 - R_{ca}^2 + X^2 + j2XR_{ca}}{(R_{ca}+R_{cb})^2 + X^2}
\end{aligned}
\tag{6.49}
$$

where X is given in Equation (6.38) for the symmetric step and in Equation (6.45), for the asymmetric step.

The magnitude of the transmission coefficient for the symmetrical step configuration on a polyguide substrate shown in Figure 6-8 is plotted in Figure 6-9 against experimental data and full-wave results in (Xu *et al.*, 1989).

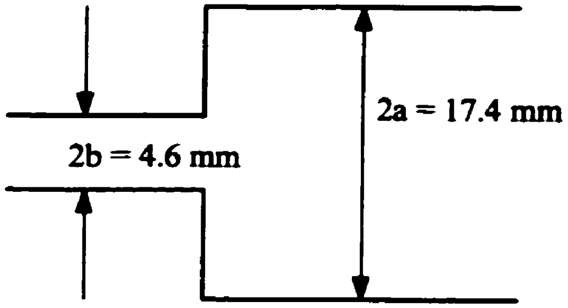

Fig. 6-8. Geometry of the microstrip step discontinuity in [79].

Substrate	2b(mm)	2a(mm)	h^*(mm)	ε_r
Polyguide	4.6	17.4	1.58	2.32

h^* is the dielectric thickness

Table 6-1. Data for the microstrip in Fig. 6-8.

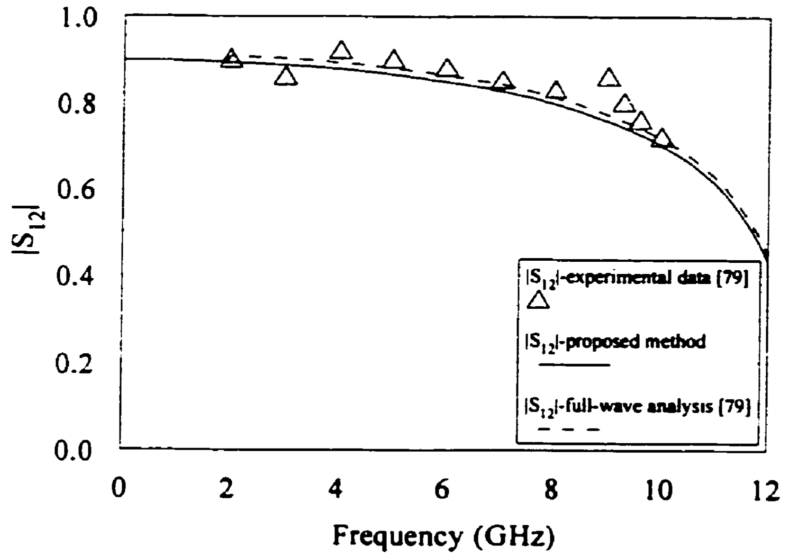

Fig. 6-9. $|S_{12}|$ versus frequency for the microstrip in Fig. 6-8.

The error in Figure 6-9 is less than 1.5 % when compared with the method of moments solution (Xu *et al.*, 1989). The necessary computer time to obtain the solution with (6.49) is *2 seconds* on a HP Vectra 300 *MHz* personal computer.

For the symmetric step discontinuity in Figure 6-10 the transmission coefficient versus frequency is plotted in Figure 6-13. In Figure 6-12 the fundamental, first higher-order, and second higher-order modes for the wide microstrip line ($2a$ in Figure 6-10), are plotted. For the symmetric step, only even-order TE_m modes (m=2, 4, 6,...) can be excited. As seen in Figure 6-13, signal blocking occurs at $f_{TE_2} \approx 23$ GHz which is the cutoff frequency of the second higher-order mode (see Figure 6-12).

For the asymmetric step discontinuity in Figure 6-11, which has the same parameters as the symmetrical step in Figure 6-10, except for an axis displacement of 0.5 mm (thus x_m = 1.5 mm in equation (6.45)), the magnitude of the transmission coefficient is plotted also in Figure 6-13. For the asymmetric step, all TE_m modes (m=1,2,...) are excited and signal blocking occurs at $f_{TE_1} \approx 11.5$ GHz, which is the cutoff frequency of the first higher-order mode (Figure 6-12). Thus, the simplified theory proposed in this thesis generates results in agreement with those published by Baican (1996), Hoffmann (1987), and Kompa (1976).

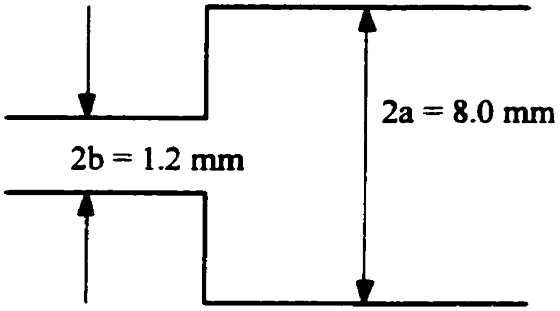

Fig. 6-10. Geometry of the symmetric step discontinuity in [24].

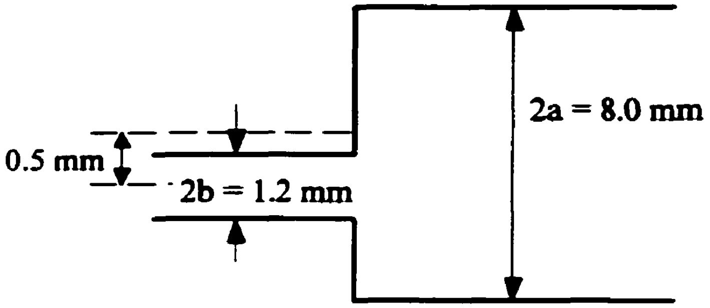

Fig. 6-11. Geometry of the asymmetric step discontinuity in [24].

Substrate	2b(mm)	2a(mm)	h^*(mm)	ε_r
Alumina	1.2	8.0	0.635	9.7

h^* is the dielectric thickness

Table 6-2. Data for the microstrip discontinuities in Figs. 6-10 and 6-11.

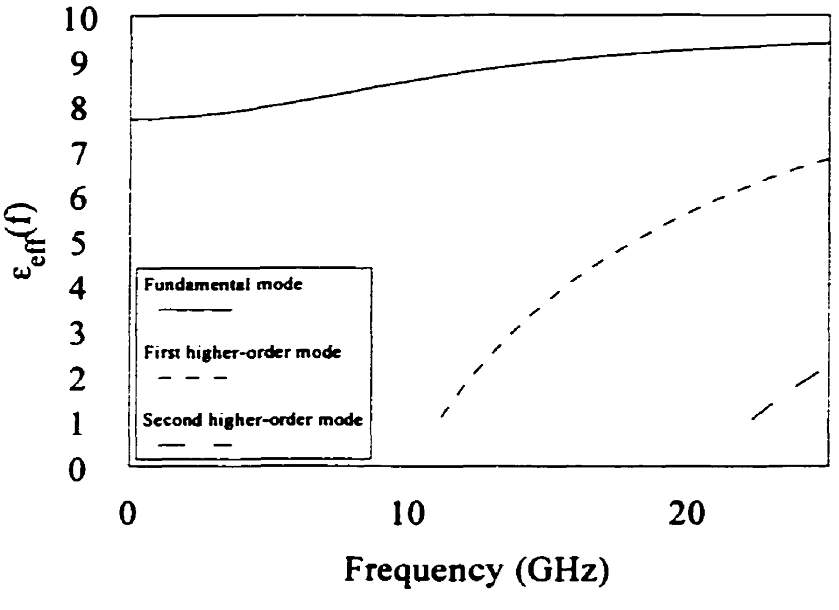

Fig. 6-12. Fundamental, first, and second higher-order modes for the wide microstrip line in Figs 6-10 and 6-11.

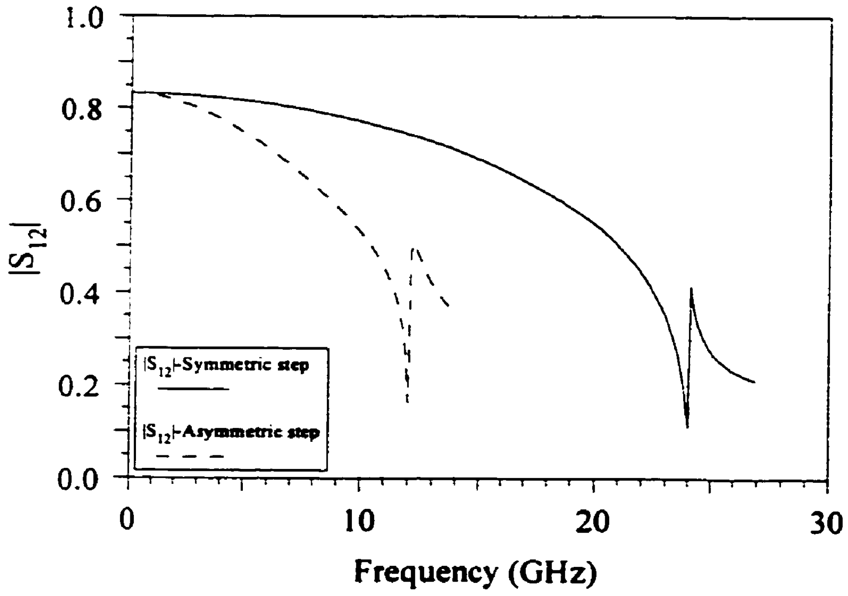

Fig. 6-13. Comparison of the magnitudes of transmission coefficients for the symmetric and asymmetric step discontinuity configurations in Figs. 6-10 and 6-11.

6.5. Cascaded Microstrip Lines

Consider the general case of an asymmetric cascaded microstrip line whose geometry is shown in Figure 6-14.

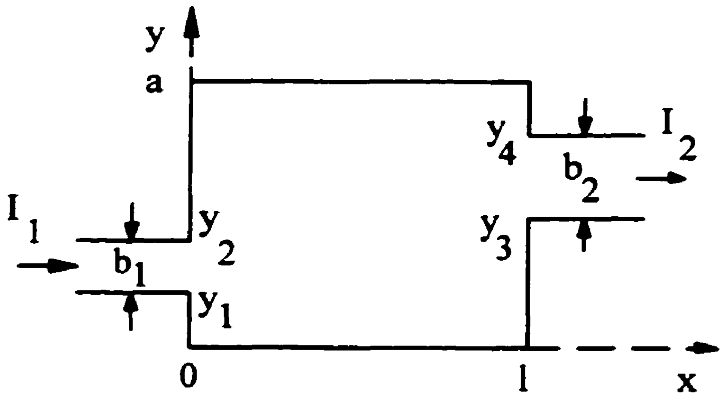

Fig. 6-14. Cascaded microstrip line.

The equations are the same as those employed in Sections 6.2, 6.3, except that this time there are more boundary conditions to be imposed, namely at $x = l$. Assuming that the currents I_1 and I_2 are uniformly distributed on the respective narrow lines, we solve the problem by superposition. The voltage U at any point in $x \in (0,l)$, $y \bullet (0,a)$ is determined as $U = U_1 + U_2$, where $U_1(x,y)$ is the voltage when $I_1 \neq 0$ and $I_2 = 0$, and $U_2(x,y)$ is the voltage when $I_1 = 0$ and $I_2 \neq 0$.

First case: $I_1 \neq 0$; $I_2 = 0$

The equation satisfied by $U_1(x,y)$ is

$$\frac{\partial^2 U_1}{\partial x^2} + \frac{\partial^2 U_1}{\partial y^2} + \beta^2 U_1 = 0 \ . \tag{6.50}$$

Enforcing the boundary conditions

$$J_{1y} = \left(-\frac{1}{j\omega L} \frac{\partial U_1}{\partial y} \right)_{\substack{y=0 \\ y=a}} = 0 \tag{6.51}$$

$$J_{1x} = \left(-\frac{1}{j\omega L} \frac{\partial U_1}{\partial x} \right)_{x=0} = J_{1x}(0, y) \neq 0, \quad y \in (y_1, y_2) \tag{6.52}$$

$$J_{1x}(l, y) = 0 \ , \tag{6.53}$$

the following solution is obtained for the voltage

$$U_1(x, y) = U_{10} \cos \beta(l - x) + \sum_{k=1}^{\infty} \left[U_{1k} \cos \beta_k (l - x) \cos \alpha_k y \right] \tag{6.54}$$

where $\alpha_k = k\pi/a$, $\beta = \omega\sqrt{LC}$ and $\beta_k = \sqrt{\nu_k^2 - \beta^2}$. By enforcing the boundary condition at $x = 0$,

$$J_{1x}(0, y) = I_{10} + \sum_{k=1}^{\infty} I_{1k} \cos \alpha_k y = -\frac{\beta U_{10}}{j\omega L} \sin \beta l - \frac{1}{j\omega L} \sum_{k=1}^{\infty} \beta_k U_{1k} \sin \beta_k l \cos \alpha_k y \,. \tag{6.55}$$

By identification

$$\begin{aligned} U_{10} &= \frac{\omega L I_{10}}{j\beta \sin \beta l} \\ U_{1k} &= \frac{\omega L I_{1k}}{j\beta_k \sin \beta_k l} \end{aligned} \tag{6.56}$$

where I_{10} and I_{1k} are

$$I_{10} = \frac{I_1}{a} \quad ; \qquad I_{1k} = 4 \frac{I_1}{b_1} \frac{\sin \alpha_k \frac{b_1}{2} \cos \alpha_k c_1}{k\pi} \tag{6.57}$$

and $c_1 = (y_1 + y_2)/2$ determines the y coordinate of the middle point of the narrow line (in Figure 6-14). The voltage U_1 is finally derived as

$$U_1(x,y) = -j\left[\frac{\omega L I_{10}}{\beta}\frac{\cos\beta(l-x)}{\sin\beta l} + \sum_{k=1}^{\infty}\frac{\omega L I_{1k}}{\beta_k}\frac{\cos\beta_k(l-x)}{\sin\beta_k l}\cos\alpha_k y\right]. \tag{6.58}$$

<u>Second case:</u> $I_1 = 0$; $I_2 \neq 0$

The solution is of the form

$$U_2(x,y) = U_{20}\cos\beta x + \sum_{k=1}^{\infty} U_{2k}\cos\beta_k x\cos\alpha_k y\ . \tag{6.59}$$

Enforcing the condition at $x = l$ we obtain

$$J_{2x}(l,y) = \left(-\frac{1}{j\omega L}\frac{\partial U_2}{\partial x}\right)_{x=l} = -\frac{1}{j\omega L}\left[-\beta U_{20}\sin\beta l + \sum_{k=1}^{\infty}(-U_{2k}\beta_k\sin\beta_k l\cos\alpha_k y)\right] =$$

$$= I_{20} + \sum_{k=1}^{\infty} I_{2k}\cos\alpha_k y \tag{6.60}$$

where I_{20} and I_{2k},

$$I_{20} = \frac{I_2}{a}\ ;\ \ I_{2k} = 4\frac{I_2}{b_2}\frac{\sin\alpha_k\frac{b_2}{2}\cos\alpha_k c_2}{k\pi} \tag{6.61}$$

and $c_2 = (y_3 + y_4)/2$ determines the y coordinate of the middle point on the other narrow line (in Figure 6-14). After identification

$$U_{20} = \frac{j\omega L I_{20}}{\beta\sin\beta l} \tag{6.62}$$

$$U_{2k} = \frac{j\omega L I_{2k}}{\beta_k \sin \beta_k l} \tag{6.63}$$

and hence

$$U_2(x,y) = j\omega L\left[\frac{I_{20}}{\beta \sin \beta l}\cos \beta x + \sum_{k=1}^{\infty}\frac{I_{2k}}{\beta_k \sin \beta_k l}\cos \beta_k x \cos \alpha_k y\right]. \tag{6.64}$$

By superposition, we obtain

$$U = U_1 + U_2 =$$

$$= j\omega L\left[\frac{I_{20}\cos \beta x - I_{10}\cos \beta(l-x)}{\beta \sin \beta\, l} + \sum_{k=1}^{\infty}\frac{I_{2k}\cos \beta_k x - I_{1k}\cos \beta_k (l-x)}{\beta_k \sin \beta_k l}\cos \alpha_k y\right]. \tag{6.65}$$

The input voltage at $x = 0$ results as

$$U(0,y) = j\omega L\left[\frac{I_{20} - I_{10}\cos \beta l}{\beta \sin \beta l} + \sum_{k=1}^{\infty}\frac{I_{2k} - I_{1k}\cos \beta_k l}{\beta_k \sin \beta_k l}\cos \alpha_k y\right]. \tag{6.66}$$

The output voltage, at $x = l$, is

$$U(l,y) = j\omega L\left[\frac{I_{20}\cos \beta l - I_{10}}{\beta \sin \beta l} + \sum_{k=1}^{\infty}\frac{I_{2k}\cos \beta_k l - I_{1k}}{\beta_k \sin \beta_k l}\cos \alpha_k y\right]. \tag{6.67}$$

Both the input and the output voltage depend on y. Calculating their average value over the width of the respective narrow microstrip lines, at the input and output, yields

$$\tilde{U}_1 = j\omega L\frac{I_{20} - I_{10}\cos \beta l}{\beta \sin \beta l} + \frac{j\omega L}{b_1}\sum_{k=1}^{\infty}\frac{a}{k\pi}\frac{I_{2k} - I_{1k}\cos \beta_k l}{\beta_k \sin \beta_k l}(\sin \alpha_k y_2 - \sin \alpha_k y_1) \tag{6.68}$$

$$\tilde{U}_2 = j\omega L \frac{I_{20}\cos\beta l - I_{10}}{\beta \sin\beta l} + \frac{j\omega L}{b_2}\sum_{k=1}^{\infty}\frac{a}{k\pi}\frac{I_{2k}\cos\beta_k l - I_{1k}}{\beta_k \sin\beta_k l}(\sin\alpha_k y_4 - \sin\alpha_k y_3) \ . \tag{6.69}$$

Finally, the average input and output voltages can be written also as

$$\begin{aligned} \tilde{U}_1 &= z_{11}I_1 + z_{12}I_2 \\ \tilde{U}_2 &= z_{21}I_1 + z_{22}I_2 \end{aligned} \tag{6.70}$$

where

$$z_{11} = -\frac{j\omega L}{\beta a}\cot\beta l - \frac{8j\omega L}{\pi^2}\sum_{k=1}^{\infty}\frac{a}{b_1^2}\frac{\sin^2\alpha_k \frac{b_1}{2}\cos^2\alpha_k c_1}{k^2\beta_k}\cot\beta_k l = jX_{11} \tag{6.71}$$

$$z_{22} = \frac{j\omega L}{\beta a}\cot\beta l + \frac{8j\omega L}{\pi^2}\sum_{k=1}^{\infty}\frac{a}{b_2^2}\frac{\sin^2\alpha_k \frac{b_2}{2}\cos^2\alpha_k c_2}{k^2\beta_k}\cot\beta_k l = jX_{22} \tag{6.72}$$

$$z_{12} = -z_{21} = \frac{j\omega L}{\beta a}\frac{1}{\sin\beta l} + \frac{8j\omega L}{\pi^2}\sum_{k=1}^{\infty}\frac{a}{b_1 b_2}\frac{\sin\alpha_k \frac{b_1}{2}\cos\alpha_k c_1 \sin\alpha_k \frac{b_2}{2}\cos\alpha_k c_2}{k^2\beta_k \sin\beta_k l} = jX_{12} \tag{6.73}$$

The corresponding equivalent circuit is given in Figure 6-15, with Z_{c1} and Z_{c2} being the characteristic impedances of the narrow lines, respectively, for which (Feldstein *et al.*, 1967)

$$z_{11} = z_1 + z_2 \ ; \ z_{22} = -(z_2 + z_3) \ ; \ z_{12} = -z_{21} = -z_2 \ . \tag{6.74}$$

Thus, the circuit parameters z_1, z_2, z_3 are determined from (6.71)-(6.73)

$$\begin{aligned} z_1 &= z_{11} + z_{12} \\ z &= -z_{12} \\ z_3 &= z_{12} - z_{22} \ . \end{aligned} \tag{6.75}$$

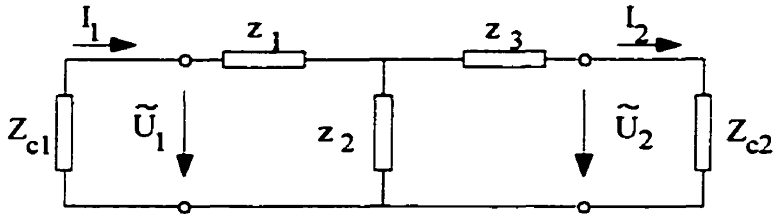

Fig. 6-15. Equivalent circuit showing the association of voltages and currents.

With the following notations

$$Z_1 = \frac{z_1}{Z_{c1}} \; ; \; Z_2 = \frac{z_2}{Z_{c1}} \; ; \; Z_3 = \frac{z_3}{Z_{c1}} \; ; \; r' = \frac{Z_{c2}}{Z_{c1}} \tag{6.76}$$

the entries of the scattering matrix (6.47) for the circuit in Figure 6-15 are

$$S_{11} = \frac{Z_2(Z_1 - 1) + (Z_3 + r')(Z_2 + Z_1 - 1)}{Z_2(Z_1 + 1) + (Z_3 + r')(Z_1 + Z_2 + 1)}$$

$$S_{12} = S_{21} = \frac{2Z_2\sqrt{r'}}{Z_2(Z_1 + 1) + (Z_3 + r')(Z_1 + Z_2 + 1)}$$

$$S_{22} = \frac{Z_2(Z_1 + 1) + (Z_3 - r')(Z_2 + Z_1 + 1)}{Z_2(Z_1 + 1) + (Z_3 + r')(Z_1 + Z_2 + 1)} \tag{6.77}$$

The results obtained using the above analysis were compared with experimental data in (Giannini *et al.*, 1992). Since in (Giannini *et al.*, 1992) there is no indication on the accuracy of the measurements or on the method used to acquire the experimental data, we also generated full-wave results in order to perform a reliable comparison. Except for the resonance regions, in most of the cases considered there is a good agreement between the two sets of results. We conducted the full-wave analysis of the structures in (Giannini *et al.*, 1992) by using two different most recent softwares, Sonnet (1999) and Microwave Office 2000-Version 3.20 (2000) that uses a modified Method of Moments to generate the solution. Both software packages require that the original circuit be enclosed in a box made of perfect conductor walls, as shown in Figure 6-16, where X, Y and H are selected to be much greater then the substrate thickness h. A gridded, variable cell size mesh is automatically generated which places smaller cells in areas that have high variations in current densities, and larger cells in areas with more uniform current variations. The cell size in each direction (ΔX or ΔY) is the dimension in each direction (X or Y) divided by the number of divisions (N_X or N_Y) in that direction. In the rest of this Section we present comparatively results for various structures considered in the literature.

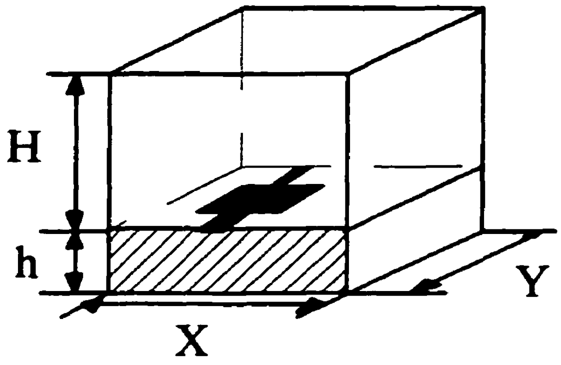

Fig. 6-16. Enclosure used for full-wave analysis [43] and [65].

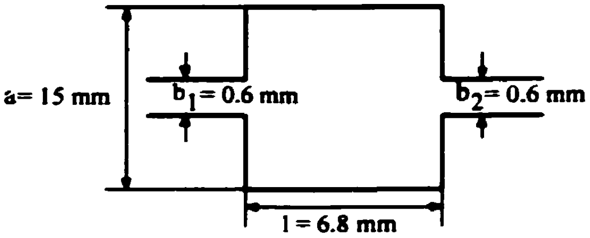

Fig. 6-17. Symmetric microstrip geometry in [17].

Substrate	a(mm)	l(mm)	b_1(mm)	b_2(mm)	h(mm)	ε_r
Alumina	15	6.8	0.6	0.6	0.635	9.7

Table 6-3. Data for the microstrip in Fig. 6-17.

Box Size			Number of Cells		Cell Size	
X(mm)	Y(mm)	H(mm)	N_X	N_Y	ΔX(mm)	ΔY(mm)
20	20	10	200	200	0.1	0.1

Table 6-4. Data used with [43] for the microstrip in Fig. 6-17.

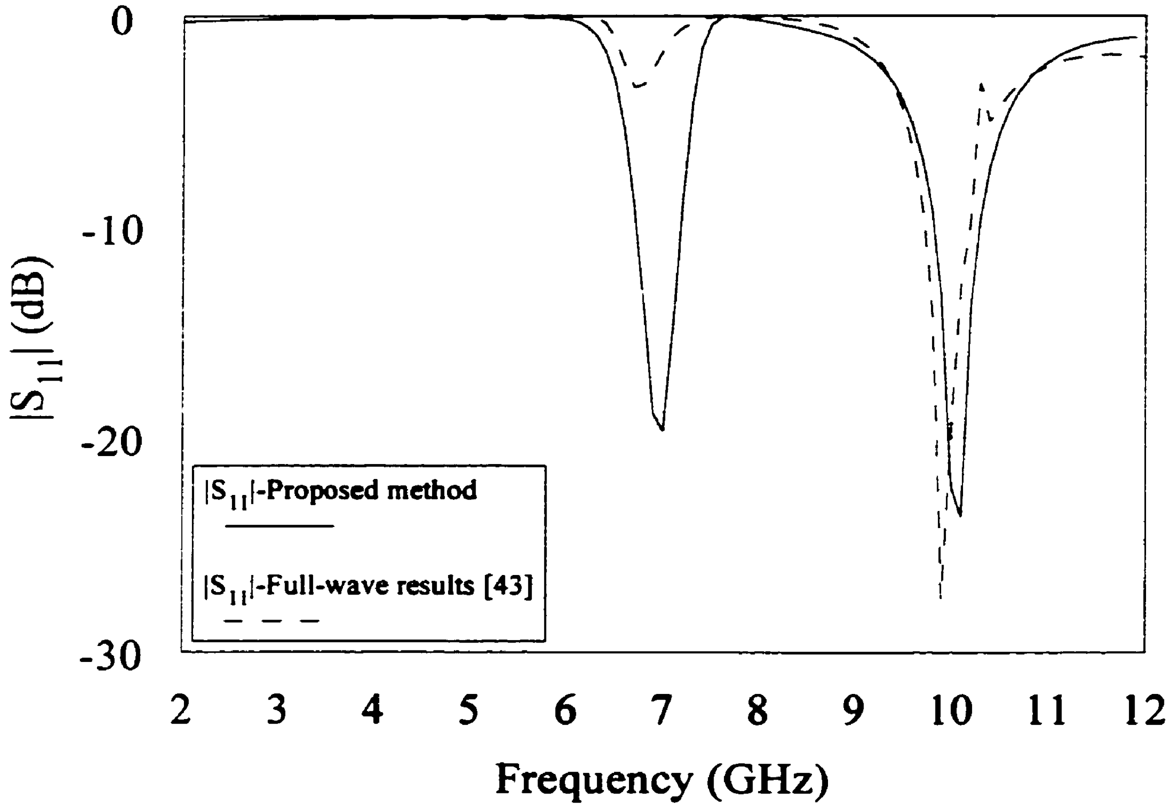

Fig. 6-18. $|S_{11}|$ versus frequency for the microstrip in Fig. 6-17.

Number of computed frequencies	Full-wave [43]		Proposed method	
	Memory used	Time	Memory used	Time
100	11.72 MB + 245 MB (swap)	2.5 hours	61 KB	1.5 sec

Table 6-5. Comparison of computer time and memory requirements in the proposed method with those in the full-wave method [43] for the microstrip in Fig. 6-17.

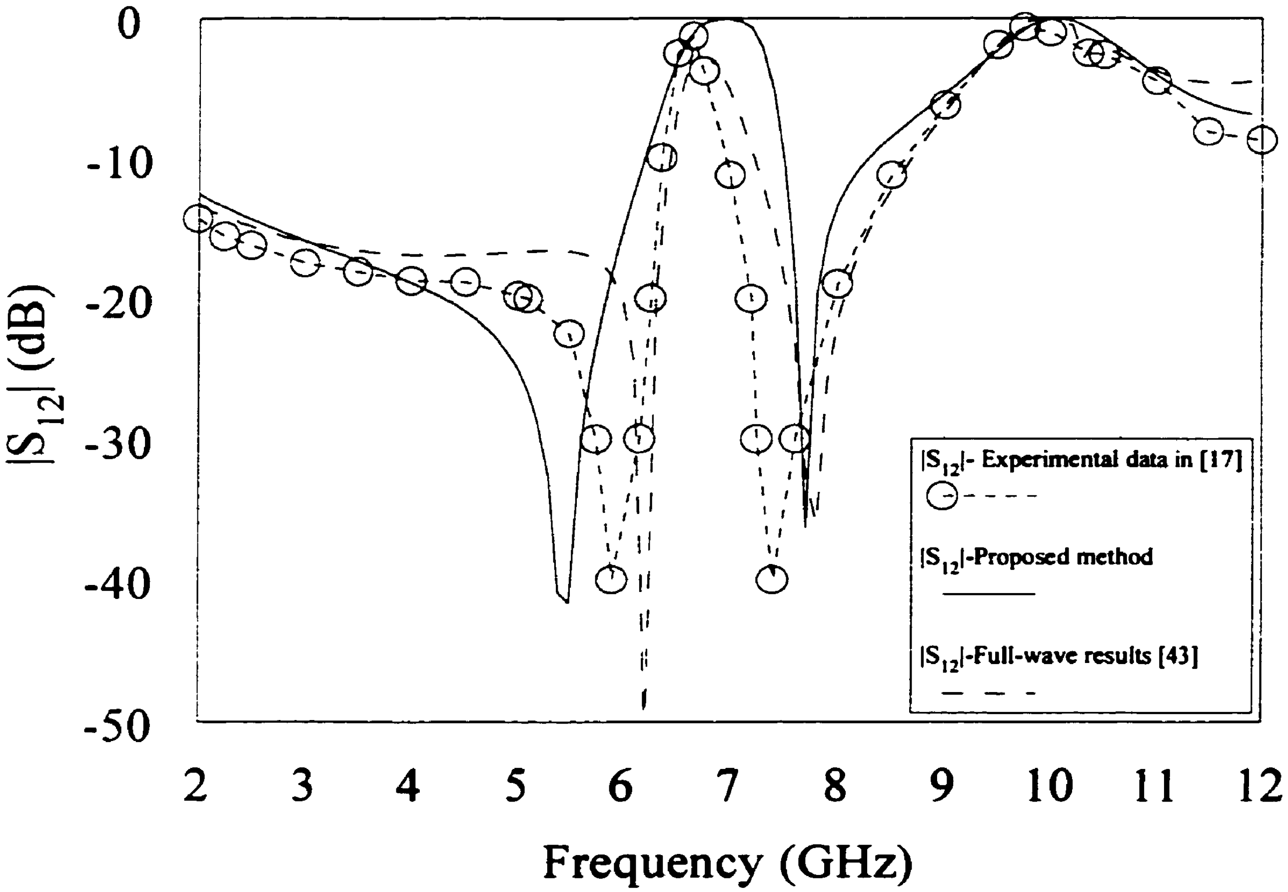

Fig. 6-19. $|S_{12}|$ versus frequency for the microstrip in Fig. 6-17.

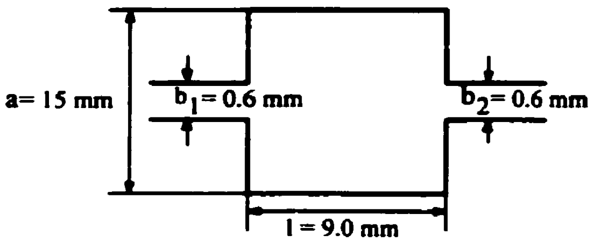

Fig. 6-20. Symmetric microstrip geometry in [17].

Substrate	a(mm)	l(mm)	b_1(mm)	b_2(mm)	h(mm)	ε_r
Alumina	15	9	0.6	0.6	0.635	9.7

Table 6-6. Data for the microstrip in Fig. 6-20.

Box Size			Number of Cells		Cell Size	
X(mm)	Y(mm)	H(mm)	N_X	N_Y	ΔX(mm)	ΔY(mm)
18	18	18	180	180	0.1	0.1

Table 6-7. Data used with [65] for the microstrip in Fig. 6-20.

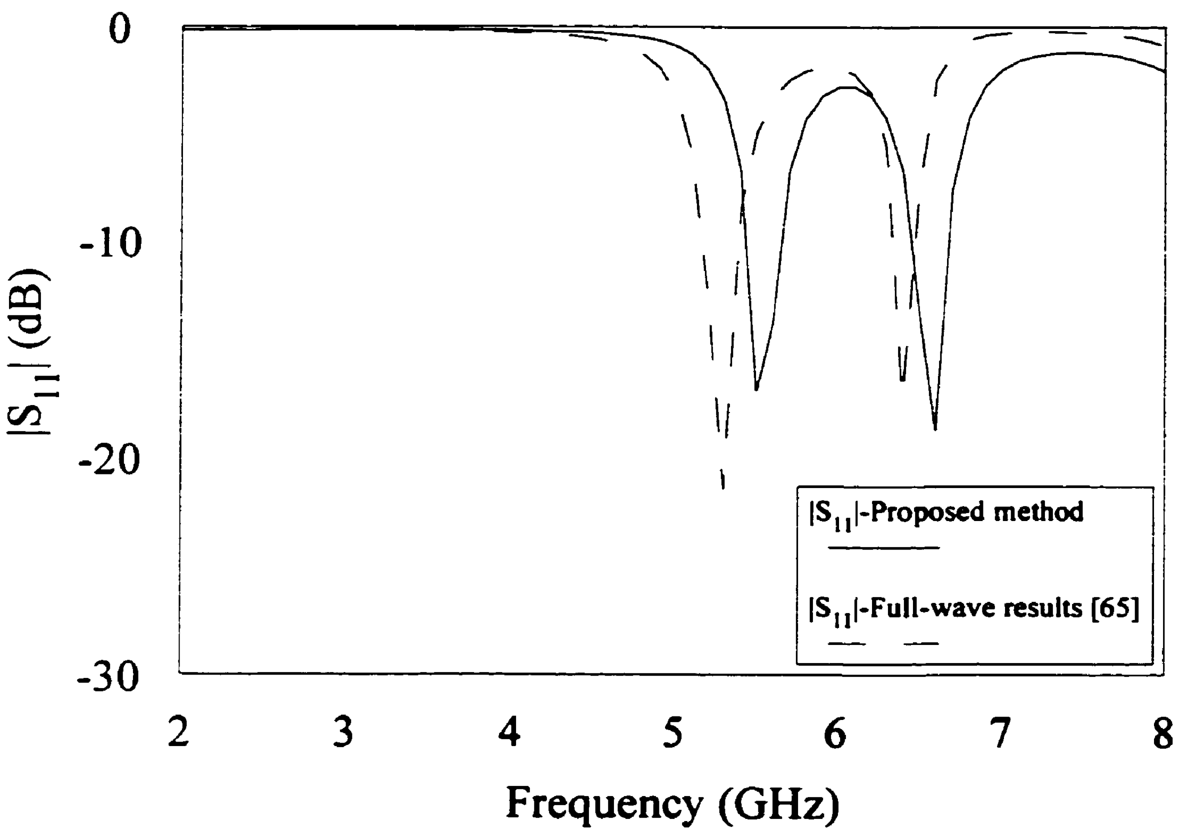

Fig. 6-21. $|S_{11}|$ versus frequency for the microstrip in Fig. 6-20.

Number of computed frequencies	Full-wave [65]		Proposed method	
	Memory used	Time	Memory used	Time
60	2 MB + 24 MB (swap)	0.236 hours	61 KB	1.5 sec

Table 6-8. Comparison of computer time and memory requirements in the proposed method with those in the full-wave method [65] for the microstrip in Fig. 6-20.

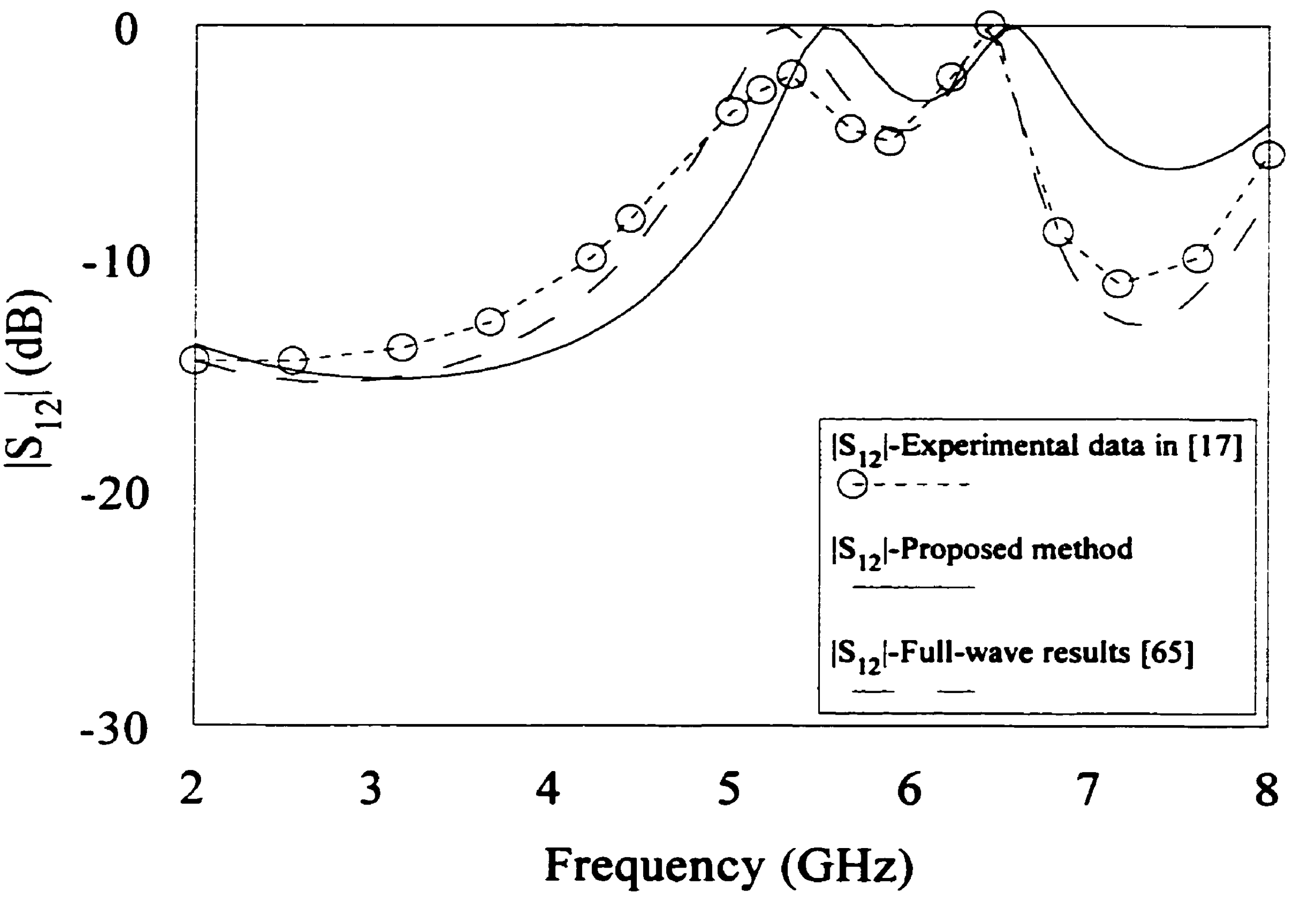

Fig. 6-22. $|S_{12}|$ versus frequency for the microstrip in Fig. 6-20.

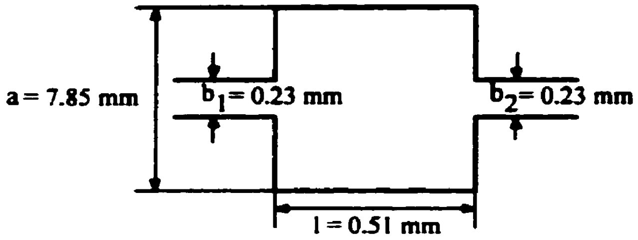

Fig. 6-23. Symmetric microstrip geometry in [17].

Substrate	a(mm)	l(mm)	b_1(mm)	b_2(mm)	h(mm)	ε_r
Alumina	7.85	0.51	0.23	0.23	0.254	9.9

Table 6-9. Data for the microstrip in Fig. 6-23.

Box Size			Number of Cells		Cell Size	
X(mm)	Y(mm)	H(mm)	N_X	N_Y	ΔX(mm)	ΔY(mm)
10	10	10	100	100	0.1	0.1

Table 6-10. Data used with [43] for the microstrip in Fig. 6-23.

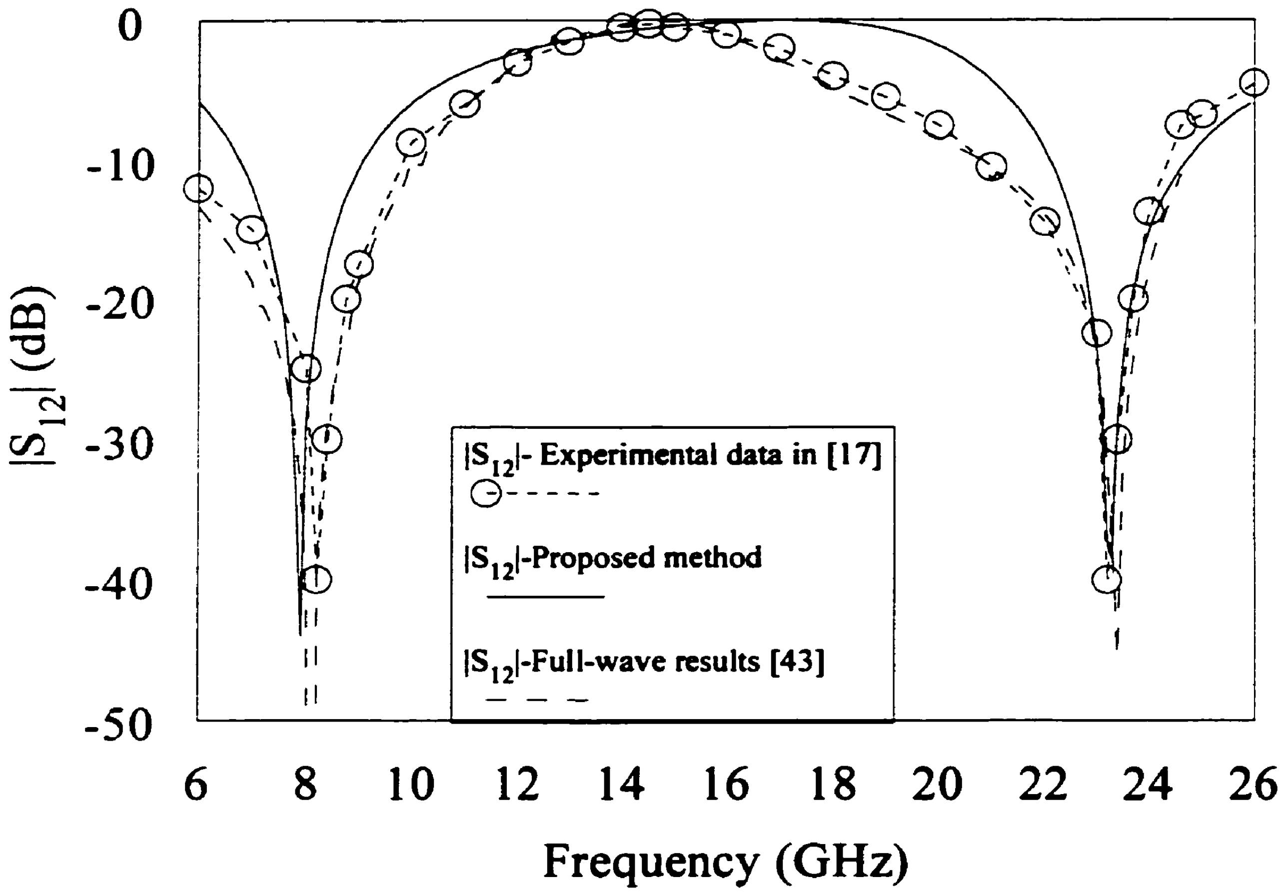

Fig. 6-24. $|S_{12}|$ versus frequency for the microstrip in Fig. 6-23.

Number of computed frequencies	Full-wave [43]		Proposed method	
	Memory used	Time	Memory used	Time
200	2.93 MB + 245.4 MB (swap)	0.33 hours	61 KB	2 sec

Table 6-11. Comparison of computer time and memory requirements in the proposed method with those in the full-wave method [43] for the microstrip in Fig. 6-23.

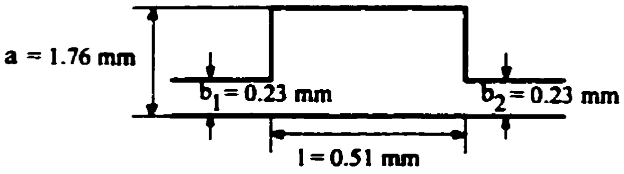

Fig. 6-25. Microstrip geometry in [17].

Substrate	a(mm)	l(mm)	b_1(mm)	b_2(mm)	h(mm)	ε_r
Alumina	1.76	0.51	0.23	0.23	0.254	9.9

Table 6-12. Data for the microstrip in Fig. 6-25.

Box Size			Number of Cells		Cell Size	
X(mm)	Y(mm)	H(mm)	N_X	N_Y	ΔX(mm)	ΔY(mm)
5	5	10	500	500	0.01	0.01

Table 6-13. Data used with [43] for the microstrip in Fig. 6-25.

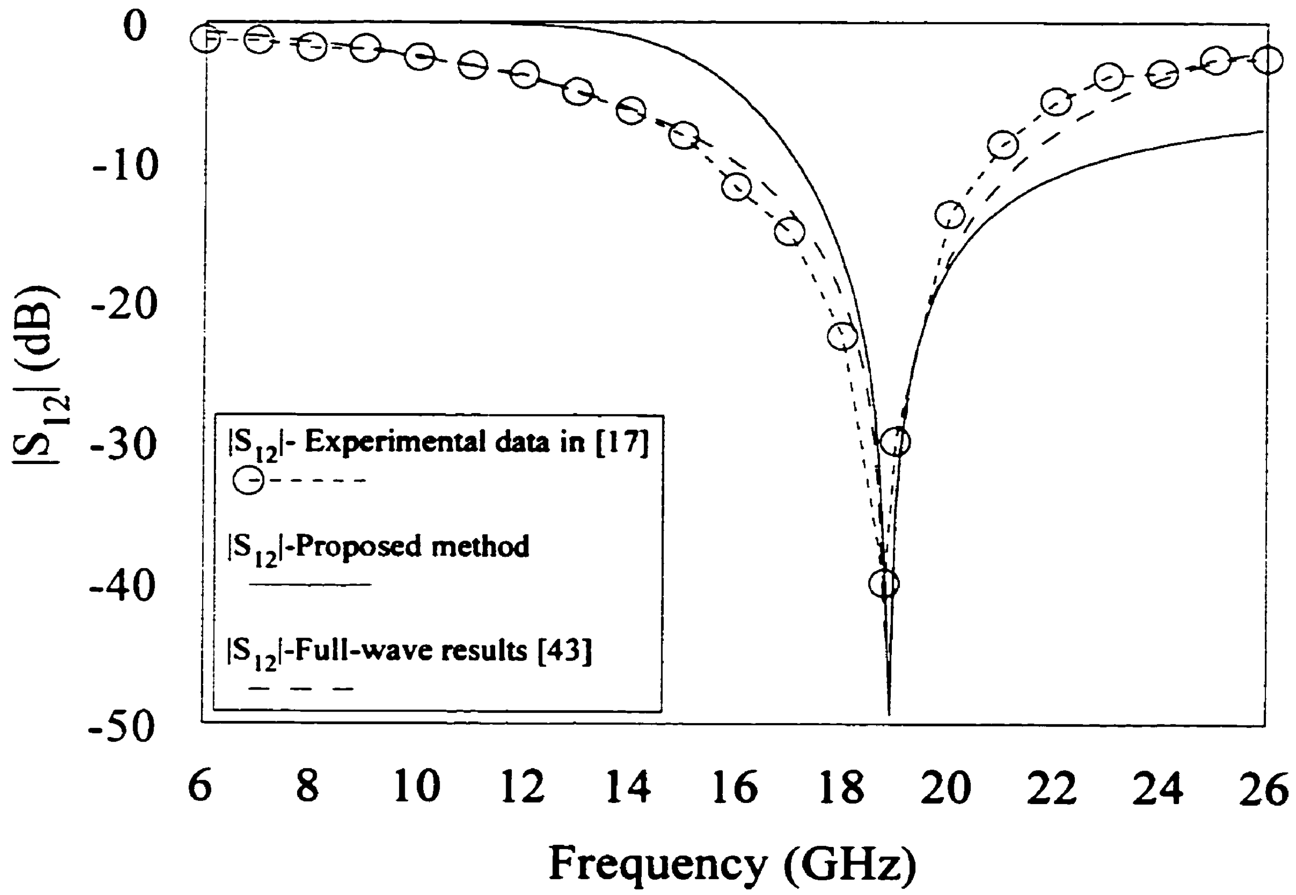

Fig. 6-26. $|S_{12}|$ versus frequency for the microstrip in Fig. 6-25.

Number of computed frequencies	Full-wave [43]		Proposed method	
	Memory used	Time	Memory used	Time
200	73.24 MB + 6134 MB (swap)	9 hours	61 KB	2 sec

Table 6-14. Comparison of computer time and memory requirements in the proposed method with those in the full-wave method [43] for the microstrip in Fig. 6-25.

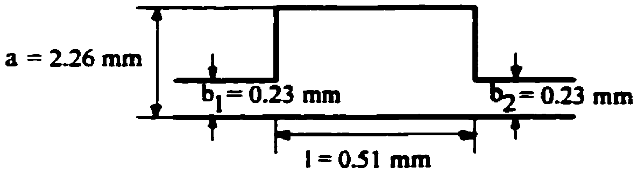

Fig. 6-27. Microstrip geometry in [17].

Substrate	a(mm)	l(mm)	b_1(mm)	b_2(mm)	h(mm)	ε_r
Alumina	2.26	0.51	0.23	0.23	0.254	9.9

Table 6-15. Data for the microstrip in Fig. 6-27.

Box Size			Number of Cells		Cell Size	
X(mm)	Y(mm)	H(mm)	N_X	N_Y	ΔX(mm)	ΔY(mm)
5	5	10	500	500	0.01	0.01

Table 6-16. Data used with [43] for the microstrip in Fig. 6-27.

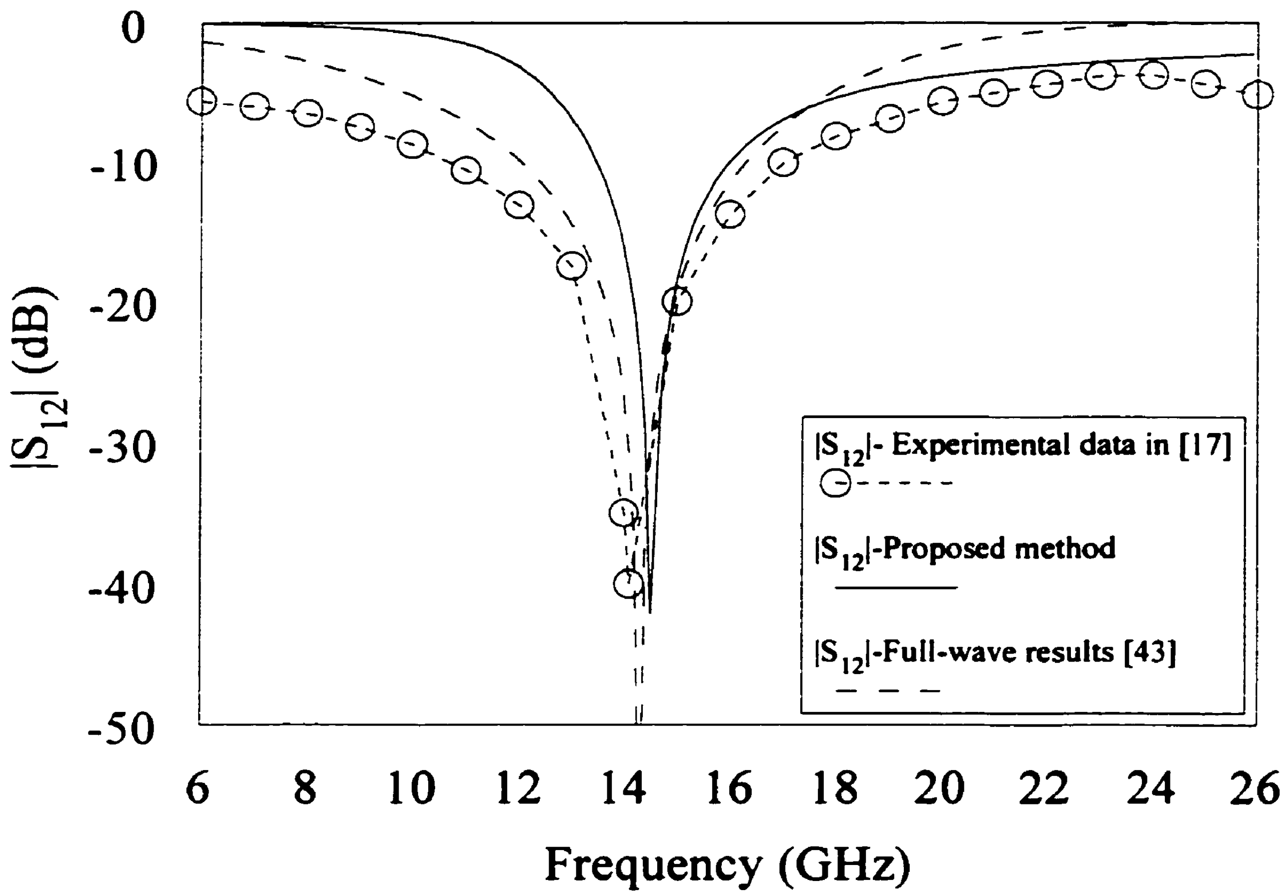

Fig. 6-28. $|S_{12}|$ versus frequency for the microstrip in Fig. 6-27.

Number of computed frequencies	Full-wave [43]		Proposed method	
	Memory used	Time	Memory used	Time
200	73.24 MB + 6134 MB (swap)	9 hours	61 KB	2 sec

Table 6-17. Comparison of computer time and memory requirements in the proposed method with those in the full-wave method [43] for the microstrip in Fig. 6-27.

On the basis of the results and comparisons presented in this Chapter, we can draw the following conclusions:

- The main advantages of the proposed method consist in that results can be generated with an insignificant computation effort and memory usage.
- The method presented can be applied initially to check approximately the performance of single and double step microstrips and, if acceptable, then a more accurate method can be used, thus reducing substantially the design time.

CHAPTER 7. MICROSTRIP RESONATORS

7.1. Circular Resonator with Homogeneous Dielectric

The resonant frequency of a microstrip resonator is usually calculated on the basis of a model where it is assumed that the electromagnetic field exists only in a bounded region between the conducting strip and the ground base. This implies that the scattered field at the side surface of the resonator is neglected. Resonant frequencies for the homogeneous rectangular, circular, and ring microstrip resonators were computed by many authors (Baican, 1996; Gopinath, 1981; Hoffmann, 1987; Khilla, 1984; Watkins, 1969; Yabuki *et al.*, 1996).

In this Chapter we determine the resonant frequency of an inhomogeneous circular microstrip resonator based on the two-dimensional equations (Tugulea and Ciric, 2000). To check the validity of the proposed solution technique, we first use the two-dimensional equations to determine the resonant frequencies of a homogeneous circular resonator for which numerical results are available in the literature (Watkins, 1969).

Consider a resonator as shown in Figure 7-1, with a homogeneous and isotropic lossless dielectric, of permittivity ε and permeability μ. The model employed and shown in Figure 7-2 consists of a cylinder with $r \in (0, a)$ and $z \in (0, h)$, bounded by vertical walls which are either ideal ferromagnetics ($\mu \to \infty$) or perfect conductors ($\sigma \to \infty$) (Bonetti and Tissi, 1978).

The two-dimensional second order voltage equation for time-harmonic fields,

$$\nabla^2 U + \beta^2 U = 0 \tag{7.1}$$

where $\beta = \omega\sqrt{\varepsilon\mu}$, can be written in circular cylindrical coordinates r, φ, z in the form

$$\frac{\partial^2 U}{\partial r^2} + \frac{1}{r}\frac{\partial U}{\partial r} + \frac{1}{r^2}\frac{\partial^2 U}{\partial \varphi^2} + \beta^2 U = 0 \ . \tag{7.2}$$

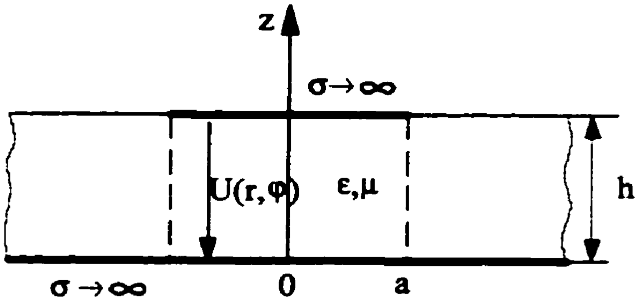

Fig. 7-1. Circular microstrip resonator.

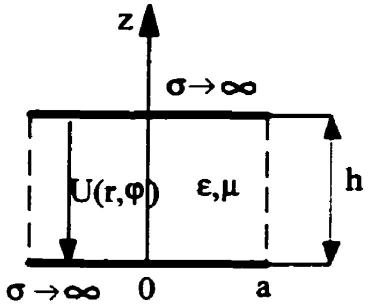

Fig. 7-2. Model for the structure in Fig. 7-1.

The associated boundary conditions are

$$\left.\frac{\partial U(r,\varphi)}{\partial r}\right|_{r=a}=0, \qquad \text{if } r=a \text{ is a magnetic wall} \tag{7.3}$$

$$U(a,\varphi)=0\ , \qquad \text{if } r=a \text{ is an electric wall.} \tag{7.4}$$

Applying the separation of variables and enforcing the regularity conditions at $r=0$ yields solutions of the form

$$U_n(r,\varphi)=(A_n\cos n\varphi+B_n\sin n\varphi)J_n(\beta r) \tag{7.5}$$

where n is an integer and $J_n(\beta r)$ is the Bessel function of the first kind and order n. Imposing the boundary conditions gives $J_n'(\beta a)=0$ for the model with a magnetic vertical wall, and $J_n(\beta a)=0$ for the model with an electric vertical wall. For $n=0$, the eigenvalues are obtained from the roots of the equations $J_1(\beta a)=0$ and $J_0(\beta a)=0$, respectively, for the magnetic wall and for the electric wall. The first root of $J_1(\beta a)=0$ is $\beta a \approx 3.831$, which corresponds to the TE_{010} mode (Baican, 1996; Khilla, 1984), and for $a = 10\,\mathrm{mm}$, $\varepsilon_r = 9.7$, $\mu_r = 1$ the resonant frequency is 5.85 GHz. For $n=1$, the equation $J_1'(\beta a)=0$ gives $\beta a \approx 1.841$, which corresponds to the TE_{110} mode and the resonant frequency is now 2.81 GHz. Similarly, for $n=2$ one has $\beta a \approx 3.054$, which corresponds to the TE_{210} mode and the respective frequency is 4.66 GHz, and for $n=3$, $\beta a \approx 4.201$, which corresponds to the TE_{310} mode with the resonant frequency 6.41 GHz. TE_{110} is the fundamental mode and TE_{210}, TE_{010}, and TE_{310} are higher modes of oscillation. These results are in agreement with those presented by Khilla (1984) using the classical field theory based on Maxwell's equations.

7.2. Circular Resonator with Inhomogeneous Dielectric

For the resonator in Figure 7-3, the substrate has the permittivity ε_1 and permeability μ_1 for $r \in (0,a)$, and ε_2 and μ_2, respectively, for $r \in (a,\infty)$. It is assumed that the dielectric materials are lossless, homogeneous, and isotropic. The resonator model, shown in Figure 7-4, has either a vertical electric wall or a magnetic wall at $r=b$. The equations for the two regions are

$$\frac{\partial^2 U_1}{\partial r^2}+\frac{1}{r}\frac{\partial U_1}{\partial r}+\frac{1}{r^2}\frac{\partial^2 U_1}{\partial \varphi^2}+\omega^2\varepsilon_1\mu_1 U_1=0, \qquad r\in(0,a) \tag{7.6}$$

$$\frac{\partial^2 U_2}{\partial r^2}+\frac{1}{r}\frac{\partial U_2}{\partial r}+\frac{1}{r^2}\frac{\partial^2 U_2}{\partial \varphi^2}+\omega^2\varepsilon_2\mu_2 U_2=0, \qquad r\in(a,b). \tag{7.7}$$

Applying the method of separation of variables and enforcing the regularity conditions at $r = 0$ yields the following solutions with no dependence on φ:

$$U_1(r) = A_1 J_0(\beta_1 r), \qquad \beta_1 = \omega\sqrt{\varepsilon_1\mu_1}, \quad r \in (0,a) \tag{7.8}$$

$$U_2(r) = A_2 J_0(\beta_2 r) + B_2 Y_0(\beta_2 r), \qquad \beta_2 = \omega\sqrt{\varepsilon_2\mu_2}, \quad r \in (a,b) \tag{7.9}$$

where Y_0 is the Bessel function of the second kind and order zero.

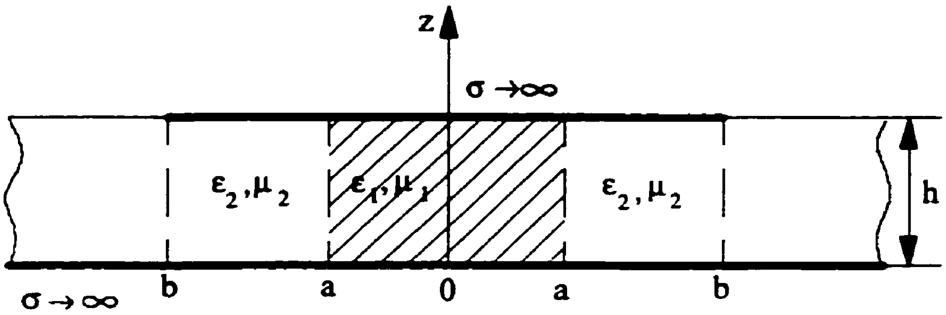

Fig. 7-3. Circular resonator with inhomogeneous dielectric.

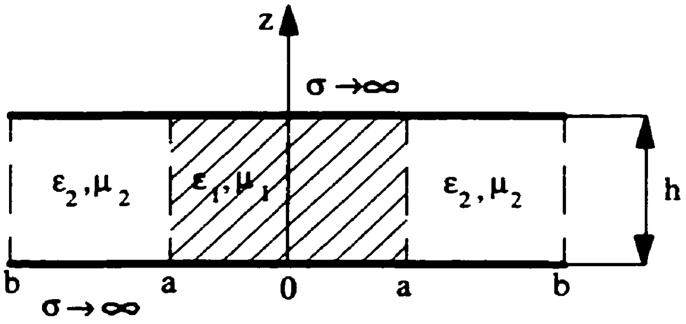

Fig. 7-4. Model for the structure in Fig. 7-3.

Imposing the boundary conditions

$$U_1(a,\varphi) = U_2(a,\varphi) \tag{7.10}$$

$$\left.\frac{1}{\mu_1}\frac{\partial U_1(r,\varphi)}{\partial r}\right|_{r=a} = \left.\frac{1}{\mu_2}\frac{\partial U_2(r,\varphi)}{\partial r}\right|_{r=a} \tag{7.11}$$

$$\left.\frac{\partial U_2(r,\varphi)}{\partial r}\right|_{r=b} = 0 \quad \text{if } r = b \text{ is a magnetic wall} \tag{7.12}$$

$$U_2(b,\varphi) = 0 \qquad \text{if } r = b \text{ is an electric wall,} \tag{7.13}$$

the following transcendental equations are derived, corresponding to (7.12) and (7.13), respectively:

$$\sqrt{\frac{\varepsilon_1}{\mu_1}}\frac{J_1(\beta_1 a)}{J_0(\beta_1 a)} = \sqrt{\frac{\varepsilon_2}{\mu_2}}\frac{J_1(\beta_2 a)Y_1(\beta_2 b) - J_1(\beta_2 b)Y_1(\beta_2 a)}{J_0(\beta_2 a)Y_1(\beta_2 b) - J_1(\beta_2 b)Y_0(\beta_2 a)} \tag{7.14}$$

$$\sqrt{\frac{\varepsilon_1}{\mu_1}}\frac{J_1(\beta_1 a)}{J_0(\beta_1 a)} = \sqrt{\frac{\varepsilon_2}{\mu_2}}\frac{J_1(\beta_2 a)Y_0(\beta_2 b) - J_0(\beta_2 b)Y_1(\beta_2 a)}{J_0(\beta_2 a)Y_0(\beta_2 b) - J_0(\beta_2 b)Y_0(\beta_2 a)}\ . \tag{7.15}$$

For instance, if $a = 10\,\text{mm}$, $b = 15\,\text{mm}$, $\varepsilon_{r1} = 9.7$, $\varepsilon_{r2} = 2.32$, and $\mu_{r1} = \mu_{r2} = 1$, the first resonant frequency from (7.14) is 3.68 GHz and the first resonant frequency from (7.15) is 2.57 GHz.

7.3. Ring Resonator with Inhomogeneous Variable Dielectric

Consider the ring resonator with variable dielectric permittivity, $\varepsilon(r)$, in Figure 7-5. The model shown in Figure 7-6, has vertical magnetic walls at $r = a$ and $r = b$. The two-dimensional second-order voltage equation is now:

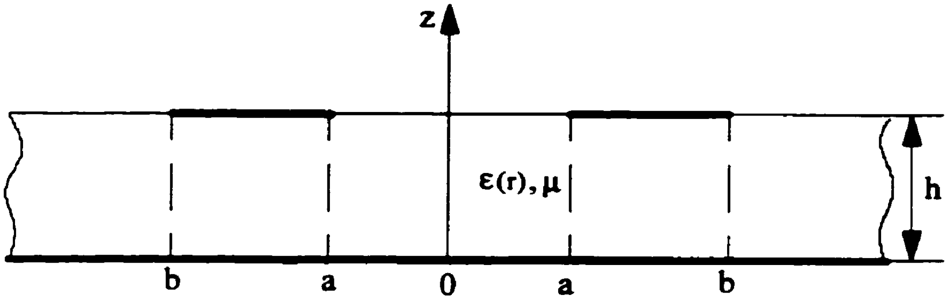

Fig. 7-5. Ring resonator with variable dielectric permittivity.

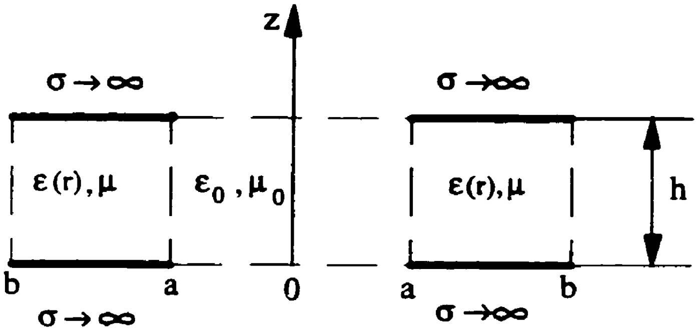

Fig. 7-6. Model for the structure in Fig. 7-5.

$$\frac{\partial^2 U}{\partial r^2}+\frac{1}{r}\frac{\partial U}{\partial r}+\frac{1}{r^2}\frac{\partial^2 U}{\partial \varphi^2}+\omega^2\varepsilon(r)\ \mu\, U\ =0, \qquad r\in(a,b). \tag{7.16}$$

We look for φ-dependent solutions of the form

$$U(r,\varphi)=U_n(r)\begin{Bmatrix}\cos n\varphi\\ \sin n\varphi\end{Bmatrix}.$$

The function $U_n(r)$ satisfies the equation

$$r^2U_n''(r)+rU_n'(r)+[\omega^2\mu\varepsilon(r)r^2-n^2]U_n(r)=0\ . \tag{7.17}$$

If $\mu=\mu_0$ and the law of variation of the dielectric permittivity is, for instance

$$\varepsilon(r)=\varepsilon_0\varepsilon_r\left(\frac{r}{a}\right)^{2m}, \tag{7.18}$$

then Equation (7.17) becomes

$$r^2U_n''(r)+rU_n'(r)+\left[\frac{4\pi^2a^2}{\lambda_0^2}\varepsilon_r\left(\frac{r}{a}\right)^{2m+2}-n^2\right]U_n(r)=0 \tag{7.19}$$

with

$$\lambda_0=\frac{2\pi}{\omega\sqrt{\varepsilon_0\mu_0}}.$$

This equation is of the form

$$x^2y''+\alpha xy'+(\beta x^p+\gamma)y=0 \tag{7.20}$$

whose solution is

$$y=x^{\frac{1-\alpha}{2}}Z_\nu\left(\frac{2}{p}\sqrt{\beta}x^{\frac{p}{2}}\right) \tag{7.21}$$

with

$$\nu = \frac{1}{p}[(1-\alpha^2)-4\gamma]^{\frac{1}{2}} \tag{7.22}$$

where $Z_\nu(x)$ is the combination $A_\nu J_\nu(x) + B_\nu Y_\nu(x)$. By identification

$$\alpha = 1;\ \gamma = -n^2;\ \beta = \frac{4\pi^2\varepsilon_r}{\lambda_0^2 a^{2m}};\ p = 2m+2;\ \nu = 2n/(2m+2) \tag{7.23}$$

and the voltage expression is

$$U(r,\varphi) = Z_\nu\left(\frac{\sqrt{\varepsilon_r}}{m+1}\frac{2\pi}{\lambda_0 a^m} r^{m+1}\right)\begin{Bmatrix}\cos n\varphi \\ \sin n\varphi\end{Bmatrix} \ . \tag{7.24}$$

Imposing the boundary conditions at $r = a$ and $r = b$,

$$\left.\frac{\partial U_n(r)}{\partial r}\right|_{\substack{r=a \\ r=b}} = 0 \tag{7.25}$$

and taking $n = 0$ and $m = 2$, the following equation is obtained

$$J_1(\xi)Y_1(k\xi) - J_1(k\xi)Y_1(\xi) = 0 \tag{7.26}$$

where

$$\xi = \frac{2\pi}{3}\sqrt{\varepsilon_r}\left(\frac{a}{\lambda_0}\right), \qquad k = \left(\frac{b}{a}\right)^3 .$$

Solving Equation (7.26) for the first root ξ_1, the corresponding resonant frequency is

$$f_1 = \frac{3c_0\xi_1}{2\pi a\sqrt{\varepsilon_r}} . \tag{7.27}$$

Choosing a different value for *m* in (7.18) modifies the law of variation of the dielectric permittivity and correspondingly the resonant frequency.

The solution technique presented is simple and equations like (7.14), (7.15) and (7.26) can be easily solved employing computation tools such as Mathematica or Matlab.

8. CONCLUSIONS

8.1. Two-Dimensional Equations

In this thesis the two-dimensional equations for microwave planar circuits have been successfully used in the analysis of specific phenomena in microstrip lines. These equations are in fact a generalization of the classical, one-dimensional transmission line equations. The two-dimensional equations allow the inclusion of losses in the analysis of microstrip structures.

The frequency range of applicability for these equations extends up to the cutoff frequency of the first TM mode, covering the practical operating range of the microstrip circuits.

8.2. Quasistatic Parameters

In the analysis of microstrip lines, accurate values for the effective dielectric permittivity at zero frequency are required. Four different methods to calculate the quasistatic parameters were developed. Two of these methods are variational methods, one for the potentials, the other for electric charges, which along with the theorems for upper and lower bound on capacitance, permit the accurate calculation of the effective dielectric permittivity and characteristic impedance at zero frequency.

These methods were employed to calculate the quasistatic parameters for all the examples considered in various chapters of this thesis. A criteria for choosing the distance where the perfect conductor walls should be placed in the models presented, based on the ratio of the strip width to the thickness of the dielectric substrate, was also given. The results obtained were compared to full-wave results available in the literature and the differences are well under 1%.

8.3. Applications of the Two-Dimensional Equations

Based on the two-dimensional equations, the following applications were developed and the results obtained were compared with those available in the literature:

- A model to calculate the dispersion for the fundamental mode *and* simultaneously, that for the higher-order modes of propagation;
- A modified model to include the losses, for the computation of *both* the dispersion and the attenuation, simultaneously;
- A simple equivalent circuit for symmetric and asymmetric step discontinuities in microstrip lines, along with efficient formulas to compute the scattering parameters, saving considerable computer resources;
- An equivalent circuit and an analytic formula for the computation of the scattering parameters of a double step discontinuity that gives acceptable results, when compared to results by full-wave methods and to experimental data, reducing the computer time by *two orders* of magnitude as compared to that required by full-wave techniques;
- A simple model and equation to calculate resonant frequencies of microstrip circular and ring resonators with inhomogeneous dielectrics.

Other results of the research performed in the thesis include:

- A detailed explanation of the existence of the higher-order modes of propagation in the proposed model based on rectangular structures filled with inhomogeneous dielectric;
- A discussion related to the existence of the evanescent modes on microstrip lines;

8.4. Future Work

The potential for engineering applications of the two-dimensional equations was demonstrated in this thesis. There are certain applications where these equations, based on the results obtained in the thesis, can be employed with a higher degree of confidence, for instance:

- Computation of the scattering parameters for T-shaped microstrip lines and for multiple step microstrip discontinuities;
- Calculation of dispersion and attenuation in parallel, coupled microstrip lines;
- Analysis of dispersion in coupled lines, including losses;
- Investigation of the attenuation for higher-order modes of propagation.

It is expected that relatively simple models, formulas, and equivalent circuits can be obtained for the above configurations and incorporated in computer aided design software, providing a fast evaluation of dispersion, attenuation and scattering parameters.

LIST OF REFERENCES

1. S. Akhtarzad and P. Jahus, "Dispersion characteristics of a microstrip line with a step discontinuity", *Electronics Letters*, Vol. 11, pp. 310-311, 1975.
2. H.A. Atwater, "Tests of microstrip dispersion formulas", *IEEE Trans. Microwave Theory Tech.*, vol. MTT-36, pp. 619-621, March 1988.
3. R. Baican, "*Microwave Integrated Circuits*", (in Romanian), Cluj-Napoca: Promedia-Plus, 1996.
4. P. Bhartia and I.J. Bahl, "*Millimeter Wave Engineering and Applications*", New York, NY: John Wiley & Sons, 1984.
5. R. Bonetti and P. Tissi, "Analysis of planar disk networks", *IEEE Trans. Microwave Theory Tech.*, vol. MTT-26, pp. 471-477, 1978.
6. T. Bryant and J. Weiss, "Parameters of microstrip transmission lines and of coupled pairs of microstrip lines", *IEEE Trans. Microwave Theory Tech.*, vol. MTT-16, pp. 1021-1027, 1968.
7. H. J. Carlin, "A simplified circuit model for microstrip", *IEEE Trans. Microwave Theory Tech.*, vol. MTT-21, pp. 589-591, Sept. 1973.
8. R. Collin, "*Field Theory of Guided Waves*", 2nd ed. Piscataway, NJ: IEEE Press, 1992.
9. E.J. Denlinger, "A frequency dependent solution for microstrip transmission lines", *IEEE Trans. Microwave Theory Tech.*, vol. MTT-19, pp. 30-39, Jan. 1971.
10. B. Easter *et al.*, "Theoretical and experimental methods for evaluating discontinuities in microstrip", *The Radio and Electronic Engineer*, Vol. 48, pp. 73-84, 1978.
11. T. Edwards and R. Owens, "2-18 GHz dispersion measurements on 10-100 Ω microstrip lines on sapphire", *IEEE Trans. Microwave Theory Tech.*, vol. MTT-24, pp. 506-513, Aug. 1976.
12. H. Ermert, "Guided modes and radiation characteristics of covered microstrip lines", *Arch. Electronik u. Ubertragungstechn.*, Vol. 30, pp. 65-70, 1976.
13. A.L. Feldstein, L.R. Iavici and V.P. Smirnov, "*Handbook of Elements of Guided Wave Techniques*", (in Russian), Moscow: Sovietskoe Radio, 1967.
14. T.S. Forzley and G. Bridges-"Dispersion characteristics of open microstrip using a direct VSW measurement approach", *Antenna Technology and Applied Electromagnetics Symp.*

Dig., Winnipeg, Aug. 5-7, 1992.

15. R. Garg and I. Bahl, "Microstrip discontinuities", *Int. J. Electronics*, Vol. 45, pp. 81-87, 1978.
16. W. Getsinger, "Microstrip dispersion model", *IEEE Trans. Microwave Theory Tech.*, vol. MTT-21, pp. 34-39, Jan. 1973.
17. F. Giannini, G. Bartolucci, and M. Ruggieri, "Equivalent circuit models for computer aided design of microstrip rectangular structures", *IEEE Trans. Microwave Theory Tech.*, vol. MTT-40, pp. 378-388, February 1992.
18. A. Gopinath *et al.*, "Equivalent circuit parameters of microstrip step change in width and cross junctions", *IEEE Trans. Microwave Theory Tech.*, vol. MTT-24, pp. 142-144, 1976.
19. A. Gopinath, "Maximum Q-factor of microstrip resonators", *IEEE Trans. Microwave Theory Tech.*, vol. MTT-29, pp. 128-131, Feb. 1981.
20. H. Green, "The numerical solution of some important transmission-line problems", *IEEE Trans. Microwave Theory Tech.*, vol. MTT-13, pp. 676-692, 1965.
21. K.G. Gupta, R. Garg, and I.J. Bahl, "*Microstrip Lines and Slotlines*". Dedham, MA: Artech House, 1979.
22. K.G. Gupta and A. Singh, "*Microwave Integrated Circuits*", John Wiley & Sons, New York, 1982.
23. E. Hammerstad and O. Jensen, "Accurate models for microstrip computer aided design", in *IEEE MTT-S Int. Microwave Symp. Dig.*, New York, NY, pp.407-409, June 1980.
24. R. Hoffmann, "*Handbook of Microwave Integrated Circuits*". Norwood, MA: Artech House, 1987.
25. T. Itoh and R. Mittra, "Spectral-domain approach for calculating the dispersion characteristics of microstrip lines", *IEEE Trans. Microwave Theory Tech.*, vol. MTT-21, pp. 469-499, July 1973.
26. T. Itoh, "*Planar Transmission Line Structures*". Piscataway, NJ: IEEE Press, 1987.
27. R. Jansen, "High-speed computation of single and coupled microstrip parameters including dispersion, high-order modes, loss and finite strip thickness", *IEEE Trans. Microwave Theory Tech.*, vol. MTT-26, pp. 75-82, Feb. 1978.
28. A. M. Khilla, "Ring and disk resonator CAD model", *Microwave J.*, pp. 91-105, Nov. 1984.

29. M. Kirschning and R.H. Jansen, "Accurate model for effective dielectric constant of microstrip with validity up to millimeter-wave frequencies", *Electron. Lett.*, vol. 18, pp. 272-273, March 1982.

30. M. Kobayashi, "Important role of inflection frequency in the dispersive property of microstrip lines", *IEEE Trans. Microwave Theory Tech.*, vol. MTT-30, pp. 2057-2059, Nov. 1982.

31. M. Kobayashi, "A dispersion formula satisfying recent requirements in microstrip CAD", *IEEE Trans. Microwave Theory Tech.*, vol. MTT-36, pp. 1246-1250, Aug. 1988.

32. G. Kompa, "Excitation and propagation of higher order modes in microstrip discontinuities", *European Microwave Conf. Proc.*, Bruxelles, 1973.

33. G. Kompa, "Dispersion measurements of the first two higher-order modes in open microstrip", *Arch. Electronik u. Ubertragungstechn.*, Vol. 29, pp. 182-184, 1975.

34. G. Kompa and R. Mehran, "Planar waveguide model for calculating microstrip components", *Electronics Letters*, Vol. 11, pp. 459-460, 1975.

35. G. Kompa, "S-matrix computation of microstrip discontinuities with a planar waveguide model", *Arch. Electronik u. Ubertragungstechn.*, Vol. 30, pp. 58-64, 1976.

36. G. Kompa, "Design of stepped microstrip components", *The Radio and Electronic Engineer*, Vol. 48, pp. 53-63, 1978.

37. N. Koster and R. Jansen, "The microstrip step discontinuity: a revised description", *IEEE Trans. Microwave Theory Tech.*, vol. MTT-34, pp. 213-222, February 1986.

38. G. Kowalski and R. Pregla, "Dispersion characteristics of shielded microstrips with finite thickness", *Arch. Electronik u. Ubertragungstechn.*, Vol. 25, pp. 193-196, 1971.

39. E.F. Kuester and D.C. Chang, "An appraisal of methods for computation of the dispersion characteristics of open microstrip", *IEEE Trans. Microwave Theory Tech.*, vol. MTT-27, pp. 691-694, July 1979.

40. R. Levy, "Derivation of equivalent circuits of microwave structures using numerical techniques", *IEEE Trans. Microwave Theory Tech.*, vol. MTT-47, pp. 1688-1695, Sept. 1999.

41. J.L. Medina, A. Serrano, and F.J. Mendietta, "Microstrip effective dielectric constant measurement and test of CAD models up to 20 GHz", *Microwave J.*, pp.82-93, March 1993.

42. F. Mesa, C. Di Nallo, and D.R. Jackson, "The theory of surface-wave and space-wave leaky-mode excitation on microstrip lines", *IEEE Trans. Microwave Theory Tech.*, vol.

MTT-47, pp. 207-215, February 1999.

43. Microwave Office 2000-Version 3.20, courtesy of Applied Wave Research, Inc., Los Angeles, CA, February 2000.

44. R. Mittra and T. Itoh, "A new technique for the analysis of the dispersion characteristics of microstrip lines", *IEEE Trans. Microwave Theory Tech.*, vol. MTT-19, pp. 47-56, 1971.

45. C. Montgomery *et al.*, "*Principles of Microwave Circuits*", Mc Graw-Hill, New-York, 1948.

46. R. Neidert and G. Reilly, "Very large impedance steps in microstrip", *IEEE Trans. Microwave Theory Tech.*, vol. MTT-22, pp. 808-810, 1974.

47. D. Nghiem, J.T. Williams, D.R. Jackson, and A.A. Oliner, "Existence of a leaky dominant mode on microstrip line with an isotropic substrate: theory and measurements", *IEEE Trans. Microwave Theory Tech.*, vol. MTT-44, pp. 1710-1715, October 1996.

48. A.A. Oliner, "Equivalent circuits for discontinuities in balanced strip transmission line", *IEEE Trans. Microwave Theory Tech.*, vol. MTT-3, pp. 134-143, 1955.

49. A.A. Oliner and K.S. Lee, "The nature of the leakage from higher modes on microstrip line", *IEEE MTT-S Int. Symposium Dig.*, pp. 57-60, 1986.

50. T. Okoshi and T. Miyoshi, "The planar circuit-An approach to microwave integrated circuitry", *IEEE Trans. Microwave Theory Tech.*, vol. MTT-20, pp. 242-252, Apr. 1972.

51. P. Pramanick and P. Bhartia, "An accurate description of dispersion in microstrip", *Microwave J.*, pp. 89-96, Dec. 1983.

52. P. Pramanick and P. Bhartia, "A new microstrip dispersion model", *IEEE Trans. Microwave Theory Tech.*, vol. MTT-32, pp. 1379-1384, Oct. 1984.

53. M. Prouty, K. Mei, S. Schwarz, R. Pous, and Y. Liu, "Solving microstrip discontinuities by the measured equation of invariance", *IEEE Trans. Microwave Theory Tech.*, vol. MTT-45, pp. 877-885, June 1997.

54. R.A. Pucel, D.Masse, and C. Hartwig, "Losses in microstrip", *IEEE Trans. Microwave Theory Tech.*, vol. MTT-16, pp. 342-350, June 1968.

55. R. Radulet and A. Tugulea, "The circuit theory of the microwave two-dimensional structures", *Rev. Roum. Sci. Tech.-Electrotechn. et Energ.*, 28, 4, pp. 337-348, Dec. 1983.

56. C.J. Railton and T. Rozzi, "The rigorous analysis of cascaded step discontinuities microstrip", *IEEE Trans. Microwave Theory Tech.*, vol. MTT-36, pp. 1177-1185, July 1988.

57. S. Ramo, J. Whinnery, and T. Van Duzer, "*Fields and Waves in Communications Electronics*", John Wiley & Sons, Jan. 1994.

58. RT/duroid 6010/6010 LM ceramic PTFE composite-manufacturer data sheet, Rogers Corporation, Microwave Materials Division, Chandler, AZ: March 2000.

59. M. Salazar-Palma *et al.*, "*Iterative and Self-adaptive Finite-elements in Electromagnetic Modeling*", Norwood, Ma: Artech House 1998.

60. M.V. Schneider, "Microstrip dispersion", *Proc. IEEE*, vol. 60, pp. 144-146, Jan. 1972.

61. U. Schulz and R. Pregla, "A new technique for the analysis of the dispersion characteristics of planar waveguides", *Arch. Electronik u. Ubertragungstechn.*, Vol. 34, pp. 169-173, 1980.

62. P. Silvester, "TEM wave properties of microstrip transmission lines", *Proc. IEEE*, Vol. 115, pp. 43-48, 1968.

63. P. Silvester and P. Benedek, "Equivalent capacitances of microstrip open circuits", *IEEE Trans. Microwave Theory Tech.*, vol. MTT-20, pp. 511-516, August 1972.

64. P. Silvester and P. Benedek, "Equivalent capacitances of microstrip gaps and steps", *IEEE Trans. Microwave Theory Tech.*, vol. MTT-20, pp. 729-733, November 1972.

65. Sonnet-Version 6.0b, courtesy of Sonnet Software, Inc., Liverpool, NY, June 1999.

66. G. Stracca, "A simple evaluation of losses in thin microstrips", *IEEE Trans. Microwave Theory Tech.*, vol. MTT-45, pp. 281-283, February 1997.

67. A. Thomson and A. Gopinath, "Calculation of microstrip discontinuity inductances", *IEEE Trans. Microwave Theory Tech.*, vol. MTT-23, pp. 648-655, 1975.

68. A. Tugulea, "A general approximate method for the estimation of microstrip dispersion", *Rev. Roum. Sci. Tech.-Electrotechn. et Energ.*, 29, 2, pp. 215-221, April 1984.

69. A. Tugulea and I.R. Ciric, "A novel lossy microstrip model", in *IEEE MTT-S Int. Symp. Dig.*, Atlanta, GA, June 1993.

70. A. Tugulea, "Losses in microstrip lines using two-dimensional equations for planar circuits", *Grad Conf., University of Manitoba*, June 1998.

71. A. Tugulea and I.R. Ciric, "Two-dimensional equations for microwave planar circuits", *Antenna Technology and Applied Electromagnetics Symp. Dig.*, Ottawa, Aug. 9-12, 1998.

72. A. Tugulea and I.R. Ciric, "Analysis of lossy microstrips using two-dimensional equations for planar circuits", *IEEE AP-S Int. Symp. Dig.*, Orlando, FL, July 1999.

73. A. Tugulea and I.R. Ciric, "Equivalent circuit for a microstrip step discontinuity", *Antenna Technology and Applied Electromagnetics Symp. Dig.*, Winnipeg, July 30-Aug. 2, 2000.

74. A. Tugulea and I.R. Ciric, "Analysis of circular microstrip resonators using two-dimensional telegraphists' equations", *Antenna Technology and Applied Electromagnetics Symp. Dig.*, Winnipeg, July 30-Aug. 2, 2000.

75. A.K. Verma and R. Kumar, "A new dispersion model for microstrip line", *IEEE Trans. Microwave Theory Tech.*, vol. MTT-66, pp. 1183-1187, August 1998.

76. J. Watkins, "Circular resonant structures in microstrip", *Electronics Letters*, vol. 5, p.524, 1969.

77. H. Wheeler, "Transmission-line properties of parallel strips separated by a dielectric sheet", *IEEE Trans. Microwave Theory Tech.*, vol. MTT-13, pp. 172-185, 1965.

78. I. Wolf, G. Kompa, and R. Mehran., "Calculation method for microstrip discontinuities and T junctions", *Electronic Letters*, vol. 8, pp. 177-179, April 1972.

79. Q. Xu, K. Webb, and R. Mittra., "Study of modal solution procedures for microstrip step discontinuities", *IEEE Trans. Microwave Theory Tech.*, vol. MTT-37, pp. 381-387, February 1989.

80. H. Yabuki, M. Matsuo, M. Sagawa, and M. Makimoto, "Stripline dual-mode ring resonators and their application to microwave devices", *Microwave J.*, pp. 72-80, June 1996.

81. E. Yamashita and R. Mittra, "Variational method for the analysis of microstrip lines", *IEEE Trans. Microwave Theory Tech.*, vol. MTT-16, pp. 251-256, 1968.

82. E. Yamashita, K. Atsuki, and T. Ueda, "An approximate dispersion formula of microstrip lines for CAD of microwave integrated circuits", *IEEE Trans. Microwave Theory Tech.*, vol. MTT-27, pp. 1036-1038, Dec. 1979.

83. E. Yamashita, K. Atsuki, and T. Hirahata, "Microstrip dispersion in a wide-frequency range", *IEEE Trans. Microwave Theory Tech.*, vol. MTT-29, pp. 610-611, June 1981.

84. R.A. York and R.C. Compton, "Experimental evaluation of existing CAD models for microstrip dispersion", *IEEE Trans. Microwave Theory Tech.*, vol. MTT-38, pp. 327-328, March 1990.